DISSERTATION

IMPACT OF THE CELL POLARITY PROTEIN SCRIBBLE ON LIVER CANCER FORMATION AND PROGRESSION

submitted to the

Combined Faculties for the Natural Sciences
and for Mathematics

of the Ruperto-Carola University of
Heidelberg, Germany

for the degree of

Doctor of Natural Sciences

Shan Wan

2017

Dissertation

submitted to the

Combined Faculties for the Natural Sciences
and for Mathematics

of the Ruperto-Carola University of
Heidelberg, Germany

for the degree of

Doctor of Natural Sciences

presented by

Master of Science: Shan, Wan

born in: Mianyang, China

Oral-examination:

IMPACT OF THE CELL POLARITY PROTEIN SCRIBBLE ON LIVER CANCER FORMATION AND PROGRESSION

Referees: Prof. Dr. Peter Angel

Dr. Kai Breuhahn

SUMMARY

Polarization of hepatocytes is important for the liver to carry out its functions such as bile secretion and detoxification. In this context, cell polarity complexes, which are spatially segregated at specific membranous domains, define the 3-dimensional orientation of hepatocytes. The disturbance of cell polarity in early phases of tumorigenesis is associated with the activation of intracellular oncogenic signaling pathways affecting tumor initiation and progression. However, if the disturbance of hepatocellular polarity participates in the tumor formation and how the dysregulation of polarity factors affect hepatocarcinogenesis is poorly understood.

In order to define relevant cell polarity factors, which may support *hepatocellular carcinoma* (HCC) development, high-dimensional expression array data derived from HCC patients were screened for significantly dysregulated cell polarity genes. A panel of significantly dysregulated factors, including the baso-lateral complex protein *Scribble* (Scrib), correlated with poor patient outcome and tumor recurrence. Scrib overexpression in HCC tissues associated with genomics gains of the *Scribble* gene locus on chromosome 8q24.3. The loss of membranous Scrib expression or its cytoplasmic enrichment was frequently observed in HCC tissues and HCC cell lines but not in normal liver tissues. In order to analyze the biological impact of cytoplasmic Scrib accumulation, polarized HCC cell lines (HepG2) stably expressing wildtype Scrib ($Scrib^{WT}$, with membrane binding) and a mutated Scrib isoform ($Scrib^{P305L}$, with enforced cytoplasmic

enrichment) were generated. *In vitro*, cytoplasmic Scrib^{P305L} reduced the formation of *canalicular* structures and moderately supported cell proliferation. *In vivo*, hydrodynamic gene delivery of Scrib^{P305L} and c-MYC induced elevated liver tumor formation compared to Scrib^{WT} and c-MYC co-injection. Importantly, Scrib^{P305L} stimulated HCC cell invasiveness, reorganization of actin filaments and overexpression of Rho GTPases. A comparative analysis of oncogenic pathways revealed an activation of AKT by Scrib^{P305L}, which was mediated through the destabilization of negative AKT regulators *leucine rich repeat protein phosphatase 1* (PHLPP1) and phosphatase and *tensin homolog* (PTEN). Transcriptome analysis detected Scrib^{P305L}-dependent upregulation of genes, which were associated with cell motility, epithelial-mesenchymal transition (EMT) and extracellular matrix (ECM) remodeling. Among these genes, *secreted protein acidic and cysteine rich* (SPARC) was highly induced by cytoplasmic Scrib and facilitates cell invasion depending on the AP-1 transcription factor subunits ATF2 and JunB. Lastly a significant association between cytoplasmic Scrib, AKT and ATF2 activation/phosphorylation and loss of E-cadherin was confirmed in human HCC samples and Scrib^{P305L}-induced gene signatures were detected in patient subgroups with worse overall survival.

Taken together, this study illustrates that the overexpression and cytoplasmic enrichment of the cell polarity factor Scrib supports HCC development and tumor cell dissemination through the induction of distinct molecular mechanisms. These mechanisms include activation of the AKT signaling axis and stimulation of AP1-target genes, which are critical for the migratory phenotype of HCC cells.

ZUSAMMENFASSUNG

Die drei-dimensionale Ausrichtung bzw. Polarität von Hepatozyten ist von zentraler Bedeutung für die Funktion der Leber (z.B. Galleproduktion und Detoxifikation). Membranassoziierte Zellpolaritätskomplexe definieren die apikale, laterale und basale Region einer Hepatozyte und der Verlust hepatozytärer Polarität ist ein frühes Ereignis in der Lebertumorentstehung. Gleichzeitig deuten publizierte Ergebnisse darauf hin, dass der Polaritätsverlust epithelialer Zellen sowohl eine tumorinitiierende als auch eine progressionsfördernde Wirkung ausüben können. Welche Polaritätsproteine jedoch maßgeblich an der Lebertumorentstehung beteiligt sind und wie die Dysregulation dieser Faktoren die Tumorentstehung beeinflusst, ist bisher kaum unterricht.

Zur Identifikation relevanter Polaritätsfaktoren im hepatozellulären Karzinom (HCC) wurden hoch-dimensionale Expressionsdaten primärer humaner HCCs und des umgebenden gesunden Lebergewebes miteinander verglichen. Hierbei korrelierte die Überexpression des basolateralen Proteins *Scribble* (Scrib) signifikant mit einem schlechteren Überleben und frühen Tumorrezidiv von HCC-Patienten. Neben der Scrib-Überexpression, bedingt durch die Amplifikation des Scribble Gens auf Chromosom 8q24.2, ist ebenfalls ein Verlust der membranären Lokalisation sowie eine zytoplasmatische Anreicherung von Scrib in HCC-Geweben und Tumorzellen zu beobachten. Um die biologische Wirkung der zytoplasmatischen Scrib-Anreicherung zu analysieren, wurden in der HCC-Zelllinie HepG2 wildtypisches Scrib ($Scrib^{WT}$ mit Membranbindung) und mutiertes Scrib ($Scrib^{P305L}$ mit erzwungener zytoplasmatischer Anreicherung) stabil exprimiert. *In vitro* reduzierte zytoplasmatisches $Scrib^{P305L}$ die Bildung des kanalikulären Netzwerks, was auf eine gestörte Zellpolarität hinweist, und

reduziert Zellproliferation. *In vivo* induzierte die Koexpression von Scrib^{P305L} und des Onkogens c-MYC mittels hydrodynamischer Injektion eine erhöhte Lebertumorbildung im Vergleich zu Mäusen mit Scrib^{WT}/c-MYC Koexpression. Vor allem induziert Scrib^{P305L} die HCC-Zellinvasivität, die Reorganisation von Aktinfilamenten und die Überexpression von motogen-wirkenden Rho-GTPasen. Vergleichende Analysen auf zellulären Signalwegen zeigen eine Aktivierung des AKT-Signalweges in Scrib^{P305L}-exprimierenden Zellen, was sich durch eine erhöhte Destabilisierung der AKT-Regulatoren *Leucin-rich Repeat-Protein-Phosphatase 1* (PHLPP1) und *Phosphatase and Tensin-Homolog* (PTEN) erklärt. Mit Hilfe von Transkriptomanalysen konnten Scrib^{P305L}-abhängige Signaturen identifiziert werden, welche mit Zellmotilität, Epithelial-mesenchymale Transition (EMT) und dem Remodelling der Extrazellularmatrix (EZM) assoziiert sind. Unter diesen Scrib^{P305L}-abhängigen Genen befindet sich *Secreted Protein Acidic and Rich in Cysteine* (SPARC), welches die Invasivität von HCC Zellen signifikant erhöht und durch die AP-1 Transkriptionsfaktoruntereinheiten ATF2 und JunB positiv reguliert wird. In humanen Geweben konnte der Zusammenhang zwischen zytoplasmatischem Scrib, der Phosphorylierung von AKT und ATF2 als auch dem Verlust von E-Cadherin als EMT-Marker bestätigt werden. Ferner konnte eine signifikante Anreicherung von Scrib^{P305L}-abhängigen Signaturgenen in HCC-Patienten mit schlechter Prognose gezeigt werden.

Zusammenfassend zeigt diese Studie, dass die Überexpression und die zytoplasmatische Anreicherung des Zellpolaritätsfaktors Scrib die HCC-Entwicklung und die Tumorprogression durch die Induktion bestimmter molekularer Mechanismen unterstützt. Diese Mechanismen umfassen die Aktivierung der AKT-Signalkaskade und die Stimulation von AP1-Zielgenen, welche für den Migrationsphänotyp von HCC-Zellen von zentraler Bedeutung sind.

CONTENTS

COMMON ABBREVIATIONS

ATF2	activating transcription factor 2
AP1	activator protein
AJ	adherence junction
APS	ammonium persulfate
AMOT	Angiomotin
aPKC	atypical protein kinase C
BSA	bovine serum albumin
CIAP	calf intestinal alkaline phosphatase
CEACAM1	carcinoembryonic antigen-related cell adhesion
ChIP	chromatin Immunoprecipitation
CoIP	Co-Immunoprecipitation
CGH	comparative genomic hybridization
CTGF	connective tissue growth factor
CRB	Crumbs
CHX	cycloheximide
CMV	cytomegalovirus
DMSO	dimethyl sulfoxide
Dlg	discs large
EF1α	elongation factor-1 alpha
ELISA	enzyme-linked immunosorbent assay
EPP	epithelial polarity program
EMT	epithelial-mesenchymal transition
EDTA	ethylenediaminetetraacetic acid
ECM	extracellular matrix
FRMD6	FERM domain-containing protein 6
F-actin	filamentous actin
GSEA	gene set enrichment analysis
G418	Geneticin
GFP	green fluorescent protein

GAP	GTPase activating protein
GEF	guanine nucleotide exchange factor
HCV	hepatitis C virus
HCC	hepatocellular carcinoma
HRP	horseradish peroxidase
HPV	human papillomavirus
HCl	hydrochloric acid
HDTV	hydrodynamic tail-vein
IF	immunofluorescence
IHC	immunohistochemistry
IRES	internal ribosome entry site
IR	inverted repeats
Kibra	kidney and brain expressed protein
Lats1	large tumor suppressor kinase 1
Lgl	lethal giant larvae
PHLPP1	leucine rich repeat protein phosphatase 1
LRR	leucine-rich repeat
LB	Luria-Bertani
Mst1/2	macrophage stimulating 1/2
MMPs	matrix metalloproteinases
MCAM	melanoma cell adhesion molecule
MRP2	multidrug resistance-associated protein 2
NF2	neurofibromin 2
NES	normalized enrichment score
PATJ	PALS1-associated tight junction protein
PFA	paraformaldehyde
Par6	partitioning defective-6
DAB	peroxidase substrate
PMSF	phenylmethylsulfonyl fluoride
PTEN	phosphatase and tensin homolog
PBS	phosphate-buffered saline

PPxY	Proline-Proline-x–Tyrosine
PALS1	protein associated with Lin-7 1
PKC	protein kinase C
Par3	proteins partitioning defective-3
PDK	pyruvate dehydrogenase kinase
S100A10	S100 calcium binding protein A10
Scrib	scribbled planar cell polarity protein
SPARC	secreted protein acidic and cysteine rich
qPCR	semi-quantitative polymerase chain reaction
STAT3	signal transducer and activator of transcription 3
SB	sleeping beauty transposon
siRNA	small interfering RNA
NaCl	sodium chloride
TIAM1	T-Cell lymphoma invasion and metastasis 1
3D	the three-dimension
TJ	tight junction
TIMP	TIMP metallopeptidase inhibitor
TGF-β	transforming growth factor beta
Tris	Tris-hydroxymethyl-aminomethane
WB	western Immunoblotting
WWTR1, synonyms: TAZ	WW domain containing transcription regulator 1
YAP	yes-associated protein
ZEB	zinc finger E-box binding homeobox

FIGURE INDEX

TABLE INDEX

1 INTRODUCTION

1.1 Liver and Hepatocellular carcinoma (HCC)

1.1.1 Physiology of the liver

The liver has very important functions such as secretion of bile acid and salt, metabolism (anabolic and catabolic processes) of nutrients, as well as detoxification of toxic compounds [1]. The physiological function of the liver is mediated by different cell types. The parenchymal cells of the liver and metabolically active cells are hepatocytes (about 60% of all cells); while non-parenchymal cells in the liver include *liver sinusoidal endothelial cells* (LSECs), Kupffer cells and stellate cells. LSECs separate hepatocytes from blood stream and facilitate the so-called porto-central blood flow [1]. Kupffer cells are localized near the LSECs in the sinusoids and act as central regulators of immune responses in case of infections. Stellate cells are located in the *Space of Disse* between hepatocytes and LSECs and represent the 'store-house' for vitamin A. In addition， they produce *extracellular matrix* (ECM) material in case of liver damage [2].

The liver exhibits a specific “plate-like” spatial architecture, with layers of hepatocytes in between sinusoidal spaces (Figure 4A). The plasma membrane of hepatocyte forms a branching network of “*bile canaliculi*”, which is the place for the secretion of bile components [3]. The liver has a unique blood vessel system, in which 75% of the liver blood supply comes from the nutrient-rich venous arm, while hepatic arteries contribute with 25% of oxygenated blood [4]. Highly fenestrated LSECs allow a permanent contact of hepatocytes with the blood stream, which allows a highly efficient transportation between hepatocytes and blood vessels [5].

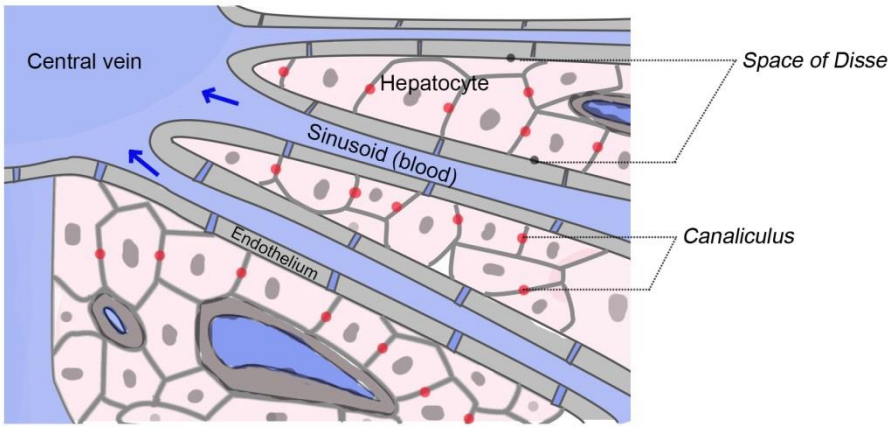

Figure 1: Liver lobe near the central area. Scheme shows the liver specific "plate-like" structure near the central area of a hepatic lobule. Dark blue arrow illustrates the direction of blood flow from the portal triad to the central vein. Red dots show the *bile canaliculus* network between two adjacent hepatocytes. Figure modified from "The two epithelial cell types in the liver" [6].

1.1.2 Epidemiology and Etiology of HCC

Hepatocellular carcinoma (HCC) is the most common primary malignant tumor of the liver. Worldwide, HCC is the fifth most common cancer type in men (7.9% of cancers) and seventh most common in women (6.5% of cancers) [7]. Its incidence is highest in Africa and Eastern Asia with more than 80% of all new HCC cases. In contrast, Northern Europe and United States have a lower HCC incidence with less than 5.0 per 100,000 individuals. However recent studies illustrated decreased HCC incidence in developing countries and an elevated number of cases in developed and industrialized countries [7]. The reasons for this phenomenon are changes in the frequency of risk factors in the respective population (e.g. viral infections and virus-independent liver diseases; see below). Compared to other malignant tumors, HCC is the third leading cause of cancer-related death and the 1-year overall survival rate is below 50% [8].

Hepatitis B virus (HBV)/*hepatitis C virus* (HCV) infections are major risk factors for HCC development [9]. About 5% of all people worldwide (around 75% in Asia) exhibit a chronic HBV infection. There is evidence showing the mechanistic connection between chronic HBV infection and cancer development, and HBV is considered to be causative for more than 50% of HCCs [7]. In contrast, 30% of the global HCC cases are due to chronic HCV infection. Compared to HBV, HCV is leading to a higher percentage of chronic hepatitis (80%) and liver cirrhosis development

(20%) [10]. In countries with low HBV/HCV prevalence such as the United States and Germany, alcohol abuse is one key etiological risk factor that may lead to *alcohol-induced liver disease* (ALD) and HCC [11]. In addition, *nonalcoholic fatty liver disease* (NAFLD) and the *nonalcoholic steatohepatitis* (NASH) represent further important risk factors for the development of HCC. NAFLD and NASH may progress to liver cirrhosis in about 5% and eventually tumor initiation. Although the relative numbers of HCCs derived from NAFLD is low (about 0.5%), this etiology is getting more relevant because of the high prevalence of obesity and diabetes in industrialized countries [12]. In addition, autoimmune disorders, cholestatic disorders, inherited disorders (e.g. hemochromatosis) and aflatoxin exposure represent further risk factors of hepatocarcinogenesis.

1.1.3 Pathogenesis of HCC

So far it is not yet fully understood how HCC progresses from damaged hepatocytes to advanced tumors. However, compared to other solid cancers, HCC has some specific histomorphological characteristics, which include the step-wise progression from normal hepatocytes to well-differentiated and premalignant lesions to poorly differentiated and malignantly transformed HCC cells [13]. Another important feature of hepatocarcinogenesis is the formation of multiple tumors, which might arise from independent tumor initiating events or satellite nodules due to intrahepatic metastasis. Especially intrahepatic metastasis is considered to be more aggressive resulting in poor patient prognosis [14]. In addition, HCC shows aberrant vascularization, which further supports the aggressiveness of tumors [15].

With regard to molecular pathogenesis, the accumulation of genomic alterations plays an important role in the development and progression of HCC. Classification approaches based on transcriptome analysis and sequencing data revealed a clear association between distinct genomic alteration patterns with biological and clinical features of HCCs [16]. For example, a subgroup of HCCs that was characterized by high tumor invasiveness, showed higher HBV copy numbers, mutations of the tumor-suppressor gene *TP53* mutation, *phosphoinositide-3-kinase* (PI3K)/AKT activation, and rare *PI3K catalytic alpha* (PIK3CA) mutations. Another subgroup with intrahepatic metastasis associated with reduced expression of E-cadherin and activation of the

wingless (Wnt) signaling pathway [16]. In addition, chromosome instability and dysregulation of DNA methylation have also been described to be involved in the pathogenesis of HCC [17, 18].

The tumor microenvironment is another important parameter affecting HCC progression. During liver fibrosis and cirrhosis under continuous inflammation, fibrotic stromal cells (so-called myofibroblasts) increase the production of secreted factors such as urokinase and matrix metalloproteinases (MMPs), which directly affect ECM composition. On the other hand, malignantly-transformed tumor cells gain properties of mesenchymal cells, with an abnormal production of these secreted factors, which leads to a degradation of basal lamina and increased invasion/metastasis of tumor cells [19]. In addition, cytokines and chemokines secreted by non-parenchymal cells, such as *tumor necrosis factor* (TNF), *interleukin-6* (IL-6), *transforming growth factor* (TGF), accelerate the process of liver fibrosis and are critical for the induction of HCC invasiveness [2].

1.1.4 Treatment for HCC

So far, surgical resection followed by liver transplantation, which improves the five-year survival from 15.2% to 77.2%, represents the only curative treatment for HCC patients. However, the treatment is limited to patients with early tumor stages (according to the TNM staging system) and good residual liver function (Child-Pugh score). Surgical resection and liver transplantation do not improve prognosis of late-stage patients with multiple nodules (>3), metastasis or severe liver dysfunction due to cirrhosis [20]. For patients with intermediate or advanced tumor stages, only palliative treatment can be offered. HCC must be considered as a chemoresistant tumor since neither doxorubicin alone nor combinations of doxorubicin, cisplatin, interferon and 5-fluorouracil or any other clinically established cytotoxic substances significantly improve patient's survival [21].

Some other therapeutic approaches have been developed for HCC patients with un-respectable lesions. For example, *transarterial chemoembolization* (TACE) treatment was established due to the aberrant vascularization of HCC [10]. TACE combines inhibition of tumor blood supply with regional delivery of chemotherapy, which shows promising effects on tumor regression and is used for intermediate-stage patients and down-staging treatment for surgical resection [22]. In addition, the small tyrosine protein kinase inhibitor Sorafenib targets multiple receptors regulating pathway in tumor cells and endothelial cells including *vascular endothelial growth*

factor receptor (VEGFR) and *platelet-derived growth factor receptor* (PDGFR). By this, Sorafenib not only affects tumor cell biology but also inhibits angiogenesis in a multi-modal manner. Although, first results illustrated that Sorafenib increase the overall survival of HCC patients about 3 months [23], a recent randomized phase III study of HCC patients (n=1,114) after surgical resection or ablation demonstrated that Sorafenib treatment did not significantly improve patient overall and recurrence-free survivals [24]. Thus, the beneficial effects of Sorafenib for HCC patients are controversially discussed.

Basic research and clinical trials are still ongoing to identify novel and druggable therapeutic targets, which may improve HCC patient's situation. For example, the PI3K/AKT pathway and *mechanistic target of rapamycin* (mTOR) are activated in HCC patients and mTOR inhibitors are currently used in clinical trials for HCC patients after surgical resection or TACE treatment [25]. This pathway is of special relevance since it has been shown that a number of oncogenic pathways and cellular mechanisms may activate the PI3K/AKT signaling axis [26]. Therefore, a deeper understanding of the underlying molecular mechanisms may help to identify HCC patients that may benefit from specific PI3K/AKT-directed inhibition approaches.

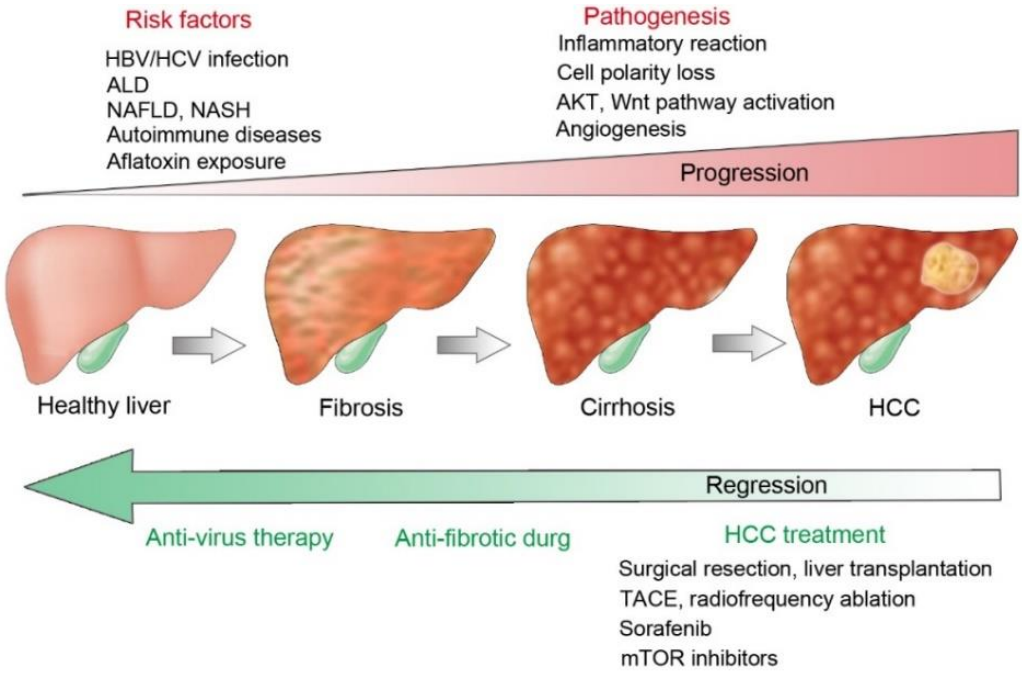

Figure 2: HCC development and current treatment options. The scheme illustrates the process of liver cancer development and progression. Risk factors that promote the progression from chronic liver diseases to HCC are summarized. Most relevant risk factors and pathogenenic mechanisms are listed. Therapeutic approaches for early/progressed HCC are mentioned next to the green arrow. Figure modified according to "Natural history of chronic liver disease" [2].

1.2 Epithelial cell polarity

1.2.1 Cell polarity is important for epithelial cell functionality

A high degree of cell polarity is a basic feature of many epithelial cells. The most important characteristic of epithelial cell polarity is the partitioning of plasma membrane into apical, lateral and basal domains. The apical domain refers to the membrane surface facing to cavities of organs. The lateral domain keeps close connection and cell-cell contact between adjacent cells, while the basal domain has direct contact with ECM or the basal lamina [27]. Cell polarity and membrane segregation are essential for epithelial cells to carry out their biological functions such as directional transport (absorption and secretion) of nutrients and salt between the extracellular environment and tissues. Intracellularly, it facilitates the molecular trafficking between organelles, e.g. from endoplasmic reticulum (ER) to the Golgi complex. In addition, cell polarity plays an essential role in keeping cell morphology, which is essential in different biological events, such as differentiation, migration and epithelial to mesenchymal transition (EMT) [28].

The establishment of cell polarity has been studied in a variety of cell types under different physiological and pathological conditions. Spatial orientation was first described during embryogenesis and tissue development, which is characterized in the following steps: a) initial appearance of cell-cell contact, b) assembly of cell junctions and c) establishment of epithelial cell morphology [29]. In these steps, cell junction-associated molecules are of special importance for the formation of cell polarity. For example, *tight junctions* (TJs), which mediate strong cell-cell contact between adjacent cells, are important in the initiation and maintenance of epithelial cell polarity and define the boundary between apical and lateral domains. TJs include transmembrane proteins (e.g. occludin and claudin), *junctional adhesion molecules* (JAM, e.g. JAM-A, JAM-B) and peripheral membrane proteins (e.g. zonula occludens-1) attached to cytoskeleton [30]. In addition to TJs, *adherens junctions* (AJs) have also been found to be indispensable in the maintenance of cell polarity. The transmembrane protein E-cadherin is the core component of AJs, which allows a tight physical interaction of neighboring cells *via* the formation of homodimer and binding of extracellular domains. In addition, E-cadherin forms a complex with intracellular catenin proteins, which on one hand mediate the interaction with the actin cytoskeleton and on the other hand affect signal transduction [31].

Establishment and maintenance of cell polarity and junctional structures are a fundamental characteristic of epithelial cells to carry out their respective functions under various biological conditions. However, in addition to the core proteins directly involved in the assembly of TJ and AJ, other proteins and lipids, which are associated with cell-cell junctions, also participate in the process of epithelial polarization. A considerable number of factors has emerged to a complex network, which include *epithelial polarity program* (EPP) polarity protein complexes, Rho GTPases and polarity lipids [28].

1.2.2 Key players of EPP: Polarity complexes

Polarity complexes refer to groups of proteins that are found in close proximity to certain polarity domains. These protein complexes are associated with the core proteins of cell junctions, and play a central role in EPP. So far, three polarity complexes have been described: the Crumbs complex, the Par complex and the Scrib complex. The Crumbs complex consists of transmembrane *Crumbs* (CRB), *protein associated with Lin-7 1* (PALS1) and *PALS1-associated tight junction protein* (PATJ). The Crumbs complex is located at apical cellular domains, which directly affect the assembly of TJ structures [32]. The Par complex comprises the proteins *partitioning defective-3* (Par3, synonym: Baz), *partitioning defective-6* (Par6) and *atypical protein kinase C* (aPKC). It is located near subapical cell domains where it interacts with core proteins of both TJ and AJ [33]. The Scrib complex is composed of *scribbled planar cell polarity protein* (Scrib), *discs large* (Dlg) and *lethal giant larvae* (Lgl, LLGL1 in human). This complex defines the basolateral domain of epithelial cells and is critically involved in the formation of AJ, probably in an E-cadherin-dependent manner [33] (Figure 3).

Although different polarity complexes are defined by their specific localization at the plasma membrane, they are not mechanistically separated from each other. Instead, polarity proteins from different complexes frequently communicate with each other in terms of an active protein exchange. These interactions result in either the recruitment of different proteins in the same complex or the competitive integration of individual proteins in different complexes. This mechanism of communication between polarity complexes is defined as “mutual exclusion” [33]. For example, the Par complex constituent aPKC is integrated in the apical Crumbs complex at early stages of Drosophila embryogenesis. In later developmental stages, it is recruited by Par3 to

the Par complex near the subapical domain [34]. In contrast, Par6, an adaptor protein for aPKC, binds and mediates the inactivation of Lgl, which is a major component of Scrib complex, *via* the phosphorylation by aPKC. Inactivated/Phosphorylated Lgl is then excluded from the subapical domain [35]; see Figure 3. Thus, through interactive communication with each other, cell polarity complexes represent highly dynamic modules that can adjust the cellular shape and functionality according to extracellular and endogenous requirements.

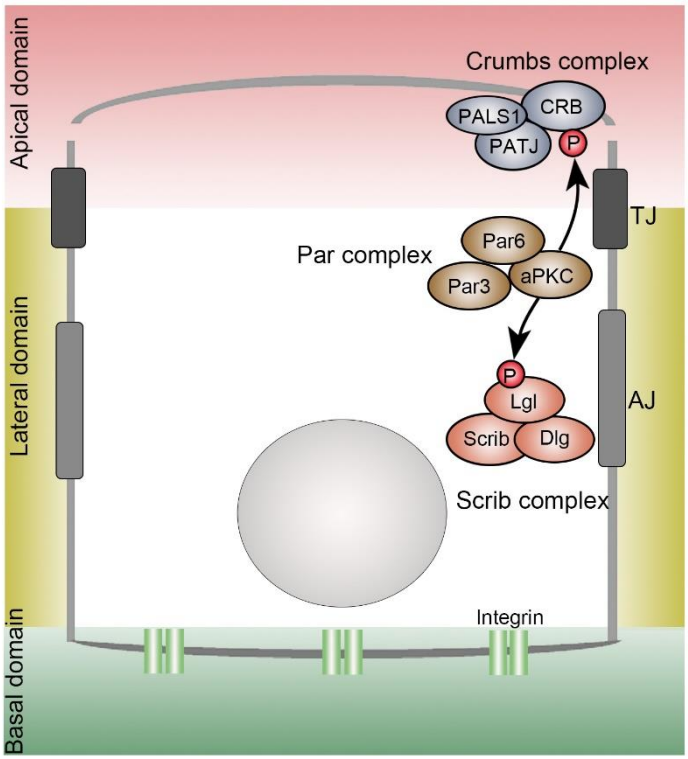

Figure 3: Polarity complexes and spatial membrane organization of epithelial cells. The scheme shows the three main polarity complexes in an epithelial cell. The specific membranous domains are indicated by different colors. The apical domain, lateral domain and basal domain of this epithelial cell are shown in dark red, yellow and green, respectively. TJ and AJ are located at the lateral domain. Integrin connects the basal domain with the underlying extracellular matrix. The arrows indicate the phosphorylation of CRB (Crumbs complex) and Lgl (Scrib complex) by aPKC (Par complex), illustrating the dynamic interaction of proteins with polarity complexes.

1.2.3 Crosstalk between Rho GTPases and polarity complexes

In addition to the polarity complexes, Rho GTPases are also central regulators of the EPP system. Rho GTPases belong to small G proteins of the Ras family, which bind to GTP or GDP and catalyze the hydrolysis of GTP [36]. During the formation and maintenance of cell polarity, Rho GTPases modulate epithelial morphology through the re-organization of the cellular cytoskeleton. The Rho GTPases family consists of about 20 different GTPases, including RhoA, Rac1 and CDC42. Importantly, different GTPases carry out their functions at specific subcellular regions [37]. For example, RhoA interacts with actin-myosin filaments in the cytoplasm, which affects

membrane retraction during different biological process, e.g. cytokinesis [38]. CDC42 and Rac1 are both found at the leading edge of migrating cells, where they regulate actin filament polarization and induce lamellipodia formation [39]. The specific subcellular localization of Rho GTPases suggests that they may have functional relevance in the regulation of polarity complexes.

Indeed, Rho GTPases and cell polarity proteins are frequently interacting under different physiological and pathological conditions. For example, in the process of EMT, CDC42 binds to Par6 and facilitates the activity of aPKC-Par6 complex [39]. In addition, the aPKC-Par6 complex activates Rac1 *via* the RAC-specific *guanine nucleotide exchange factor* (GEF) *T-cell lymphoma invasion and metastasis 1* (TIAM1) [40]. In addition, aPKC also activates p190A Rho *GTPase activating protein* (GAP), which switches off the activity of RhoA [39]. With the help of the Par complex, CDC42 induces the activity of Rac1 at lamellipodia, and inhibits the activity of RhoA in the cytosol. As a result, the Par complex promotes cell motility in the process of EMT *via* the modulation of different Rho GTPases [39]. Thus, cell polarity complexes communicate with Rho GTPases in the fine adjustment of cell cytoskeleton dynamics, which is essential in the modulation of cell morphology and motility.

1.2.4 Disturbance of cell polarity in cancer development

Loss of cell polarity is frequently found at early stages of epithelial tumor formation. For example, disruption of epithelial sheets, aberrant multilayering and loss of physiological lumen are typical features in early tumor development. However, disturbance of cell polarity is more than a consequence of tumor development [27]. This conclusion is supported by the fact that polarity proteins in different tumor types are frequently altered by genomic amplifications, deletions and mutations. For example, Dlg, Lgl and PATJ are downregulated, while Par6 is amplified and overexpressed in different cancer types [33]. Nevertheless, for some polarity proteins (e.g. Scrib, aPKC and Par3) both overexpression and downregulation have been described in several tumors suggesting that different mechanisms might be involved in the development of cancers [33, 41, 42].

Cell division/proliferation can be affected by disturbed cell polarity. During asymmetric cell division, some important proteins and RNAs are segregated into daughter cells, which determine

the fate of daughter cells in differentiation [43]. This process of asymmetric localization is dynamically modulated by the polarity proteins, e.g. aPKC and Par-proteins *via* phosphorylation and mutual exclusion. Mutation and dysfunction of these polarity proteins lead to dysfunctional asymmetric cell division. As a result, cells continue with symmetric divisions without cell cycle termination, which may give rise to tumors [43]. In addition to the disturbed asymmetric division, pathways that directly regulate mitosis such as the Hippo pathway can be activated or inactivated by disturbed cell polarity in cancer development [33].

Cell invasion/metastasis is also affected by disturbed cell polarity during tumor progression. Loss and reestablishment of cell polarity is necessary for tumor cells to leave the original localization and to achieve metastatic properties. In this context, EMT, which is highly relevant during embryogenesis, is of special importance for initial steps in tumor cell dissemination dissemination [44]. The process of EMT is directly connected with cell polarity, since the loss of the AJ molecule E-cadherin, as well as overexpression of N-cadherin and vimentin is regarded as important characteristics of EMT [19]. In addition to E-cadherin, Rho GTPases also play a central role in EMT *via* the interaction with cell polarity proteins. As described earlier, important positive regulator of EMT (CDC42 and RAC) are activated by polarity protein Par6 and aPKC (see chapter 1.2.3). Indeed, Par6 overexpression has been found to induce tumor metastasis in breast cancer *via* the activation of EMT-associated signaling pathway [33, 45].

Therefore, genetic alterations as well as abnormal localization of polarity proteins are associated with tumor progression *via* cell dedifferentiation, cell proliferation, EMT and early metastasis [33].

1.2.5 Disturbance of cell polarity affects oncogenic signaling pathways

Recent studies have focused on the molecular mechanisms how dysregulation of the EPP system affects tumorigenesis. Cell polarity proteins integrate extracellular information into intracellular pathway responses and a dysregulation of cell polarity proteins is supposed to affect these tumor-relevant downstream signaling pathways. Indeed, several oncogenic pathways have been identified to be modulated by EPP components. Here, mutations of single polarity proteins or disruptions of polarity complexes accounts for the activation of intracellular oncogenic pathways

[33]. Among these, the Hippo/*yes-associated protein* (YAP) and Wnt pathways are two examples, which affect tumor development and progression in different tissues.

The Hippo/YAP pathway is essential for organ size control and HCC development [46]. First evidences already illustrated that the apical membrane protein *FERM domain-containing protein 6* (FRMD6) regulates the Hippo/YAP pathway. Specifically, FRMD6 forms a complex with two other apical membrane proteins, *kidney and brain expressed protein* (Kibra) and *neurofibromin 2* (NF2, synonyms: Merlin). The FRMD6/NF2/Kibra complex induces the phosphorylation of Hippo pathway component *large tumor suppressor kinase 1* (Lats1), which results in the dephosphorylation and degradation of the transcriptional co-activator YAP in the cytoplasm. Thus, the apical complex FRMD6/NF2/Kibra acts as a tumor suppressor *via* the negative regulation of oncogenic YAP activity [47, 48]. In addition, other EPP components have also been identified as upstream modulators of the Hippo/YAP pathway. For example, *Angiomotin* (AMOT), which is usually localized in close proximity to apical Crumbs complex and which contains *Proline-Proline-x–Tyrosine* (PPxY) motifs, binds directly to the WW domain of YAP and its homolog *WW domain containing transcription regulator 1* (WWTR1, synonyms: TAZ). The interaction between AMOT and YAP/TAZ fosters the localization of YAP/TAZ to TJs, which is associated with their inactivation [49]. Besides this, independent studies have shown the regulatory effect on YAP/TAZ by the basolateral Scrib complex, and the apical Crumbs complexes [50, 51].

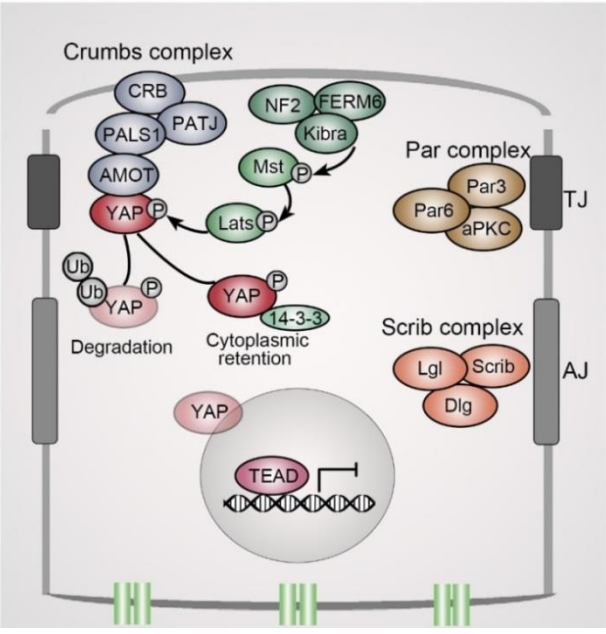

Figure 4: Known EPP regulators of Hippo/YAP pathway. Scheme shows the apical polarity complex NF2/FERM6/Kibra that mediates the phosphorylation of *macrophage stimulating 1/2* (Mst1/2), which is a major component of Hippo pathway. Phosphorylation of Mst1/2 turns on the Hippo kinase cassette, including phosphorylation of Lats1/2 and YAP. Except for the NF2/FERM6/Kibra complex, AMOT directly binds to YAP, leading to the cytoplasmic retention of YAP near TJs. The interaction between AMOT and YAP may also induce phosphorylation of YAP by the Hippo pathway components. Phosphorylated YAP is degraded by ubiquitination or kept in the cytoplasm by 14-3-3 protein binding. In this case, YAP cannot bind to its transcriptional co-activator TEAD, leading to the repression of YAP-target genes.

Wnt pathway is another example for an EPP-relevant signaling pathway, which plays an essential role in defining cell fate determination (canonical pathway) and regulation of cell movement (non-canonical pathway) [52]. The canonical Wnt pathway depends on the AJ-associated protein β-catenin, which activity is inhibited after binding to a protein complex consisting of *adenomatosis polyposis coli* (APC), *glycogen synthase kinase 3* (GSK3) and Axin [53]. Followed by Wnt ligand binding to the receptors *Frizzled* (Fz) and *low density lipoprotein receptor-related protein 5/6* (LRP5/6), the APC/GSK3/Axin complex is recruited to the plasma membrane by LRP5/6, which induces the translocation of β-catenin into the nucleus [53]. Nuclear β-catenin activates transcriptional factors *T cell-specific transcription factor* (TCF) and target genes involved in cell fate determination and oncogenesis [53]. Interestingly, Wnt signaling also activates a non-canonical pathway independent on β-catenin, which regulates cell morphology and movement *via* Rho GTPases [52]. Wnt stimulation activates a protein complex consisting of *Dishevelled* (Dsh) and *Dishevelled associated activator of morphogenesis 1* (Daam1), which further increase the activity of RhoA in the rearrangement of actin filaments [54].

It is worth mentioning that except of the Hippo/YAP and Wnt pathways, other signaling pathways (e.g. TGF-β) are also regulated by different cell polarity components [44]. Thus, EPP components play an important role in the transduction of extracellular signal, and regulation of intracellular signaling pathways related to cell division, differentiation and migration; while disruption of polarity complexes may lead to dysregulation of these pathways, which promotes cancer development *via* cell proliferation, dedifferentiation and metastasis.

1.3 Hepatocellular polarity and HCC development

1.3.1 Liver function depends on hepatocellular polarization

The important functions are carried out by the major liver cell type, the hepatocyte [1]. The physiological function of the hepatocyte strictly depends on the establishment and maintenance of hepatocellular polarity, including the formation of the well-defined apical, lateral and basal domains comparable to other epithelial cell types such as small intestinal cells [6]. However, hepatocytes establish a specific polarity domain composition, which is important for carrying out their functions [6]. For example, adjacent hepatocytes orient their apical domains towards each other to form small lumens, which further branch in 3-dimensional canalicular structures for bile secretion (Figure 5) [3]. Similar to the apical site, hepatocytes form extensions and protrusions at the basal domain in close proximity to the *Space of Disse* and LSECs, which is a requirement for a highly efficient transportation between hepatocytes and blood vessels [5]. In this way, maintenance of hepatocellular polarity supports the liver function under physiological conditions, whereas the disturbance of cell polarity can lead to dysfunction of liver and disease.

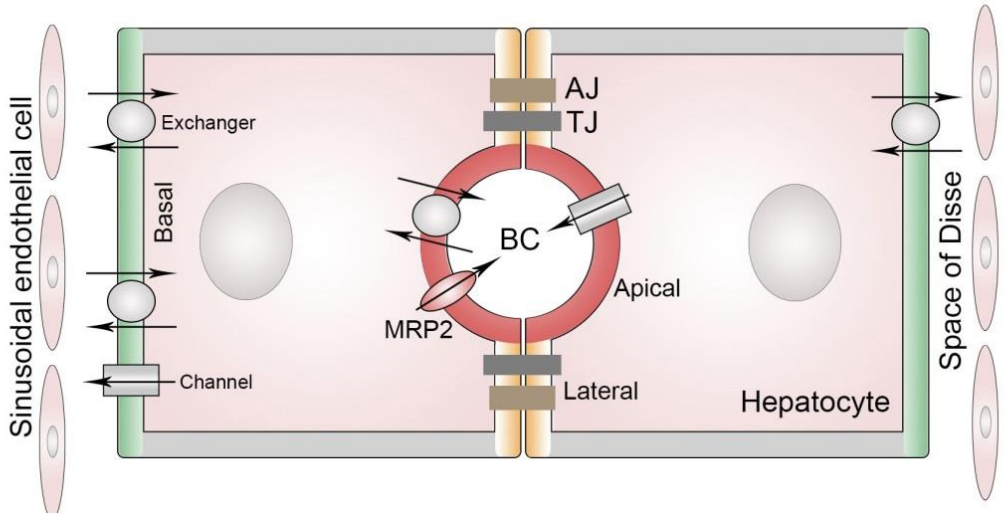

Figure 5: Hepatocellular polarity. Scheme shows cell-cell junctions, which facilitate the cell-cell contact between two adjacent hepatocytes. The red membrane indicates the apical lumen. Iron pumps and transporters, e.g. MRP2 are expressed at this domain of hepatocyte, which are important for bile secretion. The yellow membrane indicates the lateral domain of hepatocytes, where AJs and TJs are located. The green colored membrane represents the basal domain in direct contact with the *Space of Disse*. BC: bile *canaliculus*.

1.3.2 Disturbance of hepatocellular polarity in early HCC development

Disturbance of cell polarity is considered to be an early event in epithelial tumor development [27]. In the liver, during liver fibrosis and cirrhosis, excessive matrix deposition reduces the cell contact with sinusoidal blood or neighboring hepatocytes, which eventually leads to regenerative nodules [6]. In HCC, the loss of hepatocellular polarity is detected in the early stage of hepatocarcinogenesis such as dysplastic nodules. The "plate-like" structures with clear porto-central architecture are replaced by pseudoglandular structures in neoplastic livers [55]. Furthermore, discontinued *canaliculi* formation with the mislocalization of *canalicular* proteins (Na^+-K^+ ATPase and alkaline phosphatase) are detectable in preneoplastic lesions [56]. Interestingly, the morphology of neoplastic hepatocytes have a high similarity with polypotent embryonic or hepatocytes after damage, which is also mirrored by the regression of cellular polarization during liver regeneration [6]. These observations suggest that the disturbance of hepatocellular polarity happens at early steps in tumorigenesis, which may play a specific role in the pathogenesis of liver cancer.

The development HCC is associated with the dysregulation of cell polarity factors and relevant proteins such as *liver kinase B1* (LKB1) and *inositol polyphosphate phosphatase-like 1* (INPPL1), for which a direct impact on hepatocarcinogenesis have been discussed [57]. The kinases LKB1 and its effector *5'-AMP-activated protein kinase* (AMPK) play an important role in the maintenance of cell polarity *via* direct regulation on polarity protein Par1, and modulation on other polarity components (Scrib and Crumbs complexes) [58]. Mutations of LKB1 and AMPK disturb hepatocellular polarity and induce tumor formation in the liver in mouse model [57]. In addition to LKB1, the AJ protein E-cadherin also shows important function in HCC development. Loss of membranous E-cadherin is associated with an EMT phenotype and intrahepatic metastasis in HCC patients [16].

In summary, loss of hepatocellular polarity is an early event in liver tumor development. Several polarity proteins and polarity-associated pathway have been connected with hepatocarcinogenesis [57]. However, if a general loss of cell polarity or a disturbance of a certain polarity complex is important for liver tumorigenesis remains unknown.

2 OBJECTIVES

Maintenance of cell polarity is considered to facilitate tumor-suppressor functions in epithelial cells. Disturbance of the spatial epithelial cell organization leads to a loss of function and has been discussed to be involved in the initiation and progression of cancers. For the liver, a high degree of hepatocellular polarization is important to fulfill its biological functions, including deteoxification and bile production. So far, it is not fully understood if and how the spatial disturbance of hepatocellular polarization can promote liver carcinogenesis. It is also unknown which specific molecular mechanisms are induced by the dysregulation of cell polarity constituents. For these reasons, the objectives of this study are:

1. Identification of cell polarity-associated genes that are significantly dysregulated in human HCC samples in comparison to non-malignant liver tissues.

2. Defining the expression/localization of selected cell polarity proteins in HCC cells and tissues.

3. Establishment of an *in vitro* model for the functional und molecular characterization of the identified polarity proteins.

4. Confirming the *vivo* relevance of the identified polarity gene in liver tumor formation using a hydrodynamic gene delivery approach.

5. Identification of effector mechanisms induced by the dysregulation of the selected polarity proteins.

6. Corroboration of findings in an independent HCC sample cohort.

3 MATERIALS

3.1 Consumables

Consumables and plastic ware used in this study are listed in Table 1.

Table 1: Consumables

Substance	Company
Cell culture plates	TPP, Trasadingen, Switzerland
Coverslips and slides	Engelbrecht, Edermünde, Germany
Parafilm	Pechiney, Düsseldorf, Germany
Matrigel Matrix-coated Transwells	Corning, Wiesbaden, Germany
PCR 96 well plate	Applied Biosystems, Thermo Fisher Scientific, Langenselbold, Germany
PCR reaction tubes	Life science, Brand, Wertheim, Germany
Nitrocellulose membrane 0.4 µm	GE Healthcare, Freiburg, Germany
Cell scrapper	Corning
Whatman paper	GE Healthcare
Sterile vacuum-filter 0.22µm	Corning
Mr. Frosty™ Freezing Container	Thermo Fisher Scientific
Eppendorf tubes	Eppendorf, Hamburg, Germany
Precellys tubes	Bertin Technologies, Montigny-le-Bretonneux, France
Cryovials	Sigma-Aldrich, Taufkirchen, Germany

3.2 Equipment

Table 2: Equipment

Name	Company
12-Tube Magnet	Qiagen, Hilden, Germany
Agarose gel electrophoresis	Kreutz Reiskirchen, Germany
AlphaImager™ Gel Imaging System	Biozym Scientific, Hessisch Oldendorf, Germany
Laminar Flow Hood	Kojair Tech, Vilppula, Finland
Centrifuges (MIKRO 200 R)	M.S. Laboratories, Wiesloch, Germany
CO2 atmosphere	Sigma-Aldrich
FLUOstar Omega Microplate Reader	BMG Labtech, Ortenberg, Germany
Fume hood (Secuflow)	Waldner, Wangen, Germany
Immunofluorescence Microscope (CKX41)	Olympus, Eislingen, Germany
LI-COR Odyssey® Imaging System	LiCor Biosciences, Bad Homburg, Germany
Nanodrop Spectrometer (ND-1000)	Thermo Fisher Scientific
PH Meter (pH210)	Hanna Instruments, Vöhringen, Germany
PCR cycler (PTC-200)	Bio-Rad Laboratories, München, Germany
Rolling shaker (CAT RM5)	Neolab, Heidelberg, Germany
StepOne Plus	Thermo Fisher Scientific
Sonicator (S-4000)	Qsonica, Newton, USA
SDS-PAGE electrophoresis	Bio-Rad Laboratories
Thermomixer	Eppendorf
Western immunoblotting chambers	Bio-Rad Laboratories

3.3 Reagents

3.3.1 General reagents

General reagents including chemicals, transfection reagents, polymerase chain reaction (PCR) reagents etc. are listed in Table 3.

Table 3: Chemicals, transfection reagents and PCR reagents

Substance	Company
2-Mercaptoethanol	Roth, Karlsruhe, Germany
Acetic acid	Sigma-Aldrich
Agarose	Roth
Ammonium persulfate (APS)	Roth
Avidin and biotin Kit	Vector Laboratories, Burlingame, USA
ABsolute qPCR SYBR Green ROX Mix	Thermo Fisher Scientific
Bovine Serum Albumin (BSA)	Sigma-Aldrich
Bradford reagent	Sigma-Aldrich
Cycloheximide (CHX)	Sigma-Aldrich
10x Cell Lysis Buffer	Cell Signaling/New England Biolabs, Frankfurt, Germany
Dimethyl sulfoxide (DMSO)	Thermo Fisher Scientific
Dynabeads Protein G	Thermo Fisher Scientific
dNTP-Mix	Thermo Fisher Scientific
Peroxidase Substrate (DAB)	DAKO, Hamburg, Germany
Ethanol	Sigma-Aldrich
Ethylenediaminetetraacetic acid (EDTA)	Serva, Heidelberg, Germany
Fugene HD transfection reagent	Thermo Fisher Scientific
Formaldehyde (37%)	Merck, Darmstadt, Germany
Geneticin (G418)	Thermo Fisher Scientific
GeneRuler DNALadder Mix	Thermo Fisher Scientific
Glycine	Sigma-Aldrich
Hydrochloric acid (HCl)	Merck
4-(2-hydroxyethyl)-1-piperazineethanesulfonic acid (HEPES)	Roth
Horseradish peroxidase (HRP) system	DAKO
Igepal CA 6	Sigma-Aldrich
Isopropanol	Sigma-Aldrich
Rat-tail tendon collagen I	Roche, Mannheim, Germany

Lipofectamine® RNAiMAX	Life Technologies, Darmstadt, Germany
Magnesium chloride hexahydrate	Roth
Methanol	Sigma-Aldrich
Na-deoxycholate	Roth
Sodium chloride (NaCl)	Roth
Protease inhibitor	Serva, Heidelberg, Germany
Phosphotaseinhibitor PhosStop	Roche
PageRuler Prestained Protein Ladder	Thermo Fisher Scientific
Paraformaldehyde (PFA)	Merck
Phosphate-buffered saline (PBS)	GE Healthcare
Phenylmethylsulfonyl fluoride (PMSF)	Merck
REAL Hematoxylin	DAKO
Recombinant human SPARC	R&D Systems, Wiesbaden, Germany
Salmon sperm DNA	Thermo Fisher Scientific
Tetramethylethylenediamine	Roth
Tris-hydroxymethyl-aminomethane (Tris)	Roth
Triton x-100	Merck
Tween 20	Sigma-Aldrich
Trypsin/EDTA	PAA Laboratories, Cölbe, Germany
Wortmannin	Sigma-Aldrich

3.3.2 Solutions and buffers

Table 4: Solutions and buffers

Lysis Buffer (for Co-IP)		RIPA Buffer	
Tris-HCl pH 7.4	50 mM	NaCl	150 mM
Igepal CA 630 (NP40)	1%	SDS	0.1%
Na-deoxycholate	0.25%	Na-deoxycholate	0.5%
NaCl	150 mM	Igepal CA 630 (NP40)	1%
EDTA	1 mM	EDTA	5 mM
PMSF	1 mM	Tris (pH8.0)	50 mM
IP-Wasch Buffer		TE Buffer	
Tris (pH 8.5)	100 mM	Tris (pH 8.0)	70 mM
LiCl	500 mM	EDTA	1 mM
NP40	1%		
Na-deoxycholate	1%		
Talianides Buffer		4X SDS-PAGE loading buffer	
Tris (pH 8.0)	70 mM	TrisHCl (pH 6.8)	200 mM
EDTA	1 mM	DTT	400 mM
SDS	1.5%	SDS	8%
		Bromophenol blue	0.4%
		Glycerol	40%
Borate buffer		TBS Buffer	
Boric acid	100 mM	TrisHCl (pH 6.8)	50 mM
NaCl	75 mM	NaCl	150 mM
Sodium tetraborate	25 mM	Adjust the pH to 7.6	
Adjust the pH to 8.4			
Caspase Lysis Buffer		Caspase Assay Buffer	
TrisHCl (pH 7.4)	20 mM	HEPES (pH 7.5)	50 mM
NaCl	137 mM	NaCl	50 mM
Glycerin	10%	EDTA	10 mM
Triton X-100	1%	Glycerin	5%
EDTA	2 mM		

3.3.3 Enzymes

Restriction enzymes, DNA polymerase and transcriptase used for cloning and PCR reaction are shown in Table 5.

Table 5: Enzymes for cloning

Name	Company
DpnI restriction enzyme	New England Biolabs
EcoRI restriction enzyme	Thermo Fisher Scientific
Gateway® BP Clonase® II Enzyme mix	Thermo Fisher Scientific
Gateway® LR Clonase® II Enzyme mix	Thermo Fisher Scientific
Phusion® High-Fidelity DNA Polymerase	New England Biolabs
Q5® High-Fidelity DNA Polymerase	New England Biolabs
REDTaq® ReadyMix™ PCR Reaction Mix	Sigma-Aldrich
RevertAid H Minus Reverse Transcriptase	Thermo Fisher Scientific
T4 Polynucleotide (PNK) Kinase	New England Biolabs
T4 DNA Ligase	New England Biolabs
Calf intestinal alkaline phosphatase (CIAP)	Thermo Fisher Scientific

3.4 Assays and Kits

Table 6: Assays and Kits

Name	Company
NucleoSpin® Gel and PCR Clean-up kit	Macherey-Nagel, Düren, Germany
Plasmid Miniprep kit	Qiagen, Hilden, Germany
Plasmid Midprep kit	Promega, Mannheim, Germany
EndoFree Plasmid Maxiprep kit	Qiagen
NucleoSpin® RNA extraction kit	Macherey-Nagel
NE-PER Nuclear and Cytoplasmic Extraction kit	Thermo Fisher Scientific
Mem-PER Plus Membrane Protein Extraction Kit	Thermo Fisher Scientific
NucleoSpin® Gel and PCR Clean-up kit	Macherey-Nagel, Düren, Germany
SPARC Quantikine ELISA kit	R&D Systems, Wiesbaden, Germany
CellTiter-Blue® Assay	Promega
CellTox™ Green Cytotoxicity Assay	Promega
AP based DCS Detection Line system	DCS, Hamburg, Germany

3.5 Antibodies

Antibodies and concentrations used for protein biochemistry analyses are listed in Table 7.

Table 7: Antibodies

Antigen (clone)	Company	Concentrat	Application
ATF2 (20F1)	Cell signaling	0.5 µg/ml	WB
ATF2 (N-96)	Santa Cruz Biotechnology	3 µg	ChIP
Phospho-ATF2 Thr71	Cell signaling	0.5 µg/ml	WB and IHC
JunB (C37F9)	Cell signaling	3 µg	ChIP
Phospho-JunB Thr102/Thr104 (D3C6)	Cell signaling	0.5 µg/ml	WB
c-Jun (60A8)	Cell signaling	0.5 µg/ml	WB
Phospho-c-Jun Ser73	Cell signaling	0.5 µg/ml	WB
PTEN (138G6)	Cell signaling	1 µg/ml	WB
ß-Tubulin	BD Pharmingen	0.5 µg/ml	WB
Scribble (K-21)	Santa Cruz Biotechnology	0.67 µg/ml	WB and IF
Scribble	Sigma	5 µg/ml	IHC
Fascin	R&D	1 µg/ml	WB
PHLPP1	Bethyl	0.5 µg/ml	WB
E-cadherin	Epitomics	5 µg/ml	IF
N-cadherin	QED Bioscience	5 µg/ml	IF
AKT	Cell signaling	1 µg/ml	WB
Phospho-Akt Ser473	Cell signaling	1 µg/ml	WB
S6 Ribosomal protein (5G10)	Cell signaling	1 µg/ml	WB
Phospho-S6 Ribosomal protein Ser235/236	Cell signaling	1 µg/ml	WB
Na^+-K^+-ATPase	Cell signaling	1 µg/ml	WB
P38	Cell signaling	1 µg/ml	WB
Phospho-P38	Cell signaling	1 µg/ml	WB
SP1	Cell signaling	3 µg	ChIP
YAP	Cell signaling	1 µg/ml	WB
Phospho-YAP (Ser127)	Cell signaling	1 µg/ml	WB
GFP Tag	Proteintech	2 µg	IP
MCAM (ME-9F1)	Biolegend	5 µg/ml	IHC
MRP2 (R260)	Cell signaling	10 µg/ml	Sandwich culture IF
Cy™3 AffiniPure Donkey Anti-Rabbit	Jackson ImmunoResearch	3 µg/ml	IF
Alexa Fluor® 488 AffiniPure Donkey Anti-Goat	Jackson ImmunoResearch	7.5 µg/ml	IF

ChIP: Chromatin Immunoprecipitation, IHC: Immunohistochemistry, IP: Immunoprecipitation, IF: Immunofluorescence, WB: Western Immunoblotting.

3.6 Oligonucleotides

Primers for semi-quantitative polymerase chain reaction (qPCR) analysis were designed to span intronic regions of the respective genes. Primers were synthesized by Thermo Fisher Scientific and Apara-bioscience (Denzlingen, Germany).

3.6.1 Primers for qPCR

Table 8: qPCR primers

Gene	Accession Number	Forward primer (5´-3´)	Reverse primer (5´-3´)
SCRIB	NM_015356.4	AGGAAGACGCCGAAGAGGACTA	AGTGCGTCCTCTGCGAAATG
PTEN	NM_000314.6	AGTGGCGGAACTTGCAATC	GGTCCTGAATTGGAGGAA
PHLPP1	NM_194449.3	AATGCCCTGCGATCAGTC	CTTCATGTTCTCCAACTCAG
SPARC	NM_003118.3	GAAACTGTGGCAGAGGTGA	GGTTTCCTCTGCACCATCAT
FSCN1	NM_003088.3	CATCAAAGACTCCACAGGCAA	GAAGAAGTCCACAGGAGTGT
CEACAM1	NM_001712.4	GACCCAGTCACCTTGAATGT	ACGGTAATAGGTGTCTGAAG
S100A10	NM_002966.2	CCTGAGAGTACTCATGGAA	GGTCCAGGTCCTTCATTAT
TIMP1	NM_003254.2	CAATTCCGACCTCGTCATCA	ACGCTGGTATAAGGTGGTCT
TIMP2	NM_003255.4	TATCTCATTGCAGGAAAGGC	GAAGTCACAGAGGGTGATGT
JunB	NM_002229.2	CTACCACGACGACTCATACA	GCTCGGTTTCAGGAGTTTGT
ATF2	NM_001880.3	GAGGAGCCTTCTGTTGTAGA	GTGCAGTTTGTGCCAATGGT
CDH2	NM_001792.4	TGGCAGCTGGACTTGATCGAG	GACATCTGTCACTGTGATGACGG
MCAM	NM_006500.2	TGTGAGCTCAACTACCGGCT	CTCCACTTCCAGCCACACT
B2M	NM_004048.2	CACGTCATCCAGCAGAGAAT	TGCTGCTTACATGTCTCGAT

3.6.2 Primers for molecular cloning

Table 9: Cloning primers

Application	Name	Sequence (5'-3')
Amplification of hScrib for Gateway Donor vector	*Scrib forward*	GGGGACAAGTTTGTACAAAAAAGCAGGCTCCACCATGCTC AAGTGCATCCCGCTG
	Scrib reverse	GGGGACCACTTTGTACAAGAAAGCTGGGTTCTAGGAGGGC ACAGGGCCCAG
hScrib^{P305L} mutagenesis	*Scrib (mut-P305L) forward*	CTGCTGATGGCCCTGC**T**CCGCTCCCTGGGAAAGC
	Scrib (mut-P305L) reverse	GCTTTCCCAGGGAGCGG**A**GCAGGGCCATCAGCAG
Amplification of hScrib for cloning into the *pT3-EF1α* vector	*Scrib pT3 for*	tacACGCGTATGCTCAAGTGCATCCCGCTGT
	Scrib EcoRI pT3 rev	attGAATTCCTAGGAGGGCACAGGGCCCAGG

Bold and underlined letters indicate the mutation point.

3.6.3 Primers for Chromatin Immunoprecipitation (ChIP) analysis

Primers for ChIP analysis were designed to span an amplicon between 80-120 bp containing the transcription factor binding site. Control primers were designed to amplify downstream regions with no binding sites.

Table 10: ChIP primers

Name	Accession number	Sequence (5´-3´)
SPARC binding site 1 forward	ENSG00000113140	GTGGTACAAGTGGAGTTTGAGTG
SPARC binding site 1 reverse	ENSG00000113140	CAGGACTTACCACTGTACAGAC
SPARC binding site 2 forward	ENSG00000113140	GCCTGGAGAAGGAATCAACT
SPARC binding site 2 reverse	ENSG00000113140	AAAGGTTACCGTGGCAACTC
SPARC control forward	ENSG00000113140	GTCTAGCTCATGGCAGCAAATC
SPARC control reverse	ENSG00000113140	AATGTGGAGCCCAGAGGCTAT

3.6.4 Small interfering RNA (siRNA)

SiRNAs were purchased from Qiagen or Eurofins Scientific (Ebersberg, Germany). For PTEN, a 27-mer Dicer substrate siRNA method was used for the design of siRNAs [59]. For the other genes, a traditional 19-21mer siRNA method with dTdT overhangs was applied. Sequences of sense and antisense strands as well as concentrations for each siRNA are shown in the following table.

Table 11: siRNA

Gene name	Accession number	Sense (5´- 3´)	Antisense (5´- 3´)	Used concentration
PTEN#1	NM_000314.6	UAGCAGAAACAAAAGGAGAUAUCdAdA	GAUAUCUCCUUUUGUUUCUGCUAAC	20 nM
PTEN#2	NM_000314.6	GAAUCAUCUGGAUUAUAGACCAGdTdG	CUGGUCUAUAAUCCAGAUGAUUCUU	20 nM
PHLPP1#1	NM_194449.3	GAAGAGCUGAAGAGGAUUAdTdT	UAAUCCUCUUCAGCUCUUCdTdT	20 nM
PHLPP1#2	NM_194449.3	AUAACAGCCUCACAGACAAdTdT	UUGUCUGUGAGGCUGUUAUdTdT	20 nM
SCRIB#1	NM_015356.4	GGCAGCGGCTCATCCGCAAdTdT	UUGCGGAUGAGCCGCUGCCdTdT	30 nM
SCRIB#2	NM_015356.4	CAGGAUGAAGUCAUUGGAACAdTdT	UGUUCCAAUGACUUCAUCCUGdTdT	30 nM
JUN	NM_002228.3	AAGAACGUGACAGAUGAGCAGdTdT	CUGCUCAUCUGUCACGUUCUUdTdT	30 nM
ATF2	NM_001880.3	CGCGGGUGACCGAAAGGAUCAdTdT	UGAUCCUUUCGGUCACCCGCGdTdT	30 nM
JUNB	NM_002229.2	ACAGACUCGAUUCAUAUUGAAdTdT	UUCAAUAUGAAUCGAGUCUGUdTdT	30 nM
SPARC	NM_003118.3	ACCCAAGACAUGACAUUCUUAdTdT	UAAGAAUGUCAUGUCUUGGGUdTdT	30 M

3.7 Cell lines

3.7.1 Liver cancer cell lines

Liver cancer cell lines were purchased from the American Type Culture Collection (ATCC, Manassas, Virginia, USA). Cell lines were routinely confirmed by short tandem repeats profiling. Liver cancer cell lines and cell culture conditions are listed in Table 12-13. Liver cancer cell lines were seeded in hepatocyte sandwich culture, which allowed the establishment of apical lumens of canaliculi, and was used to analyze the extent of hepatic polarization [6]. MRP2 was used to visualize the canaliculi structure in hepatocyte sandwich culture. Liver cancer cell lines with different capacities of polarization were compared in Table 12.

Table 12: Liver cancer cell lines

Name	Tissue	Cell type	Disease	Cell polarity
HepG2	liver	epithelial	Hepatoblastoma	High
HuH1	liver	epithelial	HCC	High
HuH6	liver	epithelial	Hepatoblastoma	High
HuH7	liver	epithelial	HCC	Low
HLE	liver	epithelial	HCC	Low
HLF	liver	epithelial	HCC	Low
Hep3B	liver	epithelial	HCC	Low
SNU182	Liver	Epithelial	HCC	Low

3.7.2 Cell lines culture media

Table 13: Cell culture media and supplements

Name	Media	Supplement
HepG2	RPMI-1640 (GE Healthcare)	10% FCS (GE Healthcare)+ 1% Penicillin/Streptomycin (P/S) (GE Healthcare)
HuH1	DMEM (GE Healthcare)	10% FCS+ 1% P/S
HuH6	DMEM	10% FCS+ 1% P/S
HuH7	DMEM	10% FCS+ 1% P/S
HLE	DMEM	10% FCS+ 1% P/S
HLF	DMEM	10% FCS+ 1% P/S
Hep3B	MEM	10% FCS+ 1% P/S
SNU182	RPMI-1640	10% FCS+ 1% P/S

3.8 Bacterial strands

Table 14: Bacterial strands for cloning

Name	Application	Company	Description/Genotype
NEB® 5-alpha Competent E. coli	Gateway vectors	New England Biolabs	Mutations in recA1 and endonuclease I (endA1)
NEB® Stable Competent E. coli	*pT3-EF1α* vector	New England Biolabs	Eliminated activity of endA1

3.9 Plasmid maps

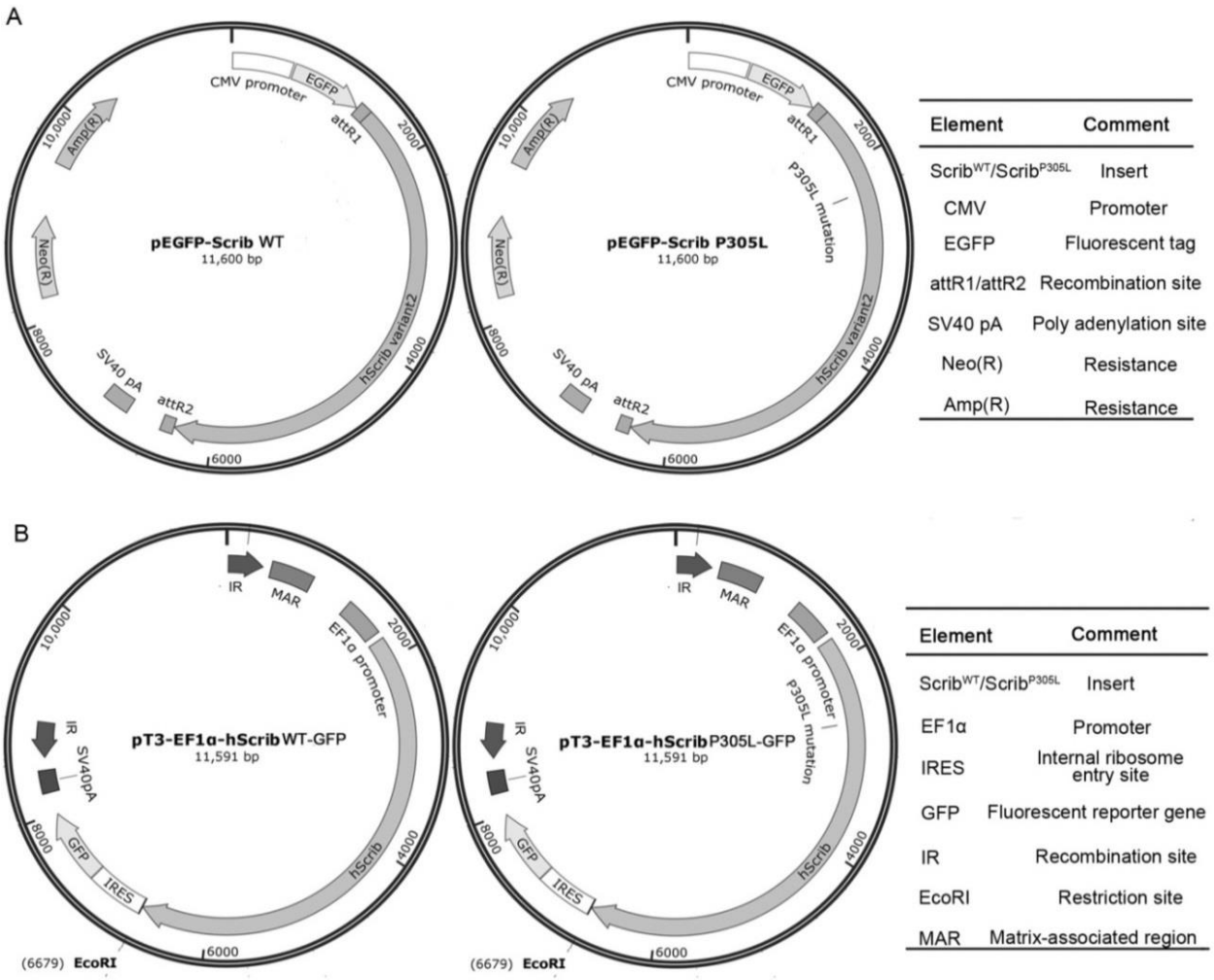

Figure 6: Plasmid maps of Scrib vectors. (A) Plasmid maps for pEGFP-Scrib^{WT} and pEGFP-Scrib^{P305L}. Inserts are located after a *cytomegalovirus* (CMV) promoter. This vector produces a fusion protein of Scrib^{WT} or Scrib^{P305L} with an N-terminal EGFP-tag. The attR recombination sites of Gateway system and Scrib mutation point (P305L) are indicated. **(B)** Plasmid maps for *pT3-EF1α-Scrib^{WT}* and *pT3-EF1α-Scrib^{P305L}* vectors. Inserts are located after a human *elongation factor-1 alpha* (EF1α) promoter, which allows long-term expression of genes in mouse hepatocytes. Inverted Repeats (IR) defines, which is recognition sites for the transponase, are indicated. Internal ribosome entry site (IRES) sequence allows independent expression of Scrib^{WT} or Scrib^{P305L} and *green fluorescent protein* (GFP).

4 METHODS

4.1 Cell culture

4.1.1 Cultivation of immortalized liver cancer cell lines

Human liver cancer cell lines were cultured in DMEM or RPMI supplemented with 10% FCS and 1% P/S at 37°C in a 5% CO_2 atmosphere. Cell lines were authenticated by STR-analysis (DSMZ, Braunschweig, Germany) and were regularly checked for mycoplasma contamination. Cell lines and cell culture conditions are described in Chapter 3.7.1-2. All liver cancer cell lines were split every 3 days. In brief, cells on 10 cm dish were washed with 4 ml PBS, and incubated with 1 ml Trypsin/EDTA at 37°C for 5 minutes. After detaching, cell suspensions were seeded on 10 cm dishes with pre-warmed cell culture media. For counting cells, 8 µl of cell suspension was added to the hemocytometer. Cells were counted in the four corners with gridded square under 10x objective using an inverted microscope. The estimated cell number per ml equals to the average cell number multiplied by 10^4. Subculture of cell lines and cell numbers used in different cell culture scales are listed in Table 15.

Table 15: Subculture and cell seeding of liver cancer cell lines

Cell line	Subcultivation ratio	Cell number (6-well)	Cell number (6 cm)	Cell number (10 cm)
HepG2	1:4	$3.0x10^5$	$6.6x10^5$	$1.8x10^6$
HuH1	1:6	$3.0x10^5$	$6.6x10^5$	$1.8x10^6$
HuH6	1:3	$4.0x10^5$	$8.8x10^5$	$2.4x10^6$
HuH7	1:8	$1.0x10^5$	$2.2x10^5$	$6.0x10^5$
HLE	1:8	$1.0x10^5$	$2.2x10^5$	$6.0x10^5$
HLF	1:10	$1.0x10^5$	$2.2x10^5$	$6.0x10^5$
Hep3B	1:3	$3.0x10^5$	$6.6x10^5$	$1.8x10^6$
SNU182	1:6	$2.0x10^5$	$4.4x10^5$	$1.2x10^6$

4.1.2 Cryconservation of liver cancer cell lines

Cells were cultured on 10 cm dishes until 70-80% confluence before cryconservation. One milliliter trypsin was added to each dish at 37°C for 5 minutes. After detaching, cells were resuspended in 8 ml cell culture media and centrifuged at 1000x rounds per minute (RPM) for 5 minutes. After removing the supernatant, the remaining cell pellet was resuspended in 800 µl cell culture media supplemented with 20% FCS and transferred to 2 ml cryovials. An equal volume (800 µl) of cell culture media supplemented with 20% FCS and 20% DMSO (final concentration 10%) was added to each cryovial. Vials were transferred into a freezing container at -80°C overnight, and stored in liquid nitrogen for long-time use.

4.1.3 Preparation of HCC cell sandwich culture

For the preparation of highly polarized 3D sandwich cultures, a collagen solution was prepared by dissolving rat-tail collagen I lyphilisate in sterile-filtered 0.2% (v/v) acetic acid overnight. Before use, the collagen solution was supplemented with concentrated DMEM medium (10x) and neutralized to pH 7.4 by adding NaOH (2 M) on ice. The collagen solution was completely dispensed on cell culture plates, which were incubated at 37°C for 1 hour to allow gelation. HCC cells (HepG2 or HuH6) were seeded on the collagen layer for at least 4 hours. After attaching, cells were washed once with ice-cold PBS. Additional collagen solution was dispensed on the upper layer of adherent cells. After 1 hour of gelation, the respective cell culture medium was added to the sandwich culture. HCC cell lines were cultured in collagen sandwich culture for 10 days before further analyses. Cell culture media were changed every 3 days. Volumes of neutralized collagen solutions, cell culture media and numbers of cells used in different cell culture scales are listed in Table 16.

Table 16: Sandwich culture preparation and cell plating

Cell culture scale	Neutralized collagen solution (for each layer)	Number of HCC cell	Media volume
12 well plate	120 µl	$5.6\text{-}7.2 \times 10^4$	1.5 ml
6 well plate	250 µl	$1.4\text{-}1.8 \times 10^5$	2 ml
6 cm plate	500 µl	$3.0\text{-}4.0 \times 10^5$	6 ml

4.1.4 Generation of cell lines stably expressing Scrib^{WT} and Scrib^{P305L}

For the generation of HCC cell lines stably expressing Scrib^{WT} or Scrib^{P305L}, Fugene HD transfection reagent was used for the delivery of expression vectors. HepG2 cells were seeded on 10 cm plates with 80% of confluence overnight. Transfection mixture consisting of pEGFP-Scrib^{WT} or pEGFP-Scrib^{P305L} plasmids (9 µg), Fugene HD transfection reagent (42 µl) and Opti-MEM was prepared with a total volume of 420 µl. After incubation at room temperature for 15 minutes, the transfection mixture was distributed thoroughly to the HCC cells in 8 ml of transfection media (with 10% FCS, without antibiotics). G418 (1 mg/ml) selection was carried out 72 hours after transfection to allow the expansion of cells with stable integration of the vector. Single colonies started to appear 2 weeks of G418 selection. Colonies were carefully transferred to 96-well plates. For single colony expansion, a lower concentration of G418 (400 ng/ml) was applied to the cell culture media. Cells were step-wise transferred to 24 -well plate, 6 -well plate, and 6 cm plates. The transgene expression was confirmed by both western immunoblotting and real-time PCR (see 4.5.2 and 4.4.3). For further functional and gene expression analysis, the stable clones were cultured with full RPMI media without G418. Overexpression of exogenous Scrib was routinely checked by western immunoblotting every month.

4.1.5 Small-interfering (siRNA)-mediated gene inhibition

A reverse transfection protocol using Lipofectamine® RNAiMAX was used for the transfection of siRNAs-mediated gene inhibition. Treatment was carried out on 6-well plates. The siRNA solution (Table 17 solution A) and the Lipofectamine® RNAiMAX solutions (Table 17 solution B) were prepared separately. SiRNA concentrations and target sequences of siRNAs are listed in Table 11. After incubation of solution A and B at room temperature for 10 minutes, solution B was added to solution A and incubated at room temperature for another 15 minutes. During this time, $3.5x10^5$ - $4x10^5$ cells were detached by trypsin and resuspended in 2.5 ml transfection media (with 10% FCS, without antibiotics). SiRNA transfection mixture (500 µl) and cell suspension (2.5 ml) were mixed well and transferred into a 6-well plate. Total RNA and proteins were extracted 48 to 72 hours after siRNA treatment. Cells without treatment as well as cells transfected with nonsense siRNA served as controls.

Table 17: Preparation of siRNA transfection solutions

Solution	Component	Amount	Final concentration
A	Opti-MEM	250 µl	-
	SiRNA (20 µM)	3.0-4.5 µl	20-30 nM
B	Opti-MEM	250 µl	-
	Lipofectamine® RNAiMAX	7.5 µl	0.25% (v/v)

4.1.6 Wortmannin treatment

For the inhibition of PI3K activity, cells were treated with Wortmannin, which was dissolved in DMSO at 100 mM and stored light-protected at -20°C. One day before treatment, cells were seeded with a cell density of $7.5x10^3$/well in a 96-well plate or $3x10^5$/well in a 6-well plate. Wortmannin was pre-diluted in PBS to a concentration of 1 mM. Different working concentrations of Wortmannin (0.05, 0.1, 0.25, and 0.5 µM) were applied to the cells for 6.5 to 24 hours. Cells treated with an equal amount of DMSO served as a control.

4.1.7 Recombinant SPARC treatment

Recombinant Human SPARC was reconstituted in PBS (final concentration: 100 µg/ml) and stored at -20°C. For the treatment, cells were seeded with a cell density of $6x10^4$ cells/well in FCS-free medium in 24-well plate of a Matrix-coated transwell chamber. In the lower chamber, a higher concentration of SPARC (200 ng/ml) was used to stimulate directional cell invasion. In the upper chamber, lower concentration of SPARC (20 ng/ml) was supplemented.

4.2 Functional assays

4.2.1 Cell viability assay

Cell viability was determined using the CellTiter-Blue reagent. Cells were seeded with a cell density of $7.5x10^3$/well in a 96-well plate. The CellTiter-Blue reagent was added to cultured cells according to the manufacturer's instructions. After 1 hour of incubation at 37°C, fluorescence was detected by a Fluostar Omega microplate reader at an excitation wavelength of 544 nm and an emission wavelength of 590 nm. Cell viability was detected 48 and 72 hours after respective treatments.

4.2.2 Cell cytotoxicity and apoptosis assays

CellTox Green reagent was employed for the measurement of cell cytotoxicity. Cells were seeded with a cell density of $7.5x10^3$/well in a 96-well plate overnight. Cell cytotoxicity was measured 48 and 72 hours after seeding. For the measurement, cells were incubated with CellTox Green reagent at room temperature for 15 minutes according to the manufacturer's instructions. The fluorescence was subsequently measured at an excitation wavelength of 485 nm and an emission wavelength of 520 nm.

Caspase-3 activity assay was used for the measurement of cell apoptosis. Proteins were extracted from cultured cells using the Protein Lysis buffer. Caspase-3 substrate Ac-DEVD-AFC (7-Amino-4-trifluoromethylcoumarin, 100 µM in HEPES-Buffer) was prepared freshly according to the manufacturer's instructions. Protein lysate (50 µg) was incubated with the Caspase-3 substrate (50 µl) at 37°C for 4 hours. Caspase activity was detected at an excitation wavelength of 400 nm and an emission wavelength of 505 nm. Cells treated with cell culture medium served as negative controls, while cells treated with Doxorubicin (1 µM) were used as positive controls.

4.2.3 Cell invasion assay

Cell invasion experiments were performed using a matrigel invasion chamber with an 8 µm pore polycarbonate membrane. Cells were seeded on top of the matrigel with a cell density of $6x10^4$/well in starvation medium. On the lower side of the invasion chamber, cell culture medium was supplemented with 10% FCS for a cell attractant. Cells remaining on the upper matrigel were removed by cotton tips after 48 to 96 hours, while transmigrating cells were fixed with paraformaldehyde (PFA, 4%, w/v) for 10 minutes. A crystal violet/methanol (5%, w/v) solution

was used for cell body staining on the polycarbonate membrane. After incubation with the crystal violet solution for 1 hour, the polycarbonate membrane was washed 3x with PBS, and 1x with distilled water. Seven different areas from each membrane were digitally documented and the numbers of transmigrating cells were visually counted (40-fold magnification).

4.3 Molecular cloning

4.3.1 Scrib cloning for the generation of stable cell lines

Empty Gateway plasmids pDONR201 and pDEST-EGFP were kindly provided by Dr. Stefan Pusch (DKFZ, Heidelberg, Germany). Human pDEST-EGFP-Scrib^{WT} and pDEST-EGFP-Scrib^{P305L} vectors for the generation of stable cell lines were constructed using the Gateway® system. Human Scrib complementary DNA (cDNA) was amplified from a human Scrib plasmid (pLK45) purchased from Addgene (Cambridge, Massachusetts, USA). For this, a proofreading Phusion® High-Fidelity DNA Polymerase was employed for the amplification of Scrib cDNA. The reaction and program are shown in Table 18-19.

Table 18: Amplification reaction of Scrib for pDONR201

Component	Amount	Final concentration
DNA template (pLK45-Scrib)	20 ng	0.4 ng/µl
dNTP (10 mM)	1 µl	200 µM
Scrib forward (10 µM)	2.5 µl	0.5 µM
Scrib reverse (10 µM)	2.5 µl	0.5 µM
5x Phusion® GC buffer	10 µl	1 x
DMSO	1.5 µl	3 %
Phusion® High-Fidelity DNA Polymerase	0.5 µl	0.02 units/µl
Nuclease free water	add to 50 µl	-

Table 19: Amplification program of Scrib for pDONR201

PCR cycle	Step	Temperature	Time
1	Initial denaturation	98 °C	30 seconds
30x	Denaturation	98 °C	30 seconds
	Combined annealing and extension	72 °C	3 minutes and 20 seconds
1	Final extension	72 °C	10 minutes

PCR product was separated on a 0.5% agarose gel, and extracted using the PCR Clean-up kit. The integration of Scrib cDNA in the Gateway® pDONR 201 vector was performed using the Gateway® BP Clonase II Enzyme Mix according to the manufacturers' instructions. In brief, 4 µl (30 fmol) of PCR product was incubated with pDONR vector (150 ng), Gateway® BP Clonase® II Enzyme mix (2 µl), and filled up with TE buffer (pH 8.0) to 10 µl. The BP reaction was done at room temperature, overnight. In order to transfer the Scrib cDNA with Gateway® expression vectors in other vectors, a LR reaction was performed using the Gateway® LR Clonase II Enzyme Mix according to the manufacturers' protocol. In brief, 5 µl pDONR-Scrib (75 ng) Gateway® destination vector pDEST-EGFP (75 ng), Gateway® LR Clonase® II Enzyme mix (1 µl) and TE buffer (pH 8.0) were incubated together. LR reaction was carried out at room temperature for 4 hours. All used constructs were confirmed by sequencing (Seqlab-Sequence Laboratories, Göttingen, Germany).

4.3.2 Site-directed Scrib^{P305L} mutagenesis

Site-directed mutagenesis was performed to include the P305L mutation in the wildtype form of Scrib [60]. For the generation of pDONR-Scrib^{P305L}, forward and reverse strands were synthesized by PCR using complementary primers containing the desired mutation (Table 9). The reaction and program for new strand synthesis are shown in Tables 20-21. After that, methylated templates were digested using 1 unit of DpnI enzyme for 3 hours. The newly synthesized DNA carrying the P305L mutation was transformed into bacteria. The pDONR-Scrib^{P305L} vector was confirmed by sequencing. Subsequently, both pDONR-Scrib^{WT} and pDONR-Scrib^{P305L} were used to transfer Scrib^{WT} and Scrib^{P305L} in the pDEST-EGFP expression vector by using Gateway® LR Clonase® II Enzyme mix (Table 5).

Table 20: Reaction for Scrib^{P305L} mutagenesis

Component	Amount	Final concentration
DNA template (pDONR-Scrib)	100 ng	2 ng/µl
dNTP (10 mM)	1 µl	200 µM
Scrib (mut-P305L) forward (10 µM)	1 µl	0.2 µM
Scrib (mut-P305L) reverse (10 µM)	1 µl	0.2 µM
5x Phusion® GC buffer	10 µl	1 x
DMSO	1.5 µl	3 %
Phusion® High-Fidelity DNA Polymerase	0.5 µl	0.02 units/µl
Nuclease free water	add to 50 µl	-

Table 21: Program for Scrib^{P305L} mutagenesis

Cycle	Step	Temperature	Time
1	Initial denaturation	98 °C	60 seconds
18 x	Denaturation	98 °C	30 seconds
	Combined annealing and extension	72 °C	4 minutes and 40 seconds
1	Final extension	72 °C	10 minutes

4.3.3 Subcloning of Scrib^{WT} and Scrib^{P305L} for hydrodynamic tail-vein injection

To generate the vectors for hydrodynamic tail-vein (HDTV) injection, human Scrib^{WT} and Scrib^{P305L} cDNAs were amplified by using *Scrib pT3 for* and *Scrib EcoRI pT3 rev* primers (Table 9). Blunt-end cloning was employed for the transfer of the insert into the *pT3-EF1α* vector. PCR reaction and program for the implication of Scrib cDNA were indicated in the following tables (Table 22-23). Fifty microliters of PCR products were loaded on a 0.5% Agarose gel for separation. The specific product with 4.8 kb was cut out under UV light and purified using the PCR Clean-up kit. To phosphorylate the insert, 17 µl of purified PCR product was incubation with 1 µl T4 Polynucleotide Kinase (PNK) and 2 µl T4 ligation buffer at 37°C for 1 hour. T4 PNK Kinase was inactivated at 65°C for 20 minutes. For the preparation of the backbone, the empty *pT3-EF1α* vector (2 µg) was digested with the restriction enzyme EcoRI (1 unit) at 37°C

for 3 hours. In order to generate blunt ends, Phusion® polymerase (1 unit) and dNTPs (0.5 µl, final concentration: 250 µM) were incubated with the digested plasmid (2 µg) at 37°C for 1 hour. The blunt-end vector (17 µl) was dephosphorylated by CIAP (2 µl, 40 units) for 1 hour. The resulting *pT3-EF1α* vector was purified by PCR clean up kit. To ligate the Scrib^{WT}/Scrib^{P305L} cDNAs with the *pT3-EF1α* vector, the phosphorylated insert (250 ng) was added to the dephosphorylated vector (100 ng) with a molar ratio of 3:1 (insert:vector). T4 ligase (1 µl, 5 units) and T4 Buffer (supplemented with ATP, 1 µl) were added to the DNA mixture and incubated at 16°C overnight.

Table 22: Amplification reaction of Scrib for *pT3-EF1α* vector

Component	Amount	Final concentration
DNA template (pDONR-Scrib^{WT}/pDONR-Scrib^{P305L})	20 ng	0.4 ng/µl
dNTP (10 mM)	1 µl	200 µM
Scrib pT3 for (10 µM)	2.5 µl	0.5 µM
Scrib EcoRI pT3 rev (10 µM)	2.5 µl	0.5 µM
5x Q5 buffer	10 µl	1 x
5x High GC Enhancer	10 µl	1 x
DMSO	1.5 µl	3 %
Q5® High-Fidelity DNA Polymerase	1 µl	0.04 units/µl
Nuclease free water	add to 50 µl	-

Table 23: Amplification program of Scrib for *pT3-EF1α* vector

PCR Cycle	Step	Temperature	Time
1	Initial denaturation	98 °C	30 seconds
38x	Denaturation	98 °C	5 seconds
	Combined annealing and extension	72 °C	3 minutes and 30 seconds
1	Final extension	72 °C	2 minutes

4.3.4 Transformation of competent bacteria

In order to amplify plasmid DNA, different vectors were transformed into competent bacteria. For bacterial transformation, 0.1-50 ng plasmid DNA was added to 50 µl of the respective bacterial strain (Table 14). After incubation on ice for 30 minutes, the plasmid/bacteria mixture was heated in a 42 °C water bath for 42 seconds, and incubated on ice for 2 minutes. For vectors containing kanamycin resistance, transformed bacteria were growing in 900 µl pre-warmed Luria-Bertani (LB) media at 37°C for 1 hour with shaking (250 RPM) before inoculation Kanamycin-containing (25 µg/ml) agar plate. For vectors with Ampicillin resistance, transformed bacteria were inoculated directly on Ampicillin-containing (50 µg/ml) agar plates. After selection overnight, single clones were picked for further testing and amplification.

For long-term storage of transformed bacteria, single clones were picked and incubated in 2 ml LB media with respective antibiotics. After growing overnight, 500 µl of the cultured bacteria was added to 500 µl glycerol (50%) in a cryovial and storted at -80°C.

4.3.5 DNA purification (MidiPrep and EndoFree Maxiprep)

For in vitro experiments, midipreps were carried out for the purification of plasmid DNA. Single bacterial clones were picked and incubated with 80 ml LB media containing Ampicillin (50 µg/ml) or Kanamycin (12.5 µg/ml) under shaking at 250 RPM. After overnight incubation, cultured bacteria were pelleted down by centrifugation at 5,000 RPM for 10 minutes. Cell pellet was resuspended in 3 ml Cell Resuspension Solution. Bacteria were lysed by adding 3 ml Cell Lysis Solution and mixed via gentle mixing. After incubation at room temperature for 3 minutes, the lysate was neutralized by adding 5 ml chilled Neutralization Solution. The neutralized lysate was incubated on ice for 5 minutes to allow sufficient precipitation. Afterwards, cell lysate was transferred on a PureYield Clearing Column to remove the precipitate. The clear supernatant was added to a DNA Binding Column. The DNA Binding Column was washed 1x 5 ml Endotoxin Removal Solution, 2x 20 ml Column Wash Solution. After drying of the DNA Binding Column, plasmid DNA was eluted by adding 600 µl nuclease free water and centrifugation at 5,000 RPM for 5 minutes.

For the purification of plasmid DNA for *in vivo* experiment, an EndoFree Maxiprep kit was applied (Table 6). Single clones were picked up and incubated in 200 ml LB media containing the respective antibiotic overnight with shaking (250 RPM). Purification was performed according to the manufacturer's instructions. Compared to the Midiprep, endotoxin produced by bacteria was removed by incubating with 2.5 ml Endotoxin Removal Buffer on ice for 30 minutes. After elution of plasmid DNA from the column, DNA was precipitated by adding 10.5 ml isopropanol and centrifuged at 5,000 RPM for 1 hour. Afterwards, the resulting DNA pellet was washed with 5 ml of 70% endotoxin-free ethanol, and centrifuged at 5,000 RPM for 40 minutes. After drying, 600 µl endotoxin-free Buffer TE was added to dissolve the plasmid DNA.

4.4 Messenger RNA (mRNA) quantification

4.4.1 RNA extraction from cultured cells

For total RNA extraction from cultured cells, the NucleoSpin RNA II kit was applied according to the manufacturer's instructions. Specifically, cells grown on 6-well plate were lysed by adding 350 µl Lysis Buffer RA1 with 1% ß-mercaptoethanol. Cell lysate was filtered by loading on a NucleoSpin® Filter and centrifuged at 11,000x g for 1 minute. Filtered lysate was mixed with 350 µl of 70 % ethanol and loaded on a RNA-binding column. After centrifugation at 11,000x g for 30 seconds, silicon membrane was desalted by adding 350 µl Membrane Desalting Buffer. The genomic DNA on silicon membrane was digested with 95 µl DNase reaction mixture at room temperature for 15 minutes. Afterwards, the RNA column was sequentially washed with 200 µl RAW2, 600 µl RA3, and 250 µl RA3. After each washing step, the column was centrifuged at 11,000x g for 30 seconds (last step for 2 minutes). RNA was eluted by adding 60 µl RNase-free water and centrifugation at 11,000x g for 1 minute. RNA concentrations were determined by Nanodrop and stored at -80°C.

4.4.2 cDNA synthesis

Reactions and program for cDNA synthesis are listed in Table 24-25. cDNA was diluted 1:50 for further analysis.

Table 24: Reaction of cDNA synthesis

Component	Amount	Final concentration
Total RNA	1 µg	50 ng/µl
dNTP (10 mM)	2 µl	1 mM
Random Hexamer primers (100 µM)	1 µl	5 µM
5x RT reaction buffer	4 µl	1x
RevertAid H Minus Reverse Transcriptase	0.9 µl	9 units/µl
Nuclease free water	add to 20 µl	-

Table 25: Program of cDNA synthesis

Step	Temperature	Time	Comment
Denaturation	75 °C	5 minutes	5x RT reaction buffer was added at the end of this step
Annealing	25 °C	15 minutes	Reverse Transcriptase was added after 5 minutes of this step
cDNA synthesis	42 °C	1 hour	-
Enzyme inactivation	70 °C	10 minutes	-

4.4.3 Semi-quantitative real-time PCR analysis

Real-time PCR reactions were set up using the ABsolute qPCR SYBR Green ROX Mix (Table 26-27). β2-Microglobulin was used for the normalization of *in vitro* experiments. StepOnePlus™ The standard curve method was used for quantification. Different dilutions of cDNA from HepG2 cells (1:12.5, 1:25, 1:50, 1:100, 1:200, and 1:400) were used for generation of the standard curves for each primer pair.

Table 26: Reaction of real-time PCR

Component	Amount	Final concentration
cDNA (1:50)	2 µl	1:500
SYBR Green ROX Mix (2x)	5 µl	1x
Forward primer (10 µM)	0.3 µl	0.3 µM
Reverse primer (10 µM)	0.3 µl	0.3 µM
Nuclease free water	2.4 µl	-

Table 27: Program of real-time PCR

PCR Cycle	Step	Temperature	Time
1	Initial denaturation	95 °C	15 minutes
40 x	Denaturation	95 °C	15 seconds
	Combined annealing and extension	60 °C	60 seconds
1	Melting curve	60 °C - 95 °C	Increase at 0.5 °C/minute

4.4.4 Gene expression profiling

Affymetrix Human Gene 2.0 ST Arrays were used for the expression analysis of total mRNA derived from HepG2 cells stably expressing $Scrib^{WT}$ or $Scrib^{P305L}$. After extraction of total RNA from both cell lines, complementary RNA labeled with biotin was prepared according to the Affymetrix standard labelling protocol. The complementary RNA was purified, fragmented, and hybridized uisng the GeneChip Hybridization oven 640. The arrays were washed and stained with the GeneChip Fluidics Station 450, and detected by using the GeneChip Scanner 3000. Custom CDF with Entrez-based gene definitions were used for the annotation of the arrays [61]. Values from the arrays were rearranged by quantile normalization, and analyzed using the software package SAS JMP7. Array data was uploaded in the Gene Expression Omnibus database (available: http://www.ncbi.nlm.nih.gov/geo/; accession number GSE93742).

4.5 Protein biochemistry analyses

4.5.1 Protein extraction from cultured cells

Cells on culture plates were washed briefly with ice-cold PBS. A certain volume (80 µl for 6-well plate, 300 µl for 10 cm dish) of cell lysis buffer supplemented with Proteinase Inhibitor (1x), PMSF (1 mM) and PhosStop (1x) was incubated with cultured cell on ice for 2 minutes. Cell lysate was collected and briefly frozen in liquid nitrogen. After thawing, the cell lysate was sonicated for ten seconds to shear DNA. Afterwards, the suspension was centrifuged at 14,000 RPM for 15 minutes. The supernatant containing total proteins were isolated and stored at -20°C before analysis.

4.5.2 SDS-Polyacrylamide gel electrophoresis (PAGE) and western immunoblotting

For western immunoblotting analysis, equal amount of proteins ranging from 30-50 µg were prepared in 3x SDS-protein sample buffer and denatured at 95°C for 5 minutes. Protein samples were loaded on polyacrylamide gels (8% to 12%) next to 8 µl of a 10-250 kDa Prestained Protein Ladder (Table 3). Electrophoresis was carried out with 120 V in electrophoresis buffer for 2 hours. Proteins on polyacrylamide gel were transferred to a 0.45 µm nitrocellulose membrane using a blotting chamber with ice-cold borate buffer at 90 V and 1000 mA/chamber for 1.5 hours. After blocking unspecific bands with 5% (w/v) milk powder or 5% (w/v) BSA in TBST (0.1% Tween 20 in TBS, v/v) for 1 hour, membranes were incubated with primary antibodies (concentrations are listed in Table 7) at 4°C overnight. After incubation, the membranes were washed 3x with TBST (0.1%), and incubated with respective fluorophore-labeled secondary antibodies (1:20,000; IRDye 680 and 800) at room temperature for 1 hour. After washing 3x TBST (0.1%), signals on the membranes were detected using a LI-COR fluorescent imaging (Odyssey SA Infrared Imaging System). Actin was used as a loading control.

4.5.3 Fractionation of subcellular proteins

For the fractionation of cytoplasmic and nuclear proteins, a NE-PER™ Nuclear and Cytoplasmic Extraction Reagents kit was used. Cells were seeded on 10 cm dishes at high cell density (>80% confluence). For experiments with low cell density, 4 dishes were prepared and pooled. Fractionation was performed according to the manufacturer's instructions. After quantification, cytoplasmic and nuclear protein extracts were loaded on polyacrylamide gel with the ratio of 2:1 (cytoplasmic: nuclear fraction) for western immunoblotting (see 4.5.2). β-Tubulin and PARP (poly-ADP ribose polymerase) served as loading controls for cytoplasmic and nuclear fractions, respectively.

Membranous and cytoplasmic protein fractionation was performed by using the Mem-PER Plus Membrane Protein Extraction Kit. Cells were seeded on 10 cm dishes and fractionation was performed according to the manufacturer's instructions. For western immunoblotting of membranous proteins, an antibody detecting Na^+-K^+-ATPase was used for a loading control. For cytoplasmic proteins, β-Tubulin was used as a loading control.

4.5.4 Enzyme-linked immunosorbent assay (ELISA)

Human SPARC Quantikine ELISA kit was used to determine the secreted concentrations of SPARC in the supernatant of cultured cells. For this, cells were starved in the respective medium without FCS for at least 12 hours. Media (100 µl) from cultured cells were collected from each sample and centrifuged for 15 minutes at 1,000x g to remove particles. The resulting supernatants were diluted 1:2 in Calibrator Diluent RD6-59. Samples, SPARC standards, and blank control (Diluent RD6-59) were incubated in the ELISA microplate at room temperature with 300 RPM shaking for 3 hours. After that, wells were washed simultaneously with wash buffer and incubated with of human SPARC conjugate antibody (200 µl) in the dark at 4°C for 1.5 hours. After an additional washing step, 200 µl of the substrate solution was added. Fluorescence was detected using the Fluostar Omega microplate reader at wavelengths of 450 nm and 550 nm. The absorbance of 550 nm was subtracted from the absorbance of 450 nm. For each sample and standard solution, the respective absorbance was corrected for the blank control. Absolute concentrations for SPARC were calculated according to the standard curves of recombinant SPARC provided by the manufacturer.

4.5.5 Protein half-life determination

Cycloheximide (CHX) chase analysis was performed to compare protein stability. To define the optimal CHX concentration for HepG2 cells, the lowest concentration which efficiently blocked protein synthesis was analyzed. Specifically, different amounts of CHX (50, 100, 150, 200, and 250 µg/ml) were applied to HepG2 cells for 16 hours. Proteins were extracted (see 4.5.1) and analyzed by western immunoblotting (see 4.5.2). Measurement of a known unstable protein (e.g. c-MYC) revealed that that 100 µg/ml CHX efficiently blocked protein synthesis without killing cells in this time-frame.

For the analysis of PHLPP1 and PTEN stability, HepG2 stable cell lines were seeded with a cell density of $8x10^4$/well in a 12-well plate. PHLPP1 with short half-life was chased until 8 hours, with 0.5 to 2-hours intervals. PTEN with longer half-life was chased until 72 hours, with 2 to 8-hours intervals. Protein extracts from each time points were collected and analyzed by western immunoblotting (see 4.5.2). The relative protein amounts for PHLPP1 and PTEN were quantified compared to the original protein levels at time-point '0'. Image Studio software was employed for the quantification of proteins.

4.5.6 Immunofluorescence analysis of tissue cryosections

A methanol-acetone fixation method was used for immunofluorescence stains of cryosections derived from human livers. Tissues were fixed in ice-cold methanol for 5 min followed by ice-cold acetone for 1 min on ice. The permeabilization step was performed by incubation with Triton X-100/PBS (0.2%, v/v) at room temperature for 5 min. For blocking, tissue sections were incubated with BSA/PBS (1%, w/v) for 30 min. Samples were then incubated with primary antibodies (listed in Table 7) in a wet chamber at 4°C overnight. After three times of wash with PBST (0.01%, Tween in PBS, v/v), tissue sections were incubated with the respective secondary antibodies in a wet chamber for 1 hour. After washing 3x with PBST, and rinsed with distilled water, cryosections were dehydrated with 100% ethanol. The visualization of nuclei and tissue mounting were achieved by the incubation with DAPI Fluoromount-G.

4.5.7 Immunofluorescence analysis of sandwich cultures

For the visualization of polarity markers in sandwich cultures, a published hepatocyte sandwich immunofluorescence staining method was modified [62]. In brief, sandwich cultures were prepared on coverslips in cell culture plates for 1-2 weeks. After washing 1x with $MgCl_2$/PBS (2mM), the sandwich cultures were fixed with PFA solution (4%, w/v) at room temperature for 20 minutes. This was followed by a permeabilization step with Triton/PBS (0.5%, v/v) at room temperature for 10 minutes. Afterwards, the coverslips were thoroughly washed 3x with PBS at room temperature (2x 5 minutes followed by additional 30 minutes). After blocking with BSA/PBS (5%, w/v) for 30 minutes, the coverslips were washed with PBST (0.05% Tween in PBS, v/v) and transferred into a wet chamber. On each slide 150-200 µl primary antibodies (Table 7) were incubated at 4°C, overnight. After primary antibody incubation, sandwiches were washed 3x with PBST at room temperature for 10 minutes followed by an incubation with 200 µl secondary antibodies at room temperature in a dark chamber for 2 hours. After incubation, the sandwich cultures were washed 3x with PBST for 10 minutes, and 3x with PBS for 10 minutes. Eventually, the sandwich cultures were dehydrated with 100% ethanol, and mounted by a DAPI Fluoromount-G.

4.5.8 Immunohistochemistry (IHC) and histological analyses

Paraffin embedded tissues were cut in 2-3 µm sections using a microtome and dried overnight. Tissues were deparaffinised by 3x incubation with xylene for 5 minutes. Afterwards, sections were rehydrated using an ethanol gradient (2x 100% Ethanol, 96% Ethanol, 70% Ethanol, water each 2 min). For antigen retrieval, tissue sections were incubated with 10 mM citrate buffer (pH 6.0) in a stream cooker. After cooling down, tissues were blocked with avidin and biotin at room temperature for 30 minutes (Avidin/Biotin Blocking Kit), and incubated with primary antibodies (Table 7) in a wet chamber at 4°C overnight.

For E-cadherin, ATF2, and pAKT stains, AP (alkaline phosphatase)-based DCS Detection Line system was employed. For this, tissue sections were incubated with Rabbit Enhancer for 20 min, and incubated with AP-Polymer Detection Line for further 20 min. After washing 2x with TBS for 5 minutes, sections were incubated with Permanent AP Red. For Scrib and MCAM stains, the *horseradish peroxidase* (HRP) system was used. Tissues were blocked with H_2O_2 for 10 min, and incubated with biotinylated secondary antibody for 30 min. This was followed by incubation with Streptavidin-HRP for 20 min and signal development with DAB (for Scrib stain) or AEC (for

MCAM stain). After washing 2x with TBS for 5 minutes, tissue sections were incubated with REAL Hematoxylin for nuclear visualization. All stains were performed by the IHC research facility at the Institute of Pathology, Heidelberg.

For histological analysis of liver tissues, Hematoxylin and eosin (H&E) stains from each tissue samples were analyzed by pathologist. Tumors were identified by well-vascularized nodules with necrotic areas within the tumor mass. Tumor cells were identified with a pleomorphic shape, a basophilic cytoplasm and sometimes fat droplets. In addition, hyperchromatic nuclei with increased nuclear to cytoplasmic ratio were presented in the tumor cells. Immunohistochemistry stain of Ki-67 was used to detect the increased mitotic activity of tumor cells.

4.6 Immunoprecipitation analysis

4.6.1 Co-Immunoprecipitation (CoIP) analysis

For the detection of specific protein-protein interactions, CoIP experiments with Protein A/G beads and magnetic separation were performed [63]. A 12-Tube magnet was used to capture the antibody-bound protein complexes. In brief, cells grown on a 10 cm dish were lysed with 300 µl ice-cold non-denaturing lysis buffer supplemented with protease inhibitors (3 µl). The supernatant was collected after centrifugation at 14,000x g for 10 minutes. In total, 20 µl of protein lysate were preserved as Input control. Dynabeads Protein G beads (50 µl) were incubated with 50 µl glycine solution (50 mM) for at room temperature for 5 minutes. After removing glycine solution from the Dynabeads, primary antibodies (2 µg) were pre-incubated with Dynabeads Protein G at 4°C for 4 hours under rotation. After two washing steps with PBST, the coupled antibody-Protein G beads were incubated with 1 mg protein lysate (defined by Bradford assay) under rotation at 4°C overnight. An equal amount of rabbit IgG antibody (2 µg) incubated with Dynabeads and eand quivalent amount of protein lysate were used as negative control. After incubation, Dynabeads-protein complexes were washed 3x with PBS using the magnet. After washing, the complexes were resuspended in 100 µl PBS and transferred in new 2 ml-tubes. The bound proteins were eluted from the Dynabeads by incubation with Laemmli buffer (2x concentrated, 30 µl) at 95°C and vortexing for 15 min. The supernatant containing denatured proteins were analyzed by western immunoblotting analysis (see 4.5.2).

4.6.2 Chromatin-Immunoprecipitation (ChIP) analysis

ChIP analysis was carried out to detect the interactions between transcription factors and specific promoter regions. For this, $1.1x10^7$ cells were seeded on 15 cm dishes and cultured for 2 additional days. DNA and proteins were cross-linked using 20 ml of formaldehyde/PBS (1%) for 12 min, followed by quenching with 1 ml of glycine (2.5 M) for 5 min. After washing with ice-cold PBS, cells were lysed with 1 ml ice-cold RIPA buffer on ice. The DNA fragments (500 bp-1 kb) were generated by sonication (amplitude 15, power level 1.5) for 2 minutes. Cell debris was removed by centrifugation at 16,000x g at 4°C for 15 minutes. Protein concentrations were determined by Bradford assay and equalized to 1 mg/ml with RIPA buffer. Diluted cell lysate was pre-cleared with 30 µl of Dynabeads Protein G. In parallel, 50 µl Dynabeads Protein G beads was blocked with salmon sperm DNA (15 µg) and BSA (50 µg) for 2 hours. Pre-cleared samples were incubated with blocked Dynabeads and respective antibodies (4 µg) at 4°C overnight. The resulting immunocomplex-bound-beads were washed 4x with RIPA buffer, 2x with IP wash buffer and again 2x with RIPA buffer (for 5 min each). The Dynabeads complexes were resuspended in 100 µl TE buffer. Immunocomplexes were eluted with 200 µl of Talianidis elution buffer (1.5x concentrated) at 65°C for 15 min. Reversal crosslinking was achieved by adjusting to 200 mM NaCl (4 M) and incubation at 65°C for 5 hours. DNA was extracted by the PCR Clean-Up kit according to the manufacturer's protocol. Real-time PCRs were performed to determine the quantity of precipitated promoter fragments with the normalization to a standard curve derived from serial dilutions of genomic DNA. As a negative control, primers binding to 5,200 bp downstream of the start codon was used.

4.7 Mouse work

The experimental setup and group size were approved by the German Regional Council of Baden-Wuerttemberg (ref. number: G-30/16; Karlsruhe, Germany) and in accordance with the institutional regulations of the Interfakultäre Biomedizinische Forschungseinrichtung (IBF), University of Heidelberg, Germany). Exclusion and termination criteria are defined in the ATBC criteria of the animal welfare officer of the University Hospital Heidelberg.

4.7.1 Hydrodynamic tail-vein (HDTV) plasmid delivery

A HDTV gene delivery method was employed to analyze the effect of cytoplasmic and membranous Scrib on liver tumor development. The establishment of HDTV is based on the anatomical structure of the liver, which is highly permeable between sinusoids and liver parenchymal cells (Chapter 1.1.1). The large volume of plasmid DNA solution flowing into *vena cava inferior* induces cardiac congestion, which leads to the enrichment of plasmids in the veins of mouse liver. This allows the penetration of injected plasmid DNA from blood vessels into hepatocytes under physical pressure. In order to allow a permanent integration and expression of target genes, a Sleeping Beauty transposon (SB) system was used to mediate genomic integration of the *pT3-EF1α* vectors [64]. The *pT3-EF1α-c-MYC* (12.5 μg) vector was combined with *pT3-EF1α-hScrib*^{WT}*-GFP* or *pT3-EF1α-hScrib*^{P305L}*-GFP* (12.5 μg) plasmids and mixed with SB (5 μg) in 2 ml (approximately 10% of animal body weight) sterile PBS for each mouse. Before injection, plasmid solutions were pre-warmed at 37´°C in a water bath and transferred in a 2 ml syringe. For injection, FVB/N mice at the age of 10 weeks were fixed in a mouse restrainer. Plasmid solution was injected into the lateral-tail vein within 7-10 seconds. As a control, *pT3-EF1α-c-MYC* (12.5 μg) vector combined with *pT3-EF1α-GFP* (12.5 μg) was injected. The transient transfection efficiency can be analyzed 48 hours after injection by IHC stains of GFP. However, because the SB-induced genomic integration was applied in this technique, stable expression of transgenes was analyzed 2 weeks after injection.

4.7.2 Isolation of mouse liver tissue

Four weeks after HDTV, liver tissue was isolated from injected mice for protein and histological analysis. The mice were sacrificed by CO2 asphyxiation. The abdominal cavity was carefully opened with a surgical scissor; the gastric system was removed to the right side. The ligaments on the anterior and superior liver surface were separated from the diaphragm. Afterwards, the mouse liver was slightly removed from the *porta hepatis* using a surgical tweezer. The inferior surface of liver was carefully separated from abdominal organs. The isolated livers were briefly washed with PBS, and put on a 10 cm cell culture dish. Individual lobes were separated using a surgical scalpel (blade #22).

The isolated liver tissues were immediately fixed in buffered formalin for 2 days followed by IHC staining (Chapter 4.5.8). In addition, small pieces of liver tissues were transferred into Precellys tubes and transferred to liquid nitrogen for protein and RNA purification. The methods for protein and RNA extraction are described in 4.5.1 and 4.4.1 respectively. For long-term storage, the protein and RNA samples were stored at -80°. Representative IHC photos from isolated livers showing the Scrib-positive cells 2 days after injection are presented in Figure 7.

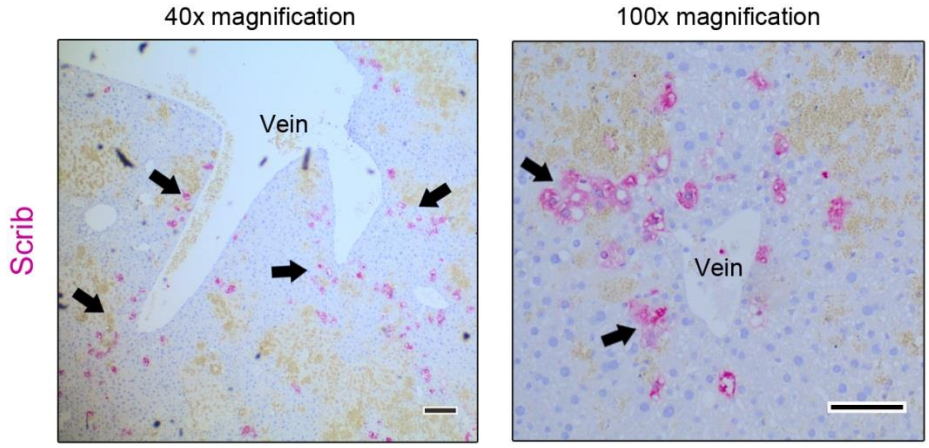

Figure 7: Transient transfection of *pT3-EF1α-hScrib^{P305L}-GFP* plasmid in mouse liver. A mouse liver was collected 2 days after the HDTV injection of *pT3-EF1α-hScrib^{P305L}-GFP* and *pT3-EF1α-c-MYC* plasmids. The mouse liver was fixed in buffered formalin for 2 days, and continued with IHC stains of Scrib. Positive cells with transient Scrib expression (indicated by arrows) were observed surrounding the veins of liver. Photos were taken under 40x magnification, with scale bar: 500 µm; and 100x magnification, with scale bar: 200 µm.

4.8 HCC Patient material

4.8.1 HCC patient gene expression and survival data

Transcriptome and clinical data derived from 249 primary HCCs and corresponding non-tumorous liver tissues were used for this study [65]. Expression levels of 33 polarity genes were compared between HCCs (n=249) and non-tumor livers (n=239). Overall survival and recurrence-free survivals of HCC patients (n=242) were analyzed using Kaplan-Meier curves and statistically compared using the Log-Rank Test. Chromosomal gains and losses were calculated by analyzing CGH array data derived from 60 HCC patients out of the transcriptome cohort [66]. In order to characterize the subcellular localization of Scrib in tissues, cryo-conserved non-tumorous livers (n=20) as well as HCC tissues (n=32) were obtained from the NCT tissue bank Heidelberg (application no. 1921). The project was approved by the ethics committee of Heidelberg University.

4.8.2 HCC tissue-microarray (TMA) analysis

The TMA used for IHC analysis consisted of non-tumor livers (n=7) and HCC tissues (n=105). The histological grading of HCC tissues was done by an experienced hepato-pathologist (G1=10, G2=75, G3=16, G4=4). Immunohistochemistry stains were analyzed according to both quantitative and qualitative parameters. For quantitative parameter, number of cells was analyzed: 0=no positive cells, 1=less than 1%, 2=less than 10%, 3=10-50%, 4=more than 50%. For qualitative parameter, staining intensity was analyzed: 0=negative, 1=low, 2=medium, 3=strong. The final score was given by multiplying quantitative and qualitative parameters. Evaluation was done by two experienced investigators.

4.9 Data acquisition and statistical analysis

Data are presented as mean ± standard deviation. IBM SPSS Statistics (21.0, Armonk, NY, USA) was used to perform statistical analysis. The Mann-Whitney U test was used to compare nonparametric variables between two independent groups. The Spearman rank coefficient test was used to find associations between variables. Patient survival and recurrence data were analyzed by the Log-Rank Test. All *in vitro* experiments were repeated 2-3 times.

Best Cutoff Finder was applied to define two groups of patients for survival analysis [67]. JASPAR data base was used to identify the potential AP1 family binding site on SPARC promoter region [68]. ImageJ software was used to add scale bars for photos. Adobe Photoshop CS5 was employed for the design and alignment of figures.

5 RESULTS

5.1 Overexpression of Scrib is associated with poor survival in HCCs

The hypothesis of this study was that dysregulation of single molecules of EPP system, which leads to a functionally disturbance of hepatocyte polarity, may also play an important role in the process of HCC development. In order to identify functionally relevant factors, mRNA expression data of polarity proteins were analyzed in a HCC cohort of 249 patients [65]. Candidate polarity genes included 33 different factors, which belong to the three major polarity complexes: Crumbs complex, PAR complex, and Scrib complex. Additional genes (e.g. CTNNA1 and CTNNB1) are closely related to cell-cell junctions. The selection criteria were (1) overexpression of the polarity gene in HCC tissues compared to the surrounding liver tissues; (2) expression level of candidate gene was associated with both overall survival and recurrence-free survival of HCC patients. Among the 33 polarity genes, six genes achieved these criteria: CDC42, CTNNA1, DLG5, MPP5, SCRIB and TJP1. A summary of the expression and survival data from all the 33 polarity genes is listed in Table 28. The comparisons of mRNA expressions between livers and HCCs, as well as the Kaplan-Meier survival curves for the six candidate genes are shown in Figure 8.

Table 28: Analysis of 33 polarity genes in human HCC and liver tissues

Gene Symbols	Gene Names	HCCs compared to livers	Survival correlation	Recurrence correlation
AMOT	Angiomotin	Underexpressed	Yes	No
AMOTL2	Angiomotin like 2	Underexpressed	No	No
CDC42	**Cell Division Cycle 42**	**Overexpressed**	**Yes**	**Yes**
CDH1	Cadherin 1	Underexpressed	Yes	Yes
CLDN1	Claudin 1	ns	No	No
CRB1	Crumbs 1, Cell Polarity Complex	ns	No	No
CTNNA1	**Catenin Alpha 1**	**Overexpressed**	**Yes**	**Yes**
CTNNB1	Catenin Beta 1	Overexpressed	No	No
DLG1	Discs Large MAGUK Scaffold Protein 1	Overexpressed	No	Yes
DLG2	Discs Large MAGUK Scaffold Protein 2	Underexpressed	Yes*	No
DLG3	Discs Large MAGUK Scaffold Protein 3	Underexpressed	No	No
DLG4	Discs Large MAGUK Scaffold Protein 4	Underexpressed	Yes	No
DLG5	**Discs Large MAGUK Scaffold Protein 5**	**Overexpressed**	**Yes**	**Yes**
INADL	PATJ, Crumbs Cell Polarity Complex Component	Underexpressed	No	No
LIN7C	Lin-7 Homolog C, Crumbs Cell Polarity Complex Component	Underexpressed	Yes	Yes
LLGL1	Lethal Giant Larvae Homolog 1	Underexpressed	Yes	Yes
LLGL2	Lethal Giant Larvae Homolog 2	Overexpressed	No	no
MPP1	Membrane Palmitoylated Protein 1	Underexpressed	No	Yes
MPP5	**Membrane Palmitoylated Protein 5**	**Overexpressed**	**Yes**	**Yes**
PARD3	Par-3 Family Cell Polarity Regulator	Overexpressed	No	No
PARD6A	Par-6 Family Cell Polarity Regulator	Underexpressed	No	No
PARD6B	Par-6 Family Cell Polarity Regulator Beta	Underexpressed	No	No
PRKCZ	Protein Kinase C Zeta	Underexpressed	No	No
SCRIB	**Scribbled Planar Cell Polarity Protein**	**Overexpressed**	**Yes**	**Yes**
TJP1	**Tight Junction Protein 1**	**Overexpressed**	**Yes**	**Yes***
TJP2	Tight Junction Protein 2	Underexpressed	Yes	No
WWC1	WW And C2 Domain Containing 1	Overexpressed	No	No
CRB2	Crumbs 2, Cell Polarity Complex Component	ns	No	No
CRB3	Crumbs 3, Cell Polarity Complex Component	ns	No	No
MPP4	Membrane Palmitoylated Protein 4	ns	No	No
MPP7	Membrane Palmitoylated Protein 7	ns	No	No
PARD6G	Par-6 Family Cell Polarity Regulator Gamma	ns	No	No
AMOTL1	Angiomotin like 2	ns	No	No

* Small group size according to the "Cutoff Finder". **Bold characters**: genes significantly overexpressed in HCC patients and associated with poor overall survival and cancer recurrence.

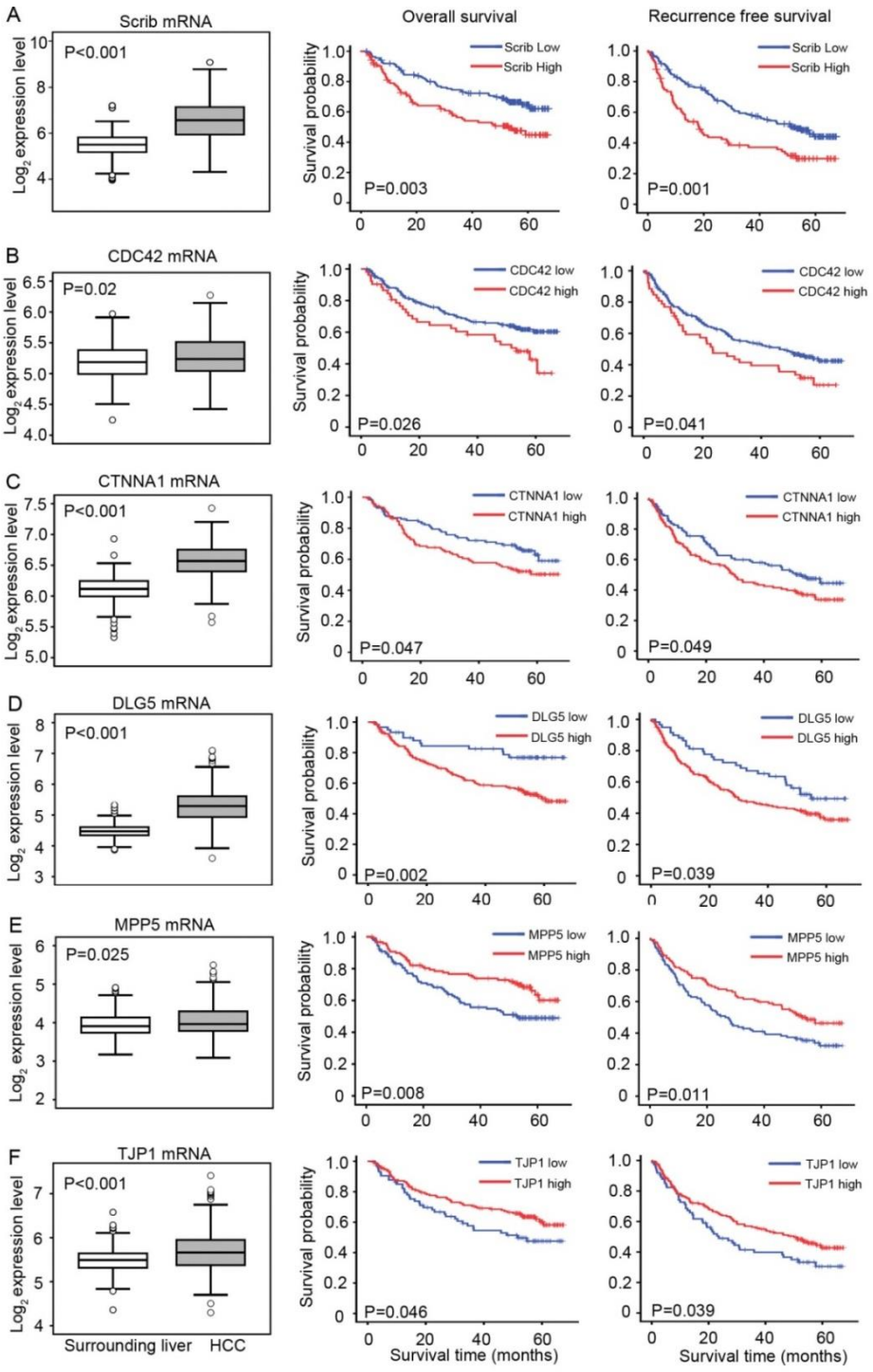

Figure 8: Polarity gene expression of five candidate polarity genes correlated with HCC patient survivals. (A) Gene transcriptome analysis of Scrib mRNA levels in HCC tissues (n=247) compared to non-tumor liver tissues (n=239). Cutoff value (Log_2 mRNA expression) was 6.742 for overall survival, and 6.879 for recurrence free survival. **(B)** For CDC42, cutoff value was 5.56 for both overall and recurrence free survivals. **(C)** For CTNNA1, cutoff value was 6.55. **(D)** For DLG5, cutoff value was 4.90. **(E)** For MPP5, cutoff value was 3.96. **(F)** For TJP1, cutoff value was 5.45. The log-rank test was used for the statistical comparison of groups.

Among the 6 polarity genes, MPP5 and TJP1 were moderately but significantly overexpressed in the group of HCCs. Nevertheless, this elevated expressed of MPP5 and TJP1 was associated with better patient survival (Figure 8 E/F). Notably, Scrib showed the strongest induction (2.14-fold) in HCC tissues compared to surrounding liver tissues. In addition, its overexpression showed the strongest association with poor overall and recurrence-free survival. For this reason and because the functional impact of Scrib overexpression was never systematically analyzed in HCC, Scrib was selected for further analysis.

In order to find out if the overexpression of Scrib in HCCs was due to genomic alterations, the mRNA expression data derived from human HCCs was compared with array-based comparative genomic hybridization (array-CGH) data [66]. In an aCGH data subset of 60 patients, amplifications of Scrib at the gene locus (chr. 8q24.3) were detected in 11 patients. Indeed, the Scrib mRNA expression levels in these patients with chromosomal gains were significantly elevated in comparison to patients without genomic alterations (Figure 9), suggesting that the gains might be causative Scrib overexpression in some HCCs.

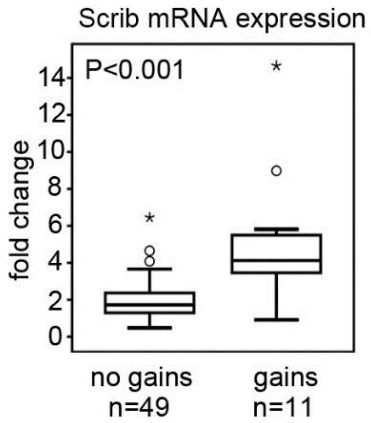

Figure 9: Scrib overexpression was associated with chromosome gains. Scrib mRNA levels were compared between HCC samples with chromosomal gains (n=49), and without chromosomal gains (n=11). The Mann–Whitney U test was used for statistical comparison.

5.2 Mislocalization of Scrib in HCC tissues and cell lines

Scrib is overexpressed in human HCC tissues and elevated Scrib levels may be due to the genetic amplifications. Interestingly, the mislocalization of Scrib has also been described in breast cancer patients [42]. For this reason, I hypothesized that also the localization of Scrib may play a role in the process of HCC development.

In order to characterize Scrib localization in human livers and HCCs, immunofluorescence stains of Scrib were carried out using cyosections from healthy livers (n=20), as well as HCC tissues (n=32). A clear membranous Scrib localization was observed in most (90%) healthy liver tissues (Figure 10A). In contrast, a frequent cytoplasmic Scrib mislocalization was found in the majority of HCC tissues (69%). In tissues with Scrib mislocalization, about 50% of patients had a partial loss of membranous Scrib, while other patients showed a complete membranous loss and cytoplasmic enrichment of Scrib (Figure 10B).

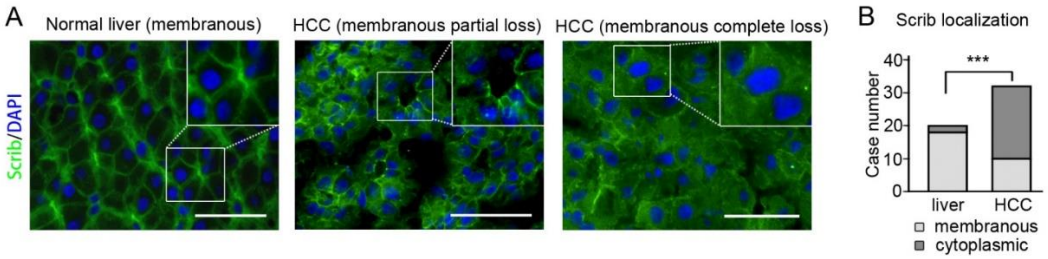

Figure 10: Mislocalization of Scrib in HCC tissues. (A) Representative pictures of Scrib immunofluorescence stains from healthy livers and HCCs. In normal livers, 90% (18/20) of all analyzed samples showed a clear membranous Scrib localization. In HCCs, most of the cases 69% (22/32) had a cytoplasmic localization of Scrib. Scale bars: 200 µm. **(B)** Quantification of Scrib localization in healthy livers and HCCs. The relative amount of cytoplasmic Scrib is significantly higher in HCC tissues compared to healthy livers. Fisher's exact test was performed ($P \leq 0.001$).

In order to test for suitable *in vitro* models for further studies, the expression and localization of Scrib were compared in different HCC cell lines (HepG2, HuH1, Huh6, Hep3B, HLF and HuH7). The mRNA levels of Scrib were higher in most HCC cell lines compared to the immortalized hepatocytes (THLE-2), (Figure 11A). Protein analysis confirmed higher Scrib expression in HCC cell lines compared to the non-malignant cell line. Highest Scrib protein levels were detected in HepG2, HuH6, HLE and HLF cells (Figure 11B). To gain further insight into Scrib localization in HCC cell lines, immunofluorescence of Scrib was carried out in lines with higher protein abundance. HepG2, HuH1 and HuH6 showed a clear membranous localization, while Hep3B, HLF and HuH7 showed a predominately cytoplasmic localization (Figure 11C). These data illustrate that next to overexpression, Scrib is also localized in the cytoplasm in a subgroup of HCC cell lines.

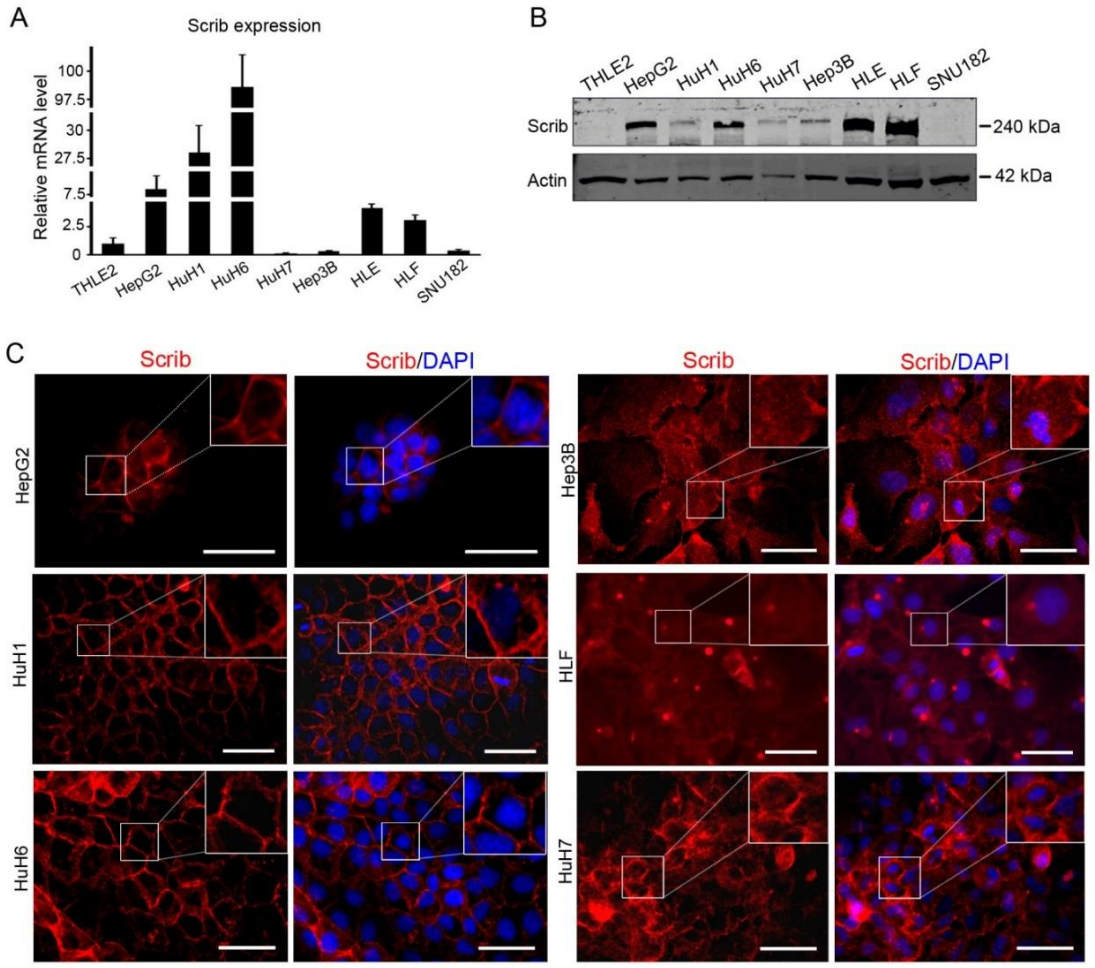

Figure 11: Different expression and localization of Scrib in HCC cell lines. (A) Comparison of Scrib mRNA levels in different HCC cell lines (HepG2, Huh1, Huh6, Huh7, Hep3B, HLE, HLF, and SNU182) and non-malignant THLE-2 cells by real-time PCR. **(B)** Comparison of Scrib protein levels in HCC cell lines and THLE-2 cells using Western immunoblotting. Actin served as the loading control. **(C)** Immunofluorescence analysis reveals differential localizations of Scrib in human HCC cell lines. Magnification: 400-fold, scale bars: 40 µm.

5.3 Scrib localization affects hepatocellular polarity

In order to study the impact of cytoplasmic Scrib in HCC cells, two cell lines stably expressing the wildtype ($Scrib^{WT}$) and mutated Scrib ($Scrib^{P305L}$) were generated. The P305L mutation in the *leucine-rich repeats* (LRR) domain abrogates the binding of Scrib with other cell polarity factor leading to its enforced cytoplasmic localization [69]. Plasmids coding for EGFP-tagged $Scrib^{WT}$ and $Scrib^{P305L}$ were transfected into HepG2 cells, which showed a polarized phenotype as well as a membranous localization of Scrib (Figure 11C). Cell lines stably expressing $Scrib^{WT}$ or $Scrib^{P305L}$ were generated and tested for the localization of exogenous Scrib by immunofluorescence. As expected, $Scrib^{WT}$ localized specifically to the plasma membrane, whereas $Scrib^{P305L}$ predominantly accumulated in the cytoplasm (Figure 12A). The localization of both Scrib isoforms was confirmed by Western immunoblotting using membranous and cytoplasmic protein fractions (Figure 12B).

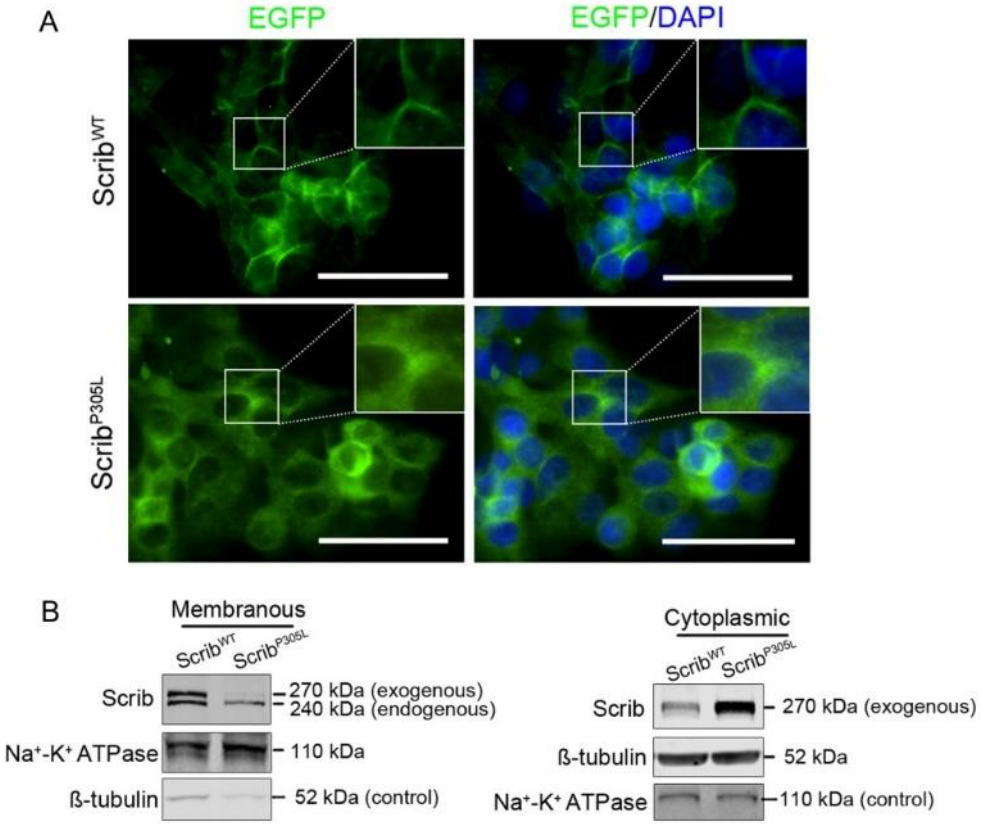

Figure 12: HepG2 stable cell lines with membranous and cytoplasmic Scrib. (A) Immunofluorescence of HepG2 cells stably expressing EGFP-tagged $Scrib^{WT}$ and $Scrib^{P305L}$. Upper right corner show higher magnifications to illustrate the expected subcellular Scrib localization. Scale bars: 40 µm. **(B)** Western immunoblots of protein fractions extracted from $Scrib^{WT}$ and $Scrib^{P305L}$ expressing cells confirm the membranous localization of $Scrib^{WT}$ and cytoplasmic localization of $Scrib^{P305L}$. Na^{+}-K^{+}-ATPase and ß-tubulin served as the loading controls for membranous and cytoplasmic proteins fractions, respectively.

Interestingly, cell lines stably overexpressing Scrib^{WT} and Scrib^{P305L} showed different morphologies when grown on a plastic surface. The Scrib^{WT} cells established a columnar shape and compact multilayer colonies, while the Scrib^{P305L} cells acquired a flattened shape and a monolayer growth pattern (Figure 13A), which is indicative for disturbed cell-cell contact. In order to further analyze the impact of membranous or cytoplasmic Scrib on the 3-dimensional hepatocellular structure, a hepatocyte sandwich culture containing two layers of collagen matrix was used, which allows the formation of highly polarized cells *in vitro* [6]. After seeding the both cell lines under sandwich culture conditions for one week, the cell layers were stained for *multidrug resistance-associated protein 2* (MRP2), which is a marker for the *canalicular* network. Elongated *canalicular* structures were detected in Scrib^{WT} cultures, while only spherical and shortened structures were found in Scrib^{P305L} cultures (Figure 13B). These results indicate that the proper localization of Scrib is critical for the maintenance of hepatocellular polarity.

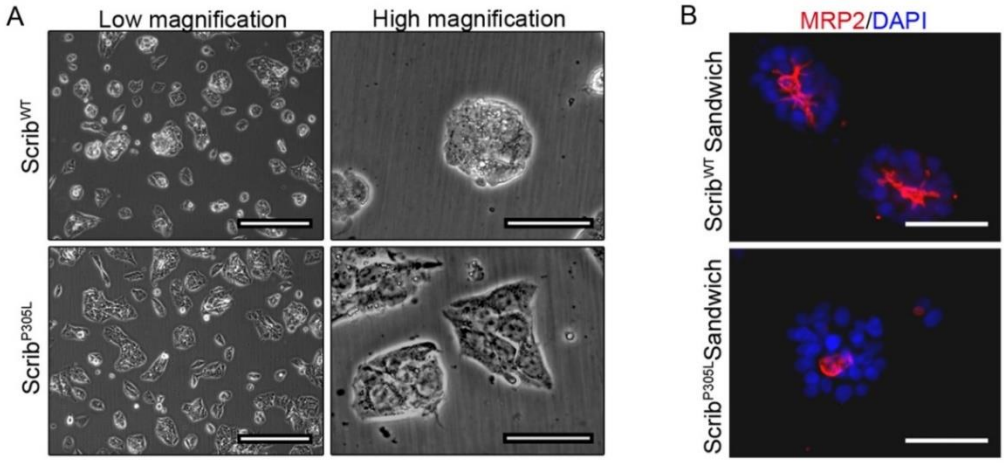

Figure 13: Disturbance of cell polarity by overexpression of cytoplasmic Scrib^{P305L}. (A) Bright field photos of HepG2 cells stably expressing Scrib^{WT} and Scrib^{P305L} indicate differences in cell morphology and cell-cell contact. Low magnification: 100-fold, scale bar: 200 µm; High magnification: 400-fold, scale bar: 40 µm. **(B)** Sandwich culture stains of MRP2 in Scrib^{WT} and Scrib^{P305L} expressed HepG2 cells. Cell lines were seeded at a cell density of 400,000 cells per 6 cm dish between collagen sheets for one week. Immunofluorescence stains of MRP2 were performed to detect the presence of *canalicular* structures. Magnification: 400-fold, Scale bars: 40 µm.

5.4 Cytoplasmic Scrib induces cell invasion in HCC cell lines

The initial correlation of Scrib expression and HCC patient data revealed an association of Scrib abundance and tumor prognosis. In addition, immunofluorescence illustrated the cytoplasmic localization of Scrib in many HCC tissues. In order to find out how cytoplasmic Scrib affects liver cancer progression, functional analyses including cell viability, apoptosis, and invasion assays were performed with $Scrib^{WT}$ and $Scrib^{P305L}$-positive HepG2 cells.

The cell viability assay revealed that cytoplasmic $Scrib^{P305L}$ induced cell viability (Figure 14A), while membranous $Scrib^{WT}$ did not affect viability for up to 48 hours. In addition, a cell cytotoxicity assay illustrated that membranous $Scrib^{WT}$ was associated with increased cell cytotoxicity (Figure 14B), while $Scrib^{P305L}$ only moderately increased cell death in comparison to untransfected HepG2 cells. To further test if the increase of cytotoxicity was due to apoptosis and if Scrib with membranous and cytoplasmic localizations can differently affect drug-induced cell death, a caspase-3 activity assay was performed with both cell lines. Interestingly, the basal caspase-3 activity was not different between $Scrib^{WT}$ and $Scrib^{P305L}$ cells, however, cells expressing $Scrib^{P305L}$ showed relatively lower caspase-3 activity after Doxorubicin treatment (Figure 14C). These data illustrate that cytoplasmic Scrib moderately affects cell apoptosis and that it may protect hepatocyte from cytotoxic challenges.

Because Scrib overexpression significantly correlated with cancer recurrence in HCC patients, additional cell invasion assays were performed. HepG2 cells stably expressing $Scrib^{WT}$ showed a low invasive capacity. In contrast, cells stably expressing $Scrib^{P305L}$ had a significantly higher invasive capacity (Figure 14D).

Together, the functional analyses revealed that cytoplasmic Scrib predominantly supports HCC cell mobility and invasion and to a lesser extent cell viability and apoptosis.

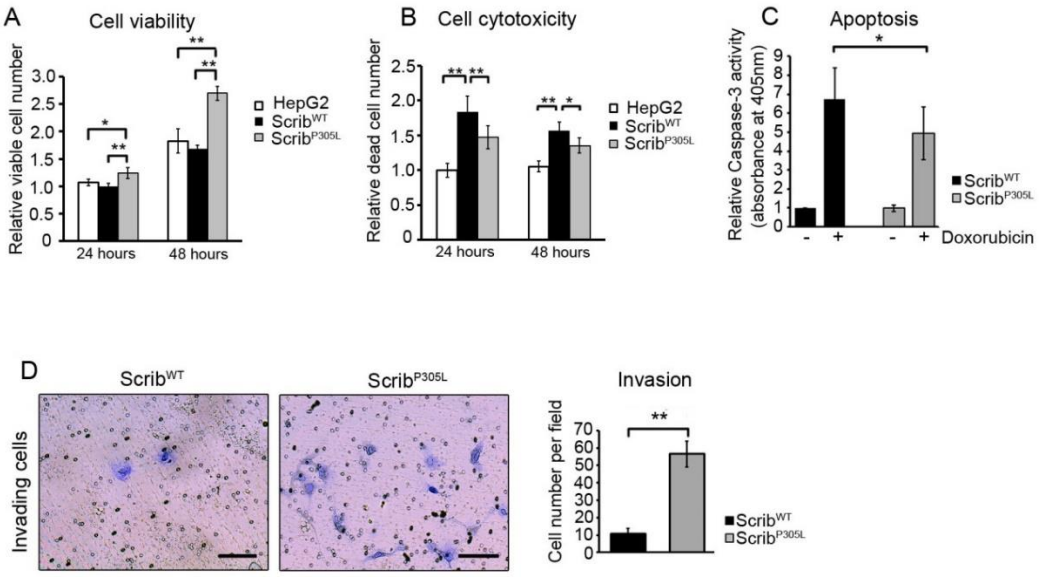

Figure 14: Functional analyses of HepG2 cells with membranous and cytoplasmic Scrib. (A) Cell viability of untransfected HepG2 and HepG2 cells expressing Scrib^{WT} or Scrib^{P305L} were measured 24 and 48 hours after seeding. **(B)** Cell cytotoxicity assay of untransfected HepG2 and cells expressing Scrib^{WT} or Scrib^{P305L} were performed 24 and 48 hours after seeding. **(C)** Scrib^{WT} and Scrib^{P305L} expressing HepG2 cells were treated with Doxorubicin (1 µM) for 24 hours followed by measurement of caspase-3 activity. Cell lysate were incubated with caspase-3 substrate for 4 hours. **(D)** HepG2 cells expressing Scrib^{WT} and Scrib^{P305L} were analyzed using Transwell chambers with Matrigel-coated inserts. The number of transmigrating cells was counted 72 hours after seeding. For each assay, cells were counted in seven different visual fields (40-fold magnification). Photos were taken with 100-fold magnification. Scale bars: 250 µm. For statistical testing, the Mann-Whitney U Test was used.

Because GTPases play an essential role in regulating actin filament in cells which undergo EMT (see Chapter 1.2.3), cytoplasmic Scrib may interaction with GTPases in the regulation of cell invasion. To further figure out the reasons why cytoplasmic Scrib induced HCC cell invasion/migration, the Scrib^{WT} and Scrib^{P305L} cell lines were analyzed with regard to their actin organization as well as the content of Rho family GTPases using immunofluorescence and Western immunoblotting. Indeed, obvious differences were found in case of the actin filament organization. Cells expressing Scrib^{P305L} showed clear actin bundles at the leading and trailing edges, which has been regarded as the typical structure of actin cytoskeleton in invading/migrating cells [70]. Such actin filament structure was less obvious in cells expressing Scrib^{WT} (Figure 15A). Differences

regarding the expressions of Rho family GTPases were also detected in the both stable cell lines. Rac 1/2/3 and CDC42, which were strong inducers of cell invasion/migration, were increased in cells expressing Scrib^{P305L}. However, the negative regulator of cell invasion/migration, RhoA, was not differentially expressed in both cell lines (Figure 15B).

In summary, these data strongly suggest that cytoplasmic Scrib predominantly supports HCC cell mobility and invasion via the regulation of actin filaments and Rho GTPases.

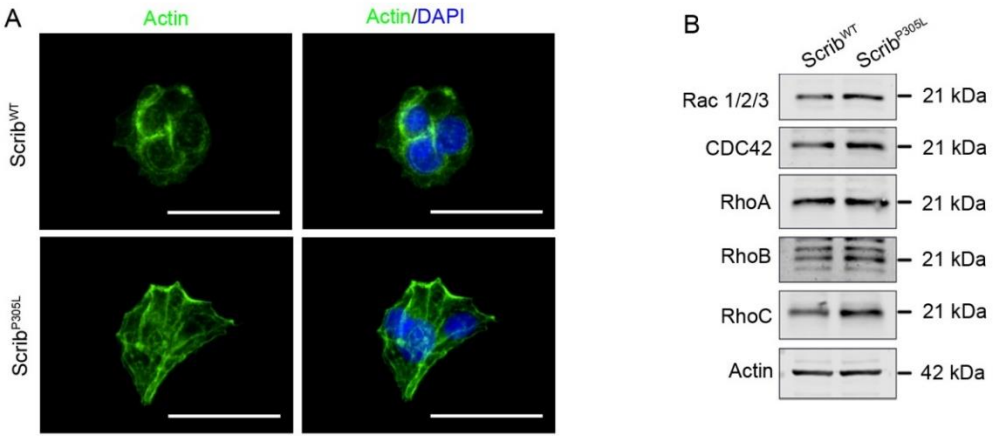

Figure 15: Effects of Scrib^{P305L} on actin filament and Rho GTPases. (A) Immunoflurescence stains of actin in cell lines stably expressing Scrib^{WT} or Scrib^{P305L} indicate differential cytoskeleton organization. Cells were documented with 400-fold magnification. Scale bars: 40 µm. (B) Western immunoblot analysis of Rho-GTPase family proteins in cells with Scrib^{WT} or Scrib^{P305L} expression.

5.5 Cytoplasmic Scrib induces tumor formation via AKT signaling

In the next step, we wanted to identify the relevant signaling pathways that were induced by cytoplasmic Scrib. Previous studies already demonstrated the regulatory effects of Scrib on *extracellular signal-regulated kinases* (ERK) and Hippo pathway activity [50, 71]. We first tested if the transcriptional downstream effector of the Hippo pathway YAP was affected by the cytoplasmic $Scrib^{P305L}$ in comparison to membranous $Scrib^{WT}$. Because YAP phosphorylation regulates its subcellular localization, the phospho-status of YAP was considered to be a good read-out for the Hippo/YAP pathway activity [46]. However, no difference regarding YAP phosphorylation was observed in HepG2 cells stably expression both Scrib isoforms (Figure 16A). In addition, the localization YAP and its paralogue TAZ after siRNA-mediated inhibition of Scrib in untransfected HepG2 cells was analyzed. Again no nuclear enrichment of YAP or TAZ was detected after Scrib silencing (Figure 16B). These results indicate that no direct effect of Scrib on Hippo/YAP pathway activity is detectable in HCC cells.

In the next step, other signaling pathways (ERK1/2, JNK and AKT pathways) that may be affected by Scrib were analyzed. In HepG2 cells stably expressing $Scrib^{WT}$ or $Scrib^{P305L}$, neither the ERK1/2 nor the JNK pathways were significantly regulated by the different Scrib isoforms (Figure 16C). However, the AKT/mTOR pathway was obviously induced by cytoplasmic Scrib. Phosphorylation of AKT and its downstream target phospho-S6 protein were both induced in cells expressing $Scrib^{P305L}$ in comparison to cells with $Scrib^{WT}$ expression (Figure 16C). In order to test if the induction of AKT depends on its physiological regulator phosphoinositide 3-kinases (PI3K), PI3K activity was inhibited by using Wortmannin. AKT activation was blocked under high dose (0.5 μM) in both tested cell lines. However, using lower doses (0.05-0.25 μM), Wortmannin completely blocked AKT phosphorylation in cells expressing $Scrib^{WT}$, but not in cells expressing $Scrib^{P305L}$ (Figure 16D). These results illustrate that AKT/mTOR pathway was activated by the overexpression of cytoplasmic Scrib in a PI3K-independent manner.

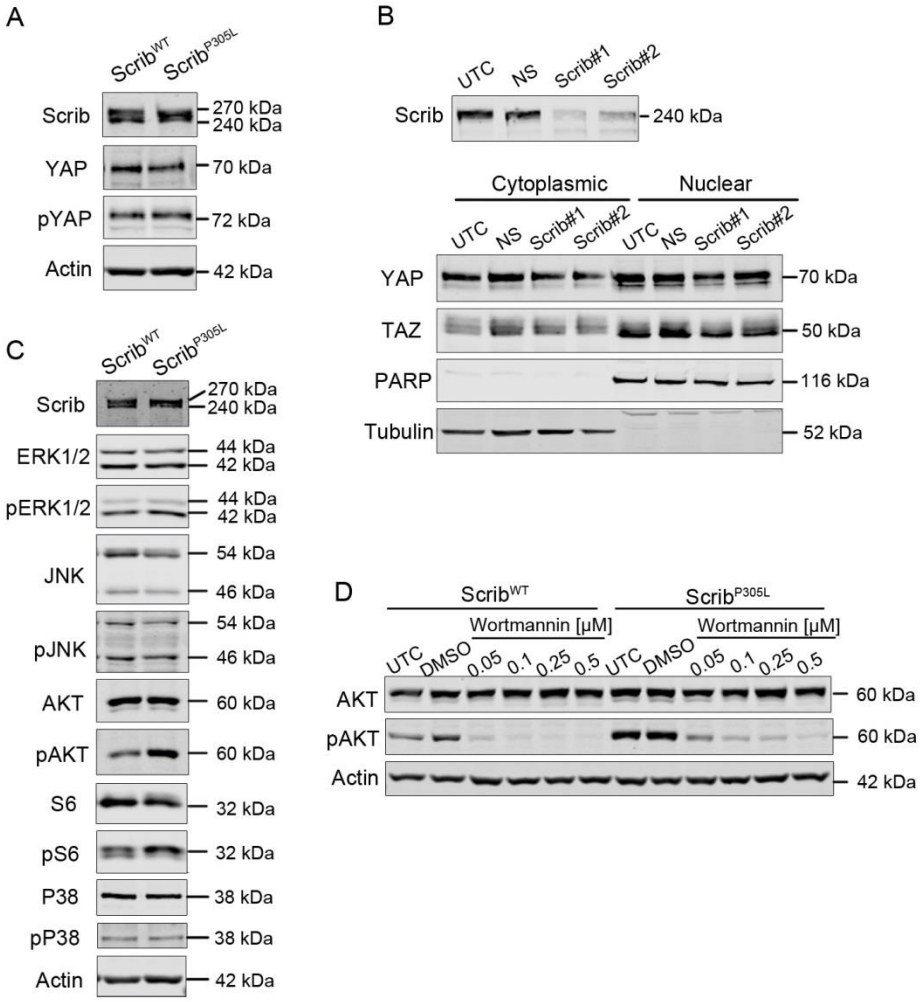

Figure 16: Cytoplasmic Scrib activates the AKT/mTOR pathway. (A) Western immunoblot analysis illustrate that neither total YAP nor phospho-YAP are differentially expressed in $Scrib^{WT}$ and $Scrib^{P305L}$ cells. **(B)** siRNA-mediated Scrib inhibition cannot induce the nuclear enrichment of YAP or its paralogue TAZ in HepG2 cells. Proteins from cytoplasmic and nuclear fractions were isolated 60 hours after siRNA treatment. PARP and ß-tubulin served as the loading controls for nuclear and cytoplasmic protein fractions, respectively. UTC: untreated cell, NS: non-sense siRNA. **(C)** Western immunoblot of protein lysates derived from $Scrib^{WT}$ and $Scrib^{P305L}$-expressing HepG2 cells shows increased phosphorylation of AKT and its downstream target S6 protein in the cells expressing $Scrib^{P305L}$. **(D)** Western immunoblot analysis of Wortmannin-treatment cells illustrates the PI3K-independent activation of the PI3K/AKT pathway in cells stable stably expressing $Scrib^{P305L}$. DMSO: DMSO-treated cells.

5.6 Cytoplasmic Scrib destabilizes the phosphatases PTEN and PHLPP1

To further define the molecular mechanism how cytoplasmic Scrib activates the PI3K/AKT pathway, two PI3K phosphatases: *phosphatase and tensin homolog* (PTEN) and *PH domain leucine-rich repeat-containing protein phosphatase 1* (PHLPP1) were chosen as candidates for further analysis. Previous studies already illustrated an interaction between Scrib and PTEN in breast cancer cells and between Scrib and PHLPP1 in colon cancer cells [42, 72]. For this reason, I hypothesized that cytoplasmic Scrib activates PI3K/AKT pathway *via* physical interactions with PHLPP1 or PTEN in HCC cells. Interestingly, Co-IP experiments confirmed the bindings of both Scrib isoforms ($Scrib^{WT}$ and $Scrib^{P305L}$) with both phosphatases (PHLPP1 and PTEN). However, no significant difference in the binding capacity was detectable, indicating that Scrib localization did not change the binding properties with PHLPP1 and PTEN (Figure 17A, B).

Because the Scrib localization did not affect PTEN/PHLPP1 binding, it was interesting to analyze if and how both phosphatases were involved in the regulation of AKT in HepG2 cells. To first confirm the inhibitory effect of PHLPP1 and PTEN on AKT phosphorylation and activity, a siRNA-mediated knockdown of PHLPP1, PTEN and both phosphatases was carried out. Silencing of PTEN or PHLPP1 resulted in a 1.6-fold and a 1.2-fold increase in phospho-AKT, respectively. The strongest effect on AKT phosphorylation was detectable after combined PTEN/PHLPP1 inhibition (1.9-fold increase, Figure 17C). These results confirmed the relevance of both phosphatases in the regulation of AKT. However, how the phosphatases affect AKT activation in HCC cells was unclear.

Although $Scrib^{WT}$ and $Scrib^{P305L}$ didn't show differential binding to PHLPP1 and PTEN, the subcellular localizations of Scrib/PHLPP1/PTEN complexes, which is closely associated with the activity of both phosphatases, might vary. For example, post-translational modifications of PTEN at its membranous-associated PDZ domain led to changed protein stability [73]. For this reason, the subcellular localizations of PHLPP1

and PTEN were compared in both cell lines stably expressing Scrib^{WT} and Scrib^{P305L} by western immunoblotting. Indeed, PHLPP1 and PTEN were predominately reduced in the membranous fractions of Scrib^{P305L}-expressing cells (PTEN: 67% reduction; PHLPP1: 62% reduction, Figure 17D). The possibility of transcriptional regulation of PHLPP1 and PTEN in these cells was excluded by real-time PCR (Figure 17E).

In cells with cytoplasmic Scrib, PHLPP1 and PTEN levels were reduced especially at the plasma membrane, which may be associated with decreased protein stabilities. To further analyze the impact of cytoplasmic Scrib on PHLPP1 and PTEN stability, protein lysates were collected at different time points after the administration of protein synthesis inhibitor CHX. Indeed, both PHLPP1 and PTEN were degraded much faster in the cells expressing Scrib^{P305L} than Scrib^{WT}. The half-life of PHLPP1 was 6 hours in Scrib^{WT} cells and 3.5 hours in Scrib^{P305L} cells. Similarly, the half-life of PTEN was 48 hours in Scrib^{WT} cells and 32 hours in Scrib^{P305L} cells (Figure 17F). In order to figure out if the decreased phosphatase stability was due to the increased proteasomal activity, Scrib^{WT} cells and Scrib^{P305L} cells were treated with proteasome inhibitor MG132 to block protein degradation. Interestingly, both phosphatases PHLPP1 and PTEN were obviously increased in Scrib^{P305L} cells but not in Scrib^{WT} cells (Figure 17G). Moreover, immunoprecipitation analysis of PHLPP1 and PTEN detected higher amount of ubiquitinated PHLPP1 and PTEN in Scrib^{P305L} cells compared to Scrib^{WT} cells (Figure 17H).

These results revealed that the interaction between membranous and cytoplasmic Scrib PHLPP1 and PTEN at specific subcellular locations. In addition, cytoplasmic-localized Scrib leads to augmented degradation of PHLPP1 and PTEN *via* ubiquitination, which eventually activates PI3K/AKT-mediated signaling.

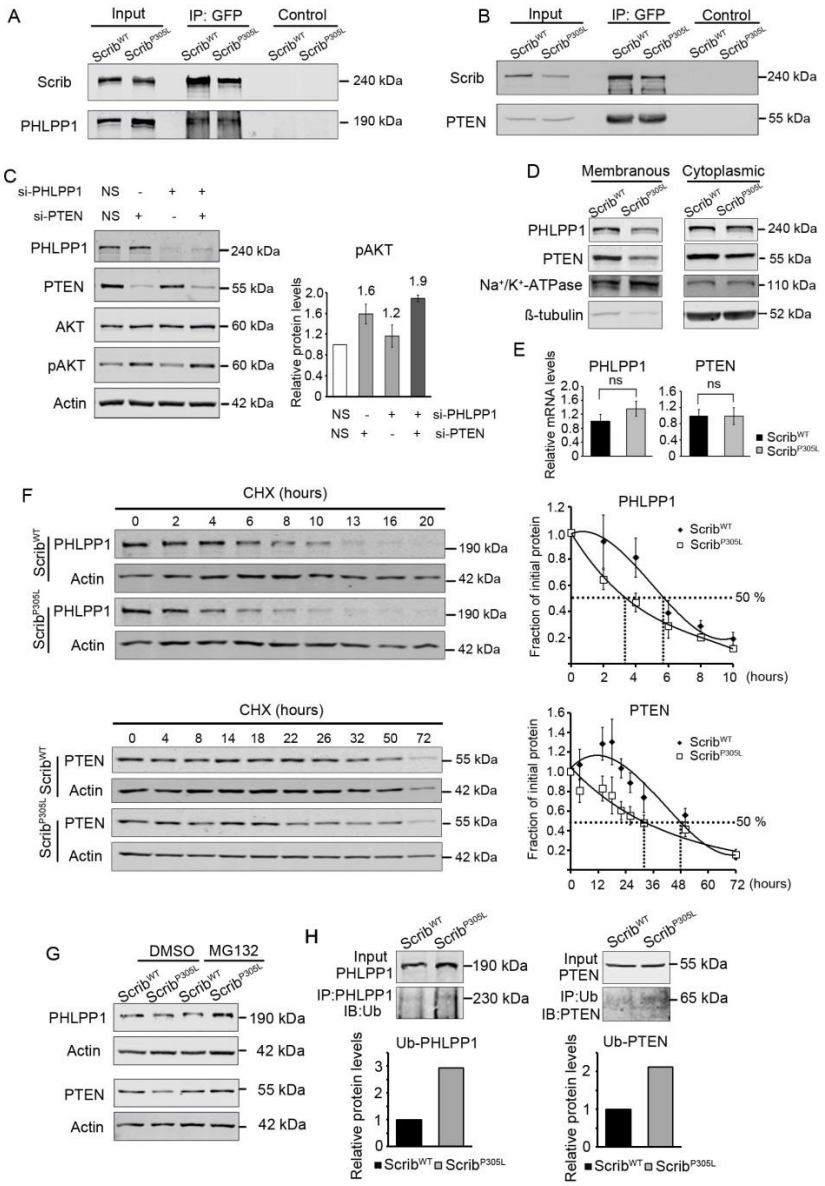

Figure 17: Cytoplasmic Scrib destabilizes the phosphatases PTEN and PHLPP1. (A) Co-IP experiments illustrate the interactions between PHLPP1 with Scrib^{WT} and Scrib^{P305L}. Scrib was precipitated using an antibody against GFP. **(B)** Co-IP experiments demonstrate the interactions between PTEN with Scrib^{WT} and Scrib^{P305L}. For (A) and (B), equal amounts of IgG antibody were used as negative controls. **(C)** Western immunoblot of phospho-AKT after siRNA-mediated inhibition of PTEN and PHLPP1. Bar chart shows the normalized results from 3 independent experiments. Nonsense siRNA (NS) was used as a control. **(D)** Protein analysis of PHLPP1 and PTEN in membranous and cytoplasmic protein fractions. Na^+-K^+-ATPase and ß-tubulin served as the loading controls for membranous and cytoplasmic fractions respectively. **(E)** Real-time PCR compares the mRNA levels of PHLPP1 or PTEN in Scrib^{WT} and Scrib^{P305L} cells. **(F)** CHX protein stability assays of PHLPP1 and PTEN in cells expressing Scrib^{P305L}. Polynomial regression graphs for PHLPP1 and PTEN were plotted from 3 independent experiments. **(G)** Cells were treated with MG132 (1 μM) overnight before protein isolation. DMSO served as a negative control. **(H)** Cells were pre-treated with MG132 (1 μM) overnight. For PHLPP1, protein was isolated under denatured condition, and detected with ubiquitination antibody. For PTEN, protein was precipitated with ubiquitin and detected with PTEN antibody. IP: immunoprecipitation, IB: immunoblotting.

5.7 Identification of target genes induced by cytoplasmic Scrib

To identify the functional relevant downstream effector mechanisms of cytoplasmic Scrib, transcriptome analysis of cells stably expressing of $Scrib^{WT}$ and $Scrib^{P305L}$ was performed. For each RNA sample, three biological replicates were analyzed. Genes with changes ≥1.6 fold or ≤0.63 fold and with adjusted P-value ≤0.05 were selected. According to these criteria, 81 upregulated genes and 54 downregulated genes were found in $Scrib^{P305L}$ expressing cells. KEGG database was used to for the network enrichment analysis of gene signatures and the GeneCards database was used for the functional annotation of selected genes [74, 75].

Two groups of target genes (downregulated or upregulated) were selected according to their differential expression in $Scrib^{P305L}$-positive cells compared to $Scrib^{WT}$-positive cells. In the group of downregulated genes (n=54), three genes were described to be the WNT pathway inhibitors (BICC1, DKK1 and DKK4) according to the functional annotation by GeneCards database (Figure 18). In the group of positively regulated genes (n=81), 19 genes (23%) were related to cell invasion/migration according to the functional annotation and relevant publications. These 19 genes play a role in epithelial-mesenchymal transition (EMT), tumor extracellular matrix (ECM) remodeling and actin reorganization (Figure 19).

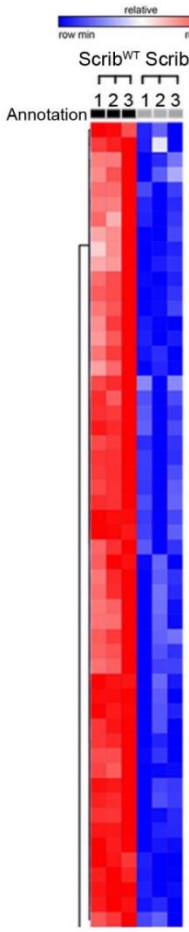

Genes downregulated in Scrib^{P305L} cells

Gene Symbol	Reference ID	Gene Name	Expression fold (Scrib^{P305L}/Scrib^{WT})
MYL9	NM_006097	myosin light chain 9	0.39
TINAG	NM_014464	tubulointerstitial nephritis antigen	0.47
SNORD116-14	NR_003329	small nucleolar RNA, C/D box 116-14	0.51
TTPA	NM_000370	tocopherol (alpha) transfer protein	0.47
SCGN	NM_006998	secretagogin, EF-hand calcium binding protein	0.42
FGL1	NM_004467	fibrinogen-like 1	0.47
PWAR5	NR_022008	Prader Willi/Angelman region RNA 5	0.45
SEC24A	NM_001252231	SEC24 homolog A, COPII coat complex component	0.55
SAR1B	NM_001033503	secretion associated Ras related GTPase 1B	0.53
FREM1	NM_001177704	FRAS1 related extracellular matrix 1	0.41
ASAH2	NM_001143974	N-acylsphingosine amidohydrolase 2	0.62
DKK1**	NM_012242	dickkopf WNT signaling pathway inhibitor 1	0.37
HTR1D	NM_000864	5-hydroxytryptamine (serotonin) receptor 1D	0.58
DKK4**	NM_014420	dickkopf WNT signaling pathway inhibitor 4	0.43
CCL20	NM_001130046	chemokine (C-C motif) ligand 20	0.56
MTTP	NM_000253	microsomal triglyceride transfer protein	0.57
ATP10D	NM_020453	ATPase, class V, type 10D	0.58
ALCAM	NM_001243280	activated leukocyte cell adhesion molecule	0.20
CDO1	NM_001801	cysteine dioxygenase type 1	0.45
GPC4	NM_001448	glypican 4	0.26
ROR1	NM_001083592	receptor tyrosine kinase like orphan receptor 1	0.35
NR5A2	NM_001276464	nuclear receptor subfamily 5, group A, member 2	0.41
FKBP11	NM_001143781	FK506 binding protein 11, 19 kDa	0.25
FABP1	NM_001443	fatty acid binding protein 1	0.62
FGB	NM_001184741	fibrinogen beta chain	0.38
BICC1**	NM_001080512	BicC family RNA binding protein 1	0.22
PAQR9	NM_198504	progestin and adipoQ receptor family member 9	0.33
TTR	NM_000371	transthyretin	0.52
UGT2B4	NM_001297615	UDP glucuronosyltransferase family 2 member B4	0.17
PIK3AP1	NM_152309	phosphoinositide-3-kinase adaptor protein 1	0.57
SLC17A2	NM_001286123	solute carrier family 17, member 2	0.62
ALDOC	NM_005165	aldolase, fructose-bisphosphate C	0.61
SLC27A2	NM_001159629	solute carrier family 27 member 2	0.56
ABCG2	NM_001257386	ATP-binding cassette, sub-family G member 2	0.59
DPYD	NM_000110	dihydropyrimidine dehydrogenase	0.49
SLC10A5	NM_001010893	solute carrier family 10, member 5	0.53
NT5E	NM_001204813	5'-nucleotidase, ecto (CD73)	0.51
CITED2	NM_001168388	Cbp/p300-interacting transactivator with Glu/Asp rich carboxy-terminal domain 2	0.58
MAT1A	NM_000429	methionine adenosyltransferase I, alpha	0.61
ONECUT1	NM_004498	one cut homeobox 1	0.34
STXBP1	NM_001032221	syntaxin binding protein 1	0.49
FST	NM_006350	follistatin	0.34
SLC6A14	NM_007231	solute carrier family 6 member 14	0.54
ROBO1	NM_001145845	roundabout guidance receptor 1	0.61
TRAJ28	NA	T cell receptor alpha joining 28	0.58
XBP1	NM_001079539	X-box binding protein 1	0.50
LINC00261	NR_001558	long intergenic non-protein coding RNA 261	0.56
THBS1	NM_003246	thrombospondin 1	0.59
ZNRF3	NM_001206998	zinc and ring finger 3	0.62
SCARA3	NM_016240	scavenger receptor class A, member 3	0.29
CLU	NM_001831	clusterin	0.49
HIST1H2AG	NM_021064	histone cluster 1, H2ag	0.24
BPIFB2	NM_025227	BPI fold containing family B, member 2	0.50
SLC22A3	NM_021977	solute carrier family 22	0.60

Figure 18: Genes downregulated in Scrib^{P305L} cells. The heatmap shows the 54 genes significantly downregulated in the cell line stably expressing cytoplasmic Scrib^{P305L} in comparison to Scrib^{WT} cells ($P \leq 0.05$, fold change ≤ 0.63). Gene expression level is depicted by the blue-red intensities (blue indicates reduced genes). RNA samples and genes names of potential downstream targets are listed in x- and y-axis respectively. ****** indicates genes negatively regulating WNT signalling pathway.

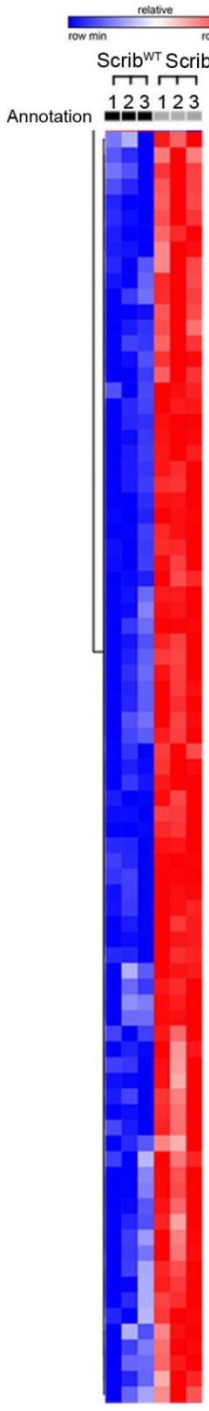

Genes upregulated in Scrib^{P305L} cells

Gene Symbol	Reference ID	Gene Name	Expression fold (Scrib^{P305L}/Scrib^{WT})
FHL2	NM_001039492	four and a half LIM domains 2	1.61
RAB31	NM_006868	RAB31, member RAS oncogene family	1.90
CKAP4	NM_006825	cytoskeleton-associated protein 4	1,90
ADGRG3*	NM_001308360	adhesion G protein-coupled receptor G3	2.99
HP	NM_001126102	haptoglobin	1.78
ITPR3	NM_002224	inositol 1,4,5-trisphosphate receptor, type 3	1.93
PYGO1	NM_015617	pygopus family PHD finger 1	2.49
LGALS1*	NM_002305	lectin, galactoside-binding, soluble, 1	1.94
LINC01234	NR_110025	long intergenic non-protein coding RNA 1	2.23
LOC100996579	NR_110163	uncharacterized LOC100996579	1.73
ISM1	NM_080826	isthmin 1, angiogenesis inhibitor	2.02
CDCA7L	NM_001127370	cell division cycle associated 7-like	3.65
SCN1A	NM_001165963	sodium voltage-gated channel alpha subunit 1	1.91
ACTA1	NM_001100	actin, alpha 1, skeletal muscle	1.66
ZNF486	NM_052852	zinc finger protein 486	1.70
CLDN6*	NM_021195	claudin 6	3.36
MB21D2	NM_178496	Mab-21 domain containing 2	1.69
CDH2*	NM_001308176	cadherin 2, type 1, N-cadherin	6.01
ANXA3	NM_005139	annexin A3	2.74
MAP1B	NM_005909	microtubule-associated protein 1B	3.61
PIEZO2	NM_022068	piezo-type mechanosensitive ion channel	3.25
CYP24A1	NM_000782	cytochrome P450, family 24, subfamily A,	4.23
ANKRD1	NM_014391	ankyrin repeat domain 1	3.27
KCNJ10	NM_002241	potassium channel, inwardly rectifying s	1.97
SLC2A3	NM_006931	solute carrier family 2	13.48
MATN3*	NM_002381	matrilin 3	2.90
CEACAM1*	NM_001024912	carcinoembryonic antigen related cell adhesion molecule 1	1.78
C12orf75	NM_001145199	chromosome 12 open reading frame 75	4.22
SULF2	NM_001161841	sulfatase 2	1.72
ERP27	NM_001300784	endoplasmic reticulum protein 27	3.19
ZNF114	NM_001301062	zinc finger protein 114	1.65
TMC7	NM_001160364	transmembrane channel-like 7	2.52
DCBLD2	NM_080927	CUB and LCCL domain containing 2	1.70
S100A10*	NM_002966	S100 calcium binding protein A10	1.88
PAM	NM_000919	peptidylglycine alpha-amidating monooxyg	2.39
FAM198B	NM_001031700	family with sequence similarity 198, mem	2.27
SERPINB9	NM_004155	serpin family B member 9	1.72
SLC16A6	NM_001174166	solute carrier family 16, member 6	2.96
NFE2L3	NM_004289	nuclear factor, erythroid 2-like 3	5.00
MXRA7*	NM_001008528	matrix-remodelling associated 7	1.82
OXCT1	NM_000436	3-oxoacid CoA transferase 1	2.91
SERPINE1	NM_000602	serpin peptidase inhibitor, clade E	2.71
KRT23	NM_001282433	keratin 23, type I	3.47
MT2A	NM_005953	metallothionein 2A	1.77
NRCAM*	NM_001037132	neuronal cell adhesion molecule	2.50
KRT19	NM_002276	keratin 19, type I	1.79
FSCN1*	NM_003088	fascin actin-bundling protein 1	3.93
SPARC*	NM_001309443	secreted protein, acidic, cysteine-rich	7.36
MCAM*	NM_006500	melanoma cell adhesion molecule	1.87
ACSS1	NM_001252675	acyl-CoA synthetase short-chain family member 1	1.74
PLA2G2A	NM_000300	phospholipase A2, group IIA (platelets,	4.73
SLC2A1	NM_006516	solute carrier family 2 member 1	1.93
TGM2	NM_004613	transglutaminase 2	1.75
C11orf74	NM_001276722	chromosome 11 open reading frame 74	1.67
PLLP	NM_015993	plasmolipin	1.61
SH3BGRL	NM_003022	SH3 domain binding glutamate rich protein like	1.77
ANTXR1*	NM_018153	anthrax toxin receptor 1	2.46
PSENEN	NM_001281532	presenilin enhancer gamma secretase subu	2.11
EPB41L1	NM_001258329	erythrocyte membrane protein band 4.1 like 1	1.81
TIMP1*	NM_003254	TIMP metallopeptidase inhibitor 1	1.81
ITIH5	NM_001001851	inter-alpha-trypsin inhibitor heavy chain family member 5	1.65
PTGFRN	NM_020440	prostaglandin F2 receptor inhibitor	1.73
NRP1	NM_001024628	neuropilin 1	1.69
KLF7	NM_001270942	Kruppel-like factor 7	2.00
ANXA2P2	NR_003573	annexin A2 pseudogene 2	1.94
LOC100507194	NR_038295	uncharacterized LOC100507194	1.93
GLIPR1	NM_006851	GLI pathogenesis-related 1	1.85
DST	NM_001144769	dystonin	1.75
RAB3B	NM_002867	RAB3B, member RAS oncogene family	1.65
HECTD2	NM_001284274	HECT domain E3 ubiquitin protein ligase 2	1.77
ENAH*	NM_001008493	enabled homolog (Drosophila)	1.83
NETO2	NM_001201477	neuropilin (NRP) and tolloid (TLL)-like	1.98
KIZ	NM_001163022	kizuna centrosomal protein	1.64
SERPINA7	NM_000354	serpin family A member 7	1.78
MPDZ	NM_001261406	multiple PDZ domain protein	1.67
TMEM185B	NM_024121	transmembrane protein 185B	1.95
MIR4435-2HG	NR_015395	MIR4435-2 host gene	1.65
BVES	NM_001199563	blood vessel epicardial substance	1.68
ASAP2*	NM_001135191	ArfGAP with SH3 domain, ankyrin repeat and PH domain 2	1.66
TIMP2*	NM_003255	TIMP metallopeptidase inhibitor 2	1.72
CCL16	NM_004590	chemokine (C-C motif) ligand 16	1.76

Figure 19: Genes upregulated in Scrib^{P305L} cells. Heatmap shows 81 genes significantly upregulated in the cell line stably expressing cytoplasmic Scrib^{P305L} in comparison to Scrib^{WT} cells ($P \leq 0.05$, fold change≥ 1.60). Gene expression level is depicted by the blue-red intensities (red indicates upregulated genes). Among the 81 upregulated genes, 19 genes (indicated by *) play have been described in the regulating cell motility, EMT, or related to tumor ECM remodelling.

Considering the gene expression levels induced by cytoplasmic Scrib, as well as the importance of genes in cell invasion/migration, eight out of 19 genes were selected for further analysis. For example, increased N-cadherin levels may affect cell-cell junctions and the induction of cell invasiveness [76]. Both *carcinoembryonic antigen-related cell adhesion molecule 1* (CEACAM1) and *melanoma cell adhesion molecule* (MCAM) are cell adhesion molecules, which are known inducers of EMT and tumor invasiveness [77]. Fascin 1 has important function in the bundling of actin filament, which induces the *filamentous actin* (F-actin) in invading cells [78]. *Secreted protein acidic and cysteine rich* (SPARC, synonym: Osteonectin), *TIMP metallopeptidase inhibitor 1* (TIMP1), *TIMP metallopeptidase inhibitor 2* (TIMP2) and *S100 calcium binding protein A10* (S100A10) are secreted factors that play roles in the remodeling of tumor ECM [79-81]. Real-time PCR were carried out to confirm the overexpression of these invasion-associated genes in Scrib^{P305L} and Scrib^{WT} cells. As expected, all the selected genes were significantly elevated in the Scrib^{P305L} cells compared to Scrib^{WT} cells with SPARC showing the highest induction (133-fold increase, Figure 20A**)**. To confirm increased SPARC secretion in Scrib^{P305L} cells, a SPARC ELISA assay was used. The SPARC protein levels were 6.5-fold higher in cultured medium of Scrib^{P305L} positive cells (15 ng/ml), compared to Scrib^{WT} positive cells (2 ng/ml) (Figure 20C). In addition, the overexpression of N-cadherin, CEACAM1 and Fascin 1 at protein levels were confirmed by western immunoblotting (Figure 20B).

Because it is known that the upregulation of N-cadherin is often accompanied by the downregulation of E-cadherin in the process of EMT in epithelial cells [76], I tested the localization of both cadherins by immunofluorescence. In Scrib^{WT} expressing cells, E-cadherin was clearly localized near the plasma membrane, while in the Scrib^{P305L} cells, E-cadherin predominantly showed a cytoplasmic localization. On the other hand, the Scrib^{P305L} expressing cells showed a strong membranous stain for N-cadherin, which was much weaker in the Scrib^{WT} cells (Figure 20D). These data demonstrate that cytoplasmic Scrib induces an EMT-like phenotype partly *via* the regulation of cadherin adhesion molecules.

Because SPARC showed the strongest induction on mRNA and protein levels in cells expressing cytoplasmic Scrib^{P305L}, this factor was chosen for further analyses. SPARC has been shown to mediate the interaction of cell surface molecules and extracellular collagen fibers, leading to the induction of tumor cell invasion in the surrounding ECM [82]. For this reason, invasion assays with recombinant SPARC protein were performed to confirm the regulatory effect of SPARC. As previously demonstrated, Scrib^{WT}-expressing cells with low-SPARC levels showed a low invasive capacity (Figure 14D). Administration of recombinant SPARC significantly induced the invasiveness of Scrib^{WT} expressing cells (Figure 20E). In addition, the invasive capacity of Scrib^{P305L} expressing cells, which have a high basal invasion potential, was suppressed when SPARC expression was inhibited by the siRNA (Figure 20F).

Taken together, these results demonstrate that overexpression of cytoplasmic Scrib induces tumor invasiveness *via* the upregulation of genes, including SPARC, which are involved in EMT and ECM remodelling.

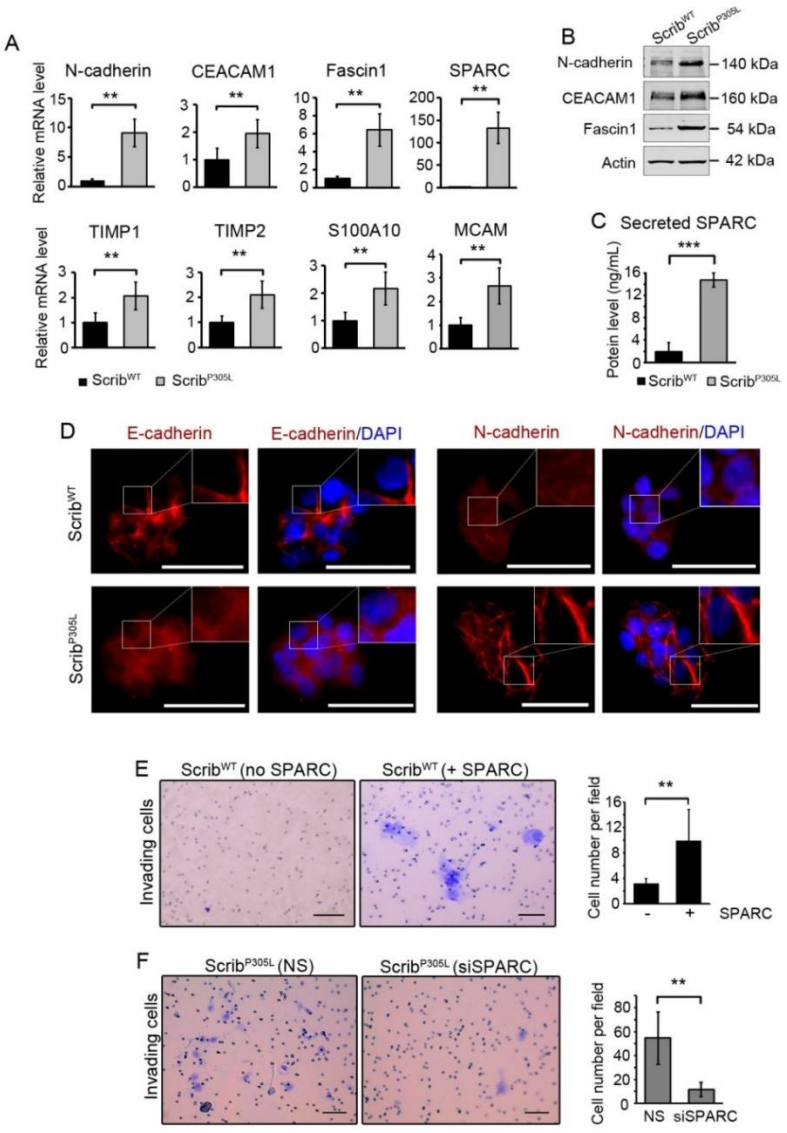

Figure 20: Cytoplasmic Scrib induces HCC cell invasiveness. (A) Real-time PCR analysis confirms the overexpression of the eight selected genes, which are involved in EMT and cell migration (N-cadherin, CEACAM1, Fascin1, SPARC, TIMP1, TIMP2, and S100A10). Mann-Whitney U test was performed ($P \leq 0.01$). **(B)** Western immunoblot analysis confirms increased amounts of N-cadherin, CEACAM1 and Fascin 1 in the cells expressing $Scrib^{P305L}$. **(C)** Human SPARC Quantikine ELISA assay was used to detect SPARC in the supernatant of cultured $Scrib^{P305L}$ expressing cells in comparison to $Scrib^{WT}$ expressing cells. Supernatant was collected from stable cell lines under starvation condition after 12 hours. **(D)** Immunofluorescence stains of N-cadherin and E-cadherin illustrates the overexpression of N-cadherin and the cytoplasmic localization of E-cadherin in $Scrib^{P305L}$ cells. Magnification: 400-fold. Scale bars: 40 µm. **(E)** Cell Invasion was measured 96 hours after SPARC stimulation. Cells were stained with crystal violet (blue color). **(F)** Invasion assays illustrate the SPARC-induced cell invasion was abolished after siRNA-mediated silencing of SPARC in $Scrib^{P305L}$ cells. The outer wells were supplemented with full FCS. Invasion was measured 72 hours after transfection. For (E) and (F), photos were taken under 100-fold magnification, scale bars: 200 µm. Invading cells were counted in seven different visual fields under 40-fold magnification.

5.8 The role of AP1 family in regulating cytoplasmic Scrib-target genes

AP1 transcriptional factors are activated by extracellular stimuli and stress, such as cytokines and growth factors. It can be activated by a variety of intracellular signaling pathways, e.g., JNK, ERK，p38 and AKT [83]. In order to define the transcriptional factor, which accounts for the upregulation of Scrib-target genes via AKT, the AP1 family constituents (c-Jun, ATF2 and JunB) were compared in nuclear fractions of cells stably expressing $Scrib^{WT}$ or $Scrib^{P305L}$. Both increased total and phosphorylated protein levels of c-Jun and JunB were observed, while induced phosphorylated level without changing the total amount of ATF2 was detected in the cells expressing $Scrib^{P305L}$ (Figure 21A). To test if Scrib affects the transcription of AP1 family constituents, real-time PCR was performed to compare c-Jun, ATF2, and JunB mRNA levels. Interestingly, c-Jun was transcriptional upregulated in $Scrib^{P305L}$ expressing cells, while ATF2 and JunB were not affected (Figure 21B).

In the next step, I evaluated the regulatory effect of these AP1 family members on cytoplasmic Scrib-target genes by siRNA-mediated gene silencing in $Scrib^{P305L}$ expressing cells. After c-Jun silencing, S100A10 was repressed, however, the other potential target genes were not drastically regulated at all or slightly induced (Figure 21C). After ATF2 inhibition, SPARC, TIMP2 and MCAM were reduced, while Jun-B silencing led to diminished SPARC, TIMP1, TIMP2, CEACAM, S100A10 and MCAM transcript levels (Figure 21D/E). Especially, the impact of ATF2 and Jun-B on SPARC protein secretion in cells stably expressing $Scrib^{P305L}$ was confirmed using the SPARC ELISA assay (Figure 21F).

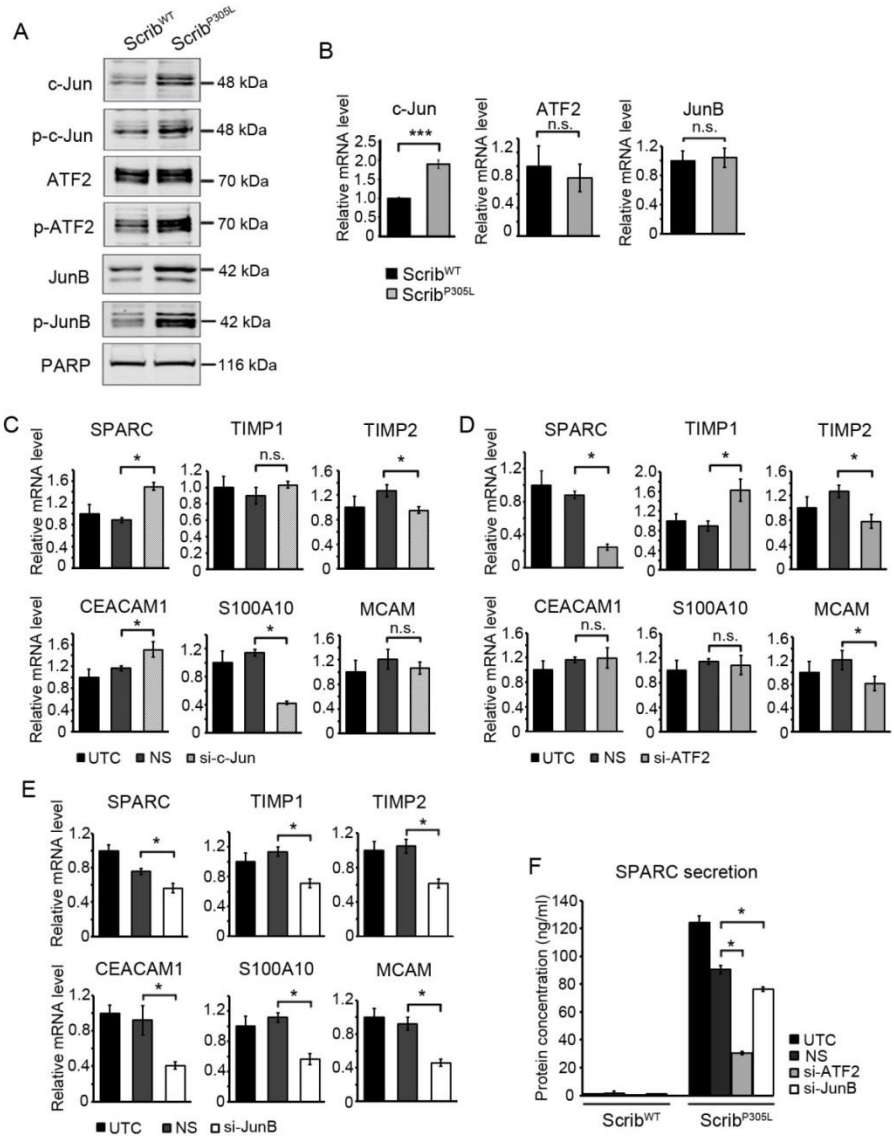

Figure 21: Scrib target genes are regulated by transcription factor AP1 subunits. (A) Western immunoblotting shows the differences of total and phosphorylated c-Jun, JunB and ATF2 in the nuclear fraction of Scrib^{P305L} expressing cells in comparison to Scrib^{WT} expressing cells. **(B)** Real-time PCR reveals an upregulation of c-Jun at the mRNA level in cells stably expressing Scrib^{P305L} in comparison to cells stably expressing Scrib^{WT}. No differences were detected for ATF2 or JunB. **(C)** Real-time PCR analysis after c-Jun inhibition in Scrib^{P305L} expressing cells. Significantly regulated genes were S100A10 (-63%) and TIMP2 (-24%). **(D)** Real-time PCR of Scrib^{P305L} expressing cells after ATF2 silencing. Significantly regulated genes were: SPARC (-73%), TIMP2 (-39%) and MCAM (-33%). **(E)** Real-time PCR analysis after JunB inhibition in Scrib^{P305L} expressing cells. Significantly regulated genes were SPARC (-26%), TIMP1 (-38%), TIMP2 (-38%), CEACAM1 (-55%), S100A10 (-49%) and MCAM (-50%). **(F)** SPARC ELISA assay confirms reduced secretion of SPARC after ATF2 (-66%) or JunB (-29%) silencing. The siRNA treatment was performed under full FCS condition. Supernatant were collected from cells after starvation for 12 hours. SPARC concentrations in Scrib^{P305L} and Scrib^{WT} cells were determined using the SPARC Quantikine ELISA assay (3 independent repetitions). For (C), (D), (E) and (F), UTC: untreated cells, NS: nonsense siRNA control. Statistical test: Mann-Whitney-U test.

To test if the AP1 subunits regulate SPARC expression through direct promoter binding, ChIP analyses were carried out in cell lines stably expressing $Scrib^{WT}$ and $Scrib^{P305L}$ lines. Two different potential AP1 binding sites were predicted by the JASPAR database (Figure 22A). The first site was located upstream of the transcriptional start (position -469 to -360). The second one was located within the second exon of SPARC (position +1890 to +1998) [84]. Primers were designed to detect these two potential binding sites, while primers that recognize an unspecific sequence downstream of the SPARC gene were designed as negative control (position +16083 to +16191). The c-Jun ChIP analysis revealed binding of c-Jun at the second binding site of the SPARC gene in the $Scrib^{P305L}$ expressing cells (Figure 22B). The ATF2 ChIP analysis demonstrated binding between ATF2 with both potential binding sites in the SPARC gene (Figure 22C). Similar to c-Jun, binding of JunB was detectable at the second binding site in the SPARC gene (Figure 22D). Importantly, none of these interactions between AP1 family members and the SPARC promoter were found in $Scrib^{WT}$ expressing cells (Figure 22B-D).

Together, these data suggest that cytoplasmic Scrib induces invasion-associated genes *via* activation of the AP1 transcriptional factors ATF2 and JunB. Interestingly, c-Jun also binds to the SPARC promoter. However, this AP1 family member negatively regulates SPARC expression.

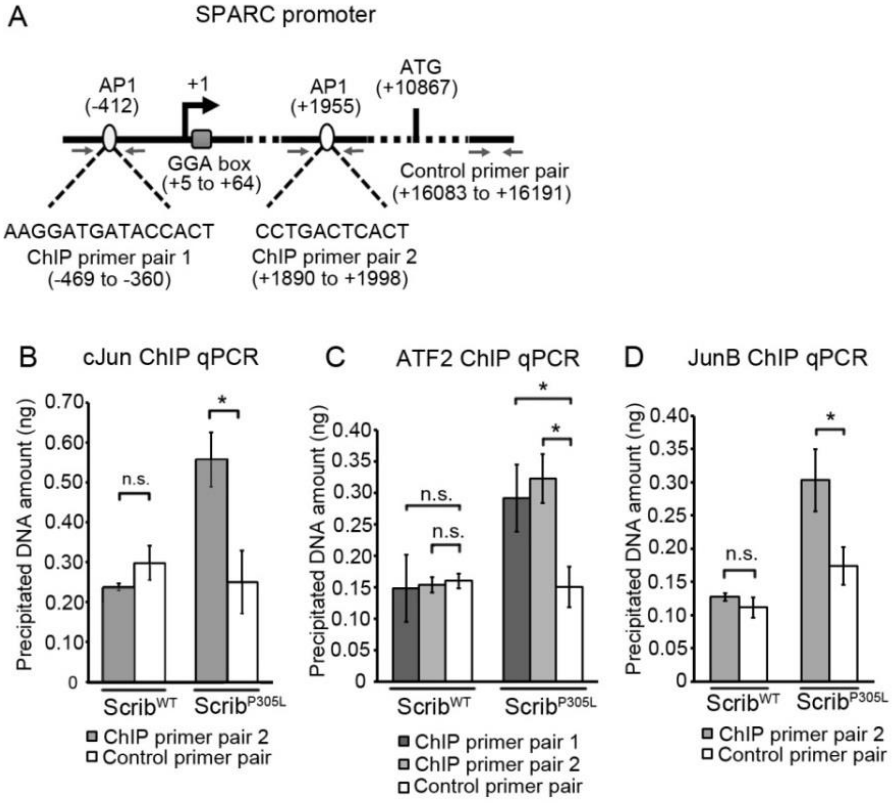

Figure 22: Interaction of the AP1 family member c-Jun, ATF2 and JunB with the SPARC promoter. (A) Scheme of two AP1 binding sites in the human SPARC gene promoter region. Primers used for ChIP analysis are indicated with grey arrows. **(B)** Real-time PCR for c-Jun ChIP analysis in cells stably expressing $Scrib^{WT}$ and $Scrib^{P305L}$. **(C)** Real-time PCR for ATF2 ChIP analysis in cells stably expressing $Scrib^{WT}$ and $Scrib^{P305L}$. **(D)** Real-time PCR for JunB ChIP analysis in cells stably expressing $Scrib^{WT}$ and $Scrib^{P305L}$. For (B), (C) and (D), the amount of precipitated DNA was normalized to a standard curve of genomic DNA. Statistical test: Mann-Whitney-U test.

5.9 Cytoplasmic Scrib promotes c-MYC-induced tumor formation

Previous studies illustrated that cytoplasmic Scrib also facilitates oncogenic properties [42]. For this reason, mouse experiments were carried out to define the oncogenic potential of cytoplasmic $Scrib^{P305L}$ in comparison to $Scrib^{WT}$ after their stable genomic integration in non-malignant hepatocytes *in vivo* by using HDTV injection. For this, human $Scrib^{WT}$ and $Scrib^{P305L}$ were cloned into *pT3-EF1α* vectors, which allowed the integration of genes in hepatocytes after co-expression of the transposase SB in mice

(HDTV injection gene delivery technique). Two ml of plasmids diluted in PBS were injected into lateral tail-vein of each mouse in 7-10 seconds. Increased pressure in liver vessels forced the entry of plasmids through highly permeable capillary endothelium into injured hepatocyte [64, 85].

We hypothesized that c-MYC overexpression might be necessary for Scrib to gain its full oncogenic properties, because c-MYC is frequently co-amplified with Scrib at the chromosome 8q.24 [86]. For this reason, the *pT3-EF1α-c-MYC* vector was co-injected with *pT3-EF1α-hScrib^{WT}-GFP* or *pT3-EF1α-hScrib^{P305L}-GFP* vectors. An IRES sequence in the *pT3-EF1α-hScrib^{WT}-GFP* and *pT3-EF1α-hScrib^{P305L}* constructs allowed the co-expression of GFP and Scrib isoforms without the formation of fusion proteins. For this reason, GFP expression was used as a reporter to determine the transfection and integration efficiency of exogenous Scrib.

Four weeks after injection, macroscopically visible tumors formed in the majority of the mice that expressing c-MYC and hScrib^{P305L}, whereas small and microscopically visible lesions were found in the mice that received c-MYC alone or c-MYC/hScrib^{WT} (Figure 23A). Increased levels of tested EMT and cell invasive signatures (SPARC, CDH2, TIMP2), and an activation of AKT was observed in samples with c-MYC/Scrib^{P305L} co-expression was observed in comparison to c-MYC/Scrib^{WT} samples (Figure 23B/C). Notably, immunohistochemical analysis revealed a prominent induction of AKT and ATF2 phosphorylation as well as SPARC production in the tumors induced by c-MYC/Scrib^{P305L} but not in control tumors (Figure 5D). Together these results indicate that cytoplasmic Scrib selectively activates AKT in hepatocytes and supports liver tumor formation in conjunction with another oncogene *in vivo*.

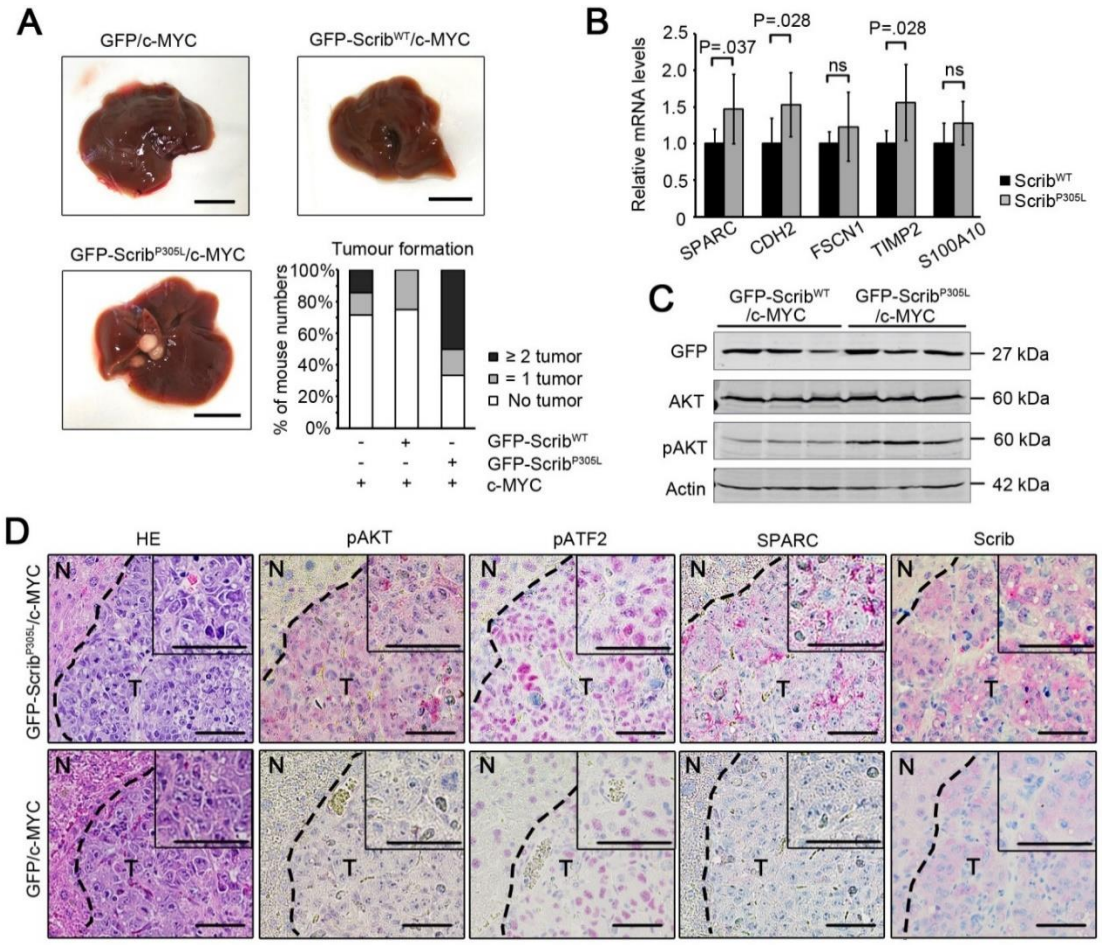

Figure 23: Cytoplasmic Scrib induces tumor formation after hydrodynamic gene delivery. (A) Eight-weeks old FVB mice were injected with vectors coding for c-MYC, SB and one of IRES-GFP (*pT3-EF1α-hScrib^{WT}-GFP*, *pT3-EF1α-hScrib^{P305L}-GFP* or *pT3-EF1α-GFP* empty vectors). Mouse livers were collected 4 weeks after injection. Scale bar: 1 cm. **(B)** Scrib target gene expressions were compared in liver tissues isolated from the mice injected with Scrib^{WT}/c-MYC (n=4) or Scrib^{P305L}/c-MYC (n=4). Statistic test: Mann-Whitney U. **(C)** Western immunoblot analysis revealed increased amounts of phospho-AKT in mouse livers injected with Scrib^{WT}/c-MYC compared to the mouse livers injected with Scrib^{P305L}/c-MYC. The presence of GFP protein confirmed the stable integration of Scrib-transgenes in mouse livers. **(D)** HE overviews and immunohistochemical analysis of pAKT, pATF2 and SPARC in Scrib^{P305L}/c-MYC- or c-MYC- induced liver tumor. Scrib^{WT}/c-MYC co-injection induced one single microscopically visible tumor, which was not suitable for histological analysis. Tumor and surrounding healthy tissues are shown. N: normal liver, T: tumor. Photos were taken under 200x magnification, scale bar: 50 µm. Dash lines indicate the hepatocyte-tumor border.

5.10 Cytoplasmic Scrib, AKT and ATF2 are associated with HCC prognosis

To confirm the previous findings in HCC patients, IHC stains of Scrib, phospho-AKT, E-cadherin and phospho-ATF2 were carried out using a HCC TMA containing human HCCs and histologically normal livers (7 histologically normal livers, 105 HCCs). Immunohistochemistry stains were scored by multiplying quantitative and qualitative parameters (see Chapter 4.8.2). In the non-tumor livers and well-differentiated HCCs, Scrib showed predominantly a membranous localization (Figure 24A). In contrast, in poorly differentiated HCC tissues, Scrib was frequently located in the cytoplasm (Figure 24A). Because the function of Scrib depends on its localization, both membranous and cytoplasmic Scrib were evaluated using individual scores. Phospho-AKT was predominantly expressed in the cytoplasm of poorly differentiated HCCs, while it was not detestable in non-tumor livers and well-differentiated HCCs. More importantly, the expression of cytoplasmic Scrib positively correlated with the expression of phospho-AKT (r_s=0.54, $p \leq 0.001$). Phospho-ATF2 was expressed in the nuclei of HCCs, which also had a positive correlation with cytoplasmic Scrib expression (r_s=0.28, p=0.037). In addition, E-cadherin was expressed on the plasma membrane of non-tumor livers and well-differentiated HCCs, which is frequently lost during the process of EMT in tumor development. Interestingly, the cytoplasmic Scrib expression negatively correlated with the membranous expression of E-cadherin (r_s=-0.49, $p \leq 0.001$) (Figure 24A).

To figure out if the IHC stains of TMAs (Scrib, phospho-AKT, phospho-ATF2 and E-cadherin) were statistically associated with tumor de-differentiation, IHC scores for the respective proteins were compared with HCC grading (Figure 24B). Cytoplasmic Scrib stains correlated with a poorer tumor differentiation (r_s=0.24, p=0.02), whereas membranous E-cadherin stains correlated with a better tumor differentiation (r_s=-0.21, p=0.04). Phospho-AKT expression also showed association with tumor de-differentiation, nevertheless this association did not reach the significance level (p=0.1).

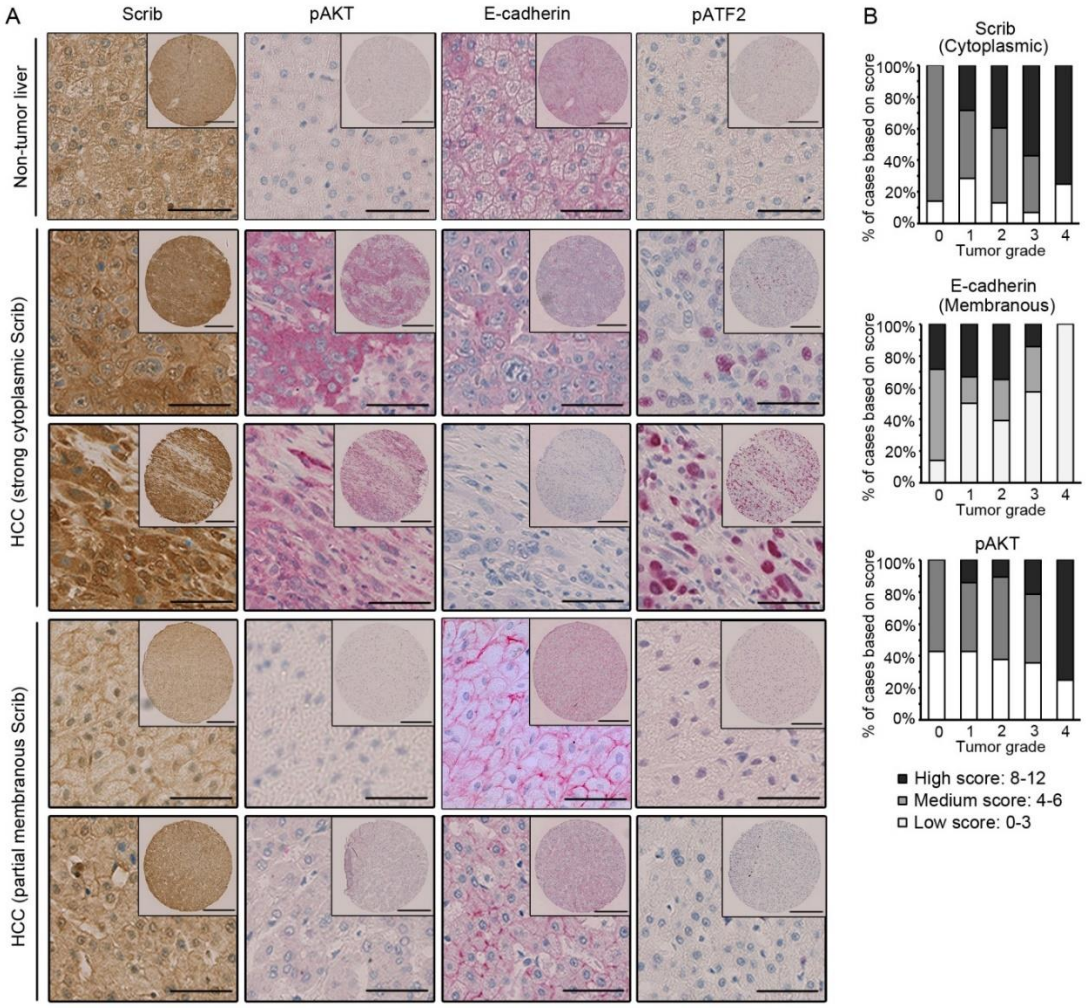

Figure 24: Cytoplasmic Scrib correlates with AKT and ATF2 activity in human HCC tissues. (A) Representative IHC stains illustrates the association of cytoplasmic Scrib with an EMT-like phenotype (loss of E-cadherin) and AKT pathway activation (phospho-AKT; pAKT). Exemplary IHC stains of one non-tumorous liver, two HCC tissues with strong cytoplasmic Scrib, and two HCC tissues with predominantly membranous Scrib are shown. Photos were taken under 400-fold magnification (scale bars: 50 µm) and 80-fold magnification (scale bars: 200 µm). **(B)** Proportional bar charts illustrate the correlation of IHC stains with tumor de-differentiation. IHC scores (0-12) were used for the correlation with the tumor grading (0: normal liver tissue, 1: G1, 2: G2. 3: G3, 4: G4). Spearman's correlation was used for statistical testing. Constituents of each scoring range (high score, medium sore and low score) are indicated with different grayscales.

The previous results strongly indicated that gene signatures induced by cytoplasmic Scrib could be used for the identification of HCC patients, who may have a higher risk to develop tumor metastasis. Therefore, I next aimed to correlate the gene signature induced by cytoplasmic Scrib with HCC patient prognosis. For this, a HCC cohort containing 91 patients with defined prognostic subgroups was applied (Figure 25). In this HCC cohort, transcriptome expression data of patients with good or poor clinical outcome was analyzed for the presence of gene induced by cytoplasmic Scrib [87]. Genes identified previously as Scrib-target genes (upregulated or downregulated) in the $Scrib^{P305L}$ cells were employed for Gene set enrichment analysis (GSEA). Interestingly, the GSEA revealed a significant correlation between the $Scrib^{P305L}$-induced gene signature (n=65) and poorer patient prognosis. Furthermore, invasion-associated genes (n=16) were selected from the upregulated genes, which again showed a significant enrichment in HCC patients with poor prognosis (Figure 25 A, B). *Vice versa*, genes that were downregulated by $Scrib^{P305L}$ (n=46) showed a significant association with better HCC prognosis (Figure 25C).

Lastly, survival data from a 249 patients HCC cohort were further used for the analysis of the eight selected Scrib-target genes SPARC, CDH2, FSCN1, CEACAM1, TIMP1, TIMP2, S100A10 and MCAM [65]. For SPARC, CDH2, TIMP2, S100A10 and MCAM, significant induction in HCC tissues compared to the corresponding normal livers were detectable (Figure 26A). Moreover, the overexpression of CDH2 and MCAM in HCC tissues positively correlated with poorer overall and recurrence-free survivals (Figure 26B). When patient data were compared with the gene expression of SPARC, CDH2, S100A10 and TIMP2 in surrounding tissues, all $Scrib^{P305L}$ target genes exhibited significant correlations with worse overall survival recurrence-free survivals (Figure 27).

To sum up, these data confirmed the association between the overexpression of cytoplasmic Scrib with the activation of AKT and ATF2 in HCC tissues. The overexpression of Scrib-target genes is associated with poorer prognosis in HCC patients.

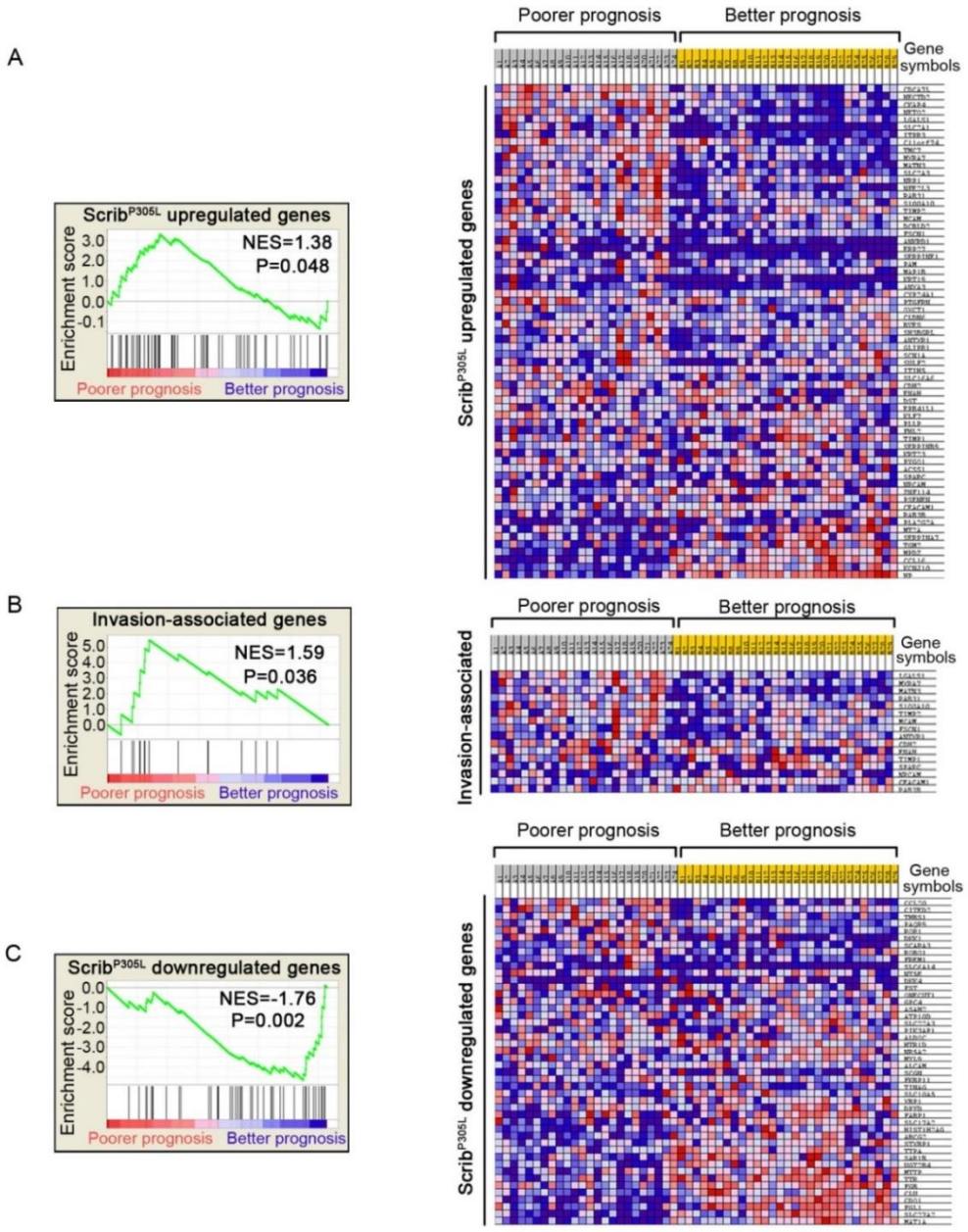

Figure 25: Expression of Scrib target genes correlates with HCC prognosis. (A) GSEA and respective heatmap of Scrib-induced target genes in the pre-defined subgroups of HCC patients with poor or better prognosis. **(B)** GSEA and heatmap of invasion-associated genes selected from Scrib-upregulated signatures in the pre-defined two subgroups. **(C)** GSEA and heatmap of Scrib-downregulated signatures in both HCC subgroups. The GSEA was performed using GSEA software provided by the Broad Institute [88]**.** For A-C, normalized enrichment score (NES) was used to reflect the enrichment of signatures for each group. Statistical significance was calculated by nominal P-value using an empirical phenotype-based permutation test. Heatmaps show the expression of Scrib-target genes in the two subgroups of HCC patients with poorer or better prognosis.

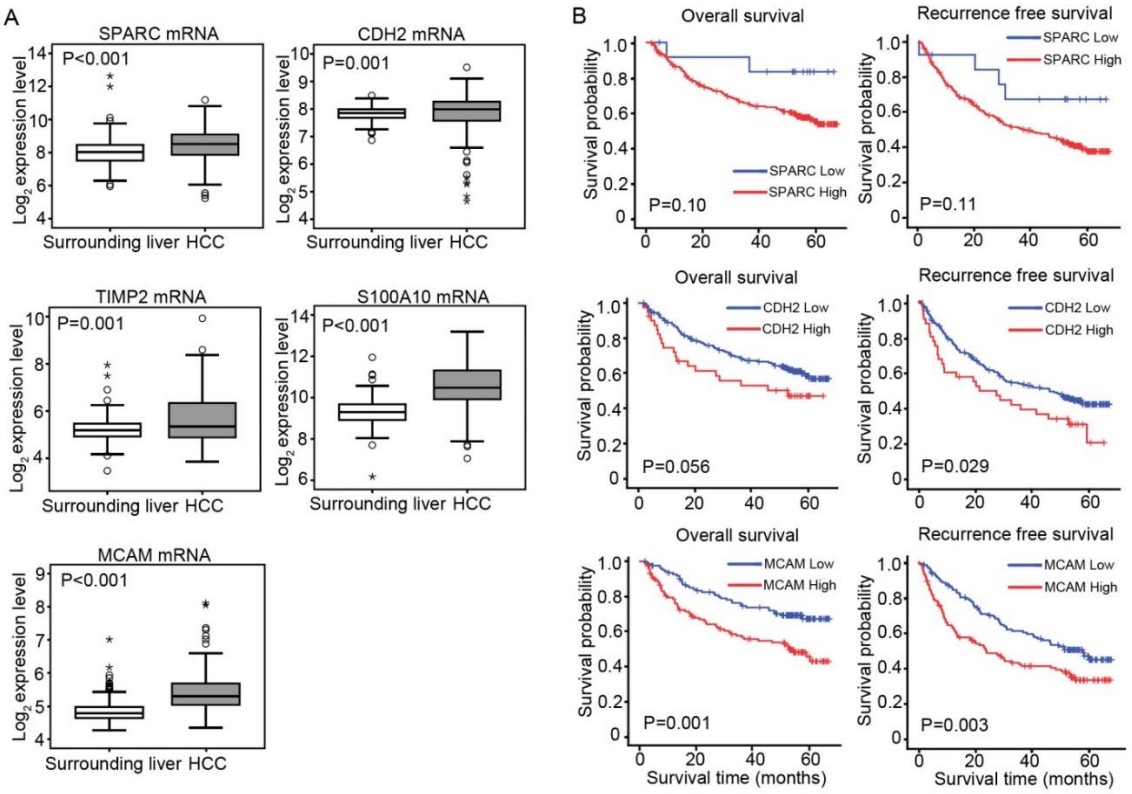

Figure 26: Overexpression of Scrib-target genes in HCC tissues. (A) Gene transcriptome analyses reveal that SPARC, CDH2, TIMP2, S100A10 and MCAM are significantly overexpressed in HCC tissues compared to surrounding livers. **(B)** Kaplan-Meier curves illustrate that higher expression of CDH2 (Log2 expression≥8.4) and MCAM (Log2 expression≥5.3) levels correlate with poorer overall and recurrence-free survivals. The overexpression of SPARC in the HCC tissues does not significantly correlate with survivals. Log-Rank test was used for the survival analyses.

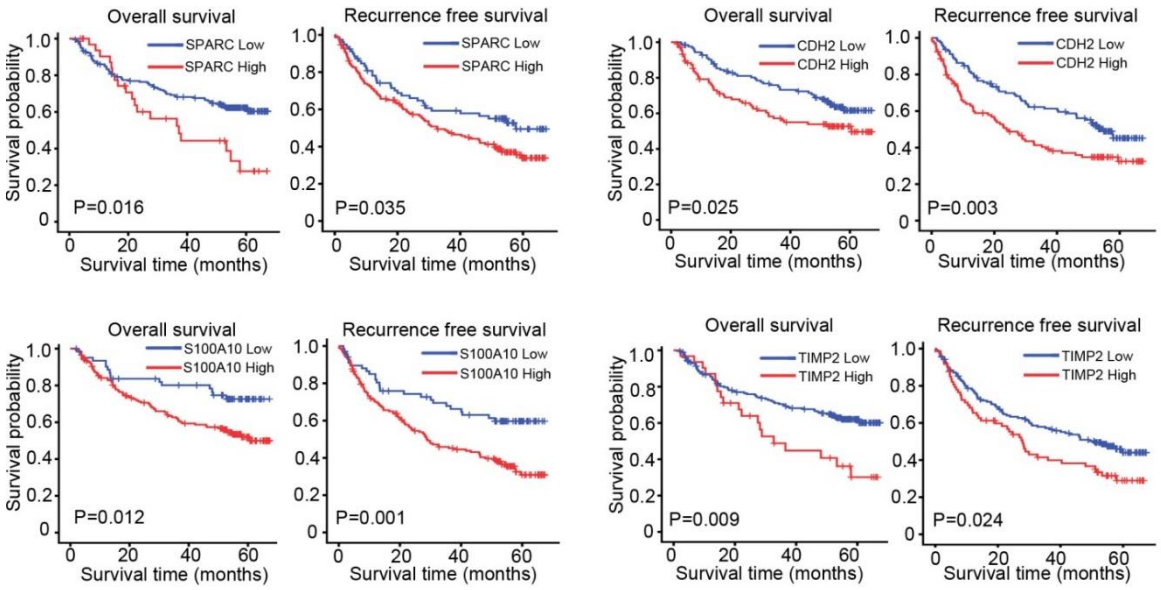

Figure 27: Overexpression of Scrib-target genes in tumor-surrounding tissues correlate with poorer survivals. Kaplan-Meier curves shows higher expression of SPARC (Log_2 expression≥8.7 for overall survival, Log_2 expression≥7.7 for recurrence-free survival), CDH2 (Log_2 expression≥7.9), S100A10 (Log_2 expression≥9.0) and TIMP2 (Log_2 expression≥5.7 for overall survival, Log_2 expression≥5.4 for recurrence-free survival) mRNA levels in the tumor-surrounding tissues positively correlate with both worse overall and recurrence-free survivals. Log-Rank test was used for the survival analyses.

6. DISCUSSION

6.1 Dysregulation of cell polarity proteins defines HCC patients with poor clinical outcome

Previous studies already identified alterations of cell polarity genes in different solid cancer cell types. These alterations include the downregulation of polarity proteins (e.g. Dlg, Lgl and PATJ), their overexpression (e.g. Par6, aPKC) or mislocalization (e.g. Par3, Scrib, aPKC) [33]. However, a systematic study of EPP components and their impact on the development and progression of HCC was missing, so far. In this study, 33 different polarity genes, which belong to the apical Crumbs complex, the subapical Par complex, and the basolateral Scrib complex were compared according to the expression levels in HCCs and surrounding tissues [65]. The comparison of transcript levels in HCCs with clinical data revealed candidate polarity genes, which may act as oncogenes (in case of overexpression) or tumor-suppressor genes (in case of downregulation). Although this transcriptome analysis allowed the identification of dysregulated factors; it cannot identify genes carrying mutations (e.g. point-mutations or small deletions) with direct impact on protein functionality.

In the subgroup of overexpressed polarity genes that were associated with oncogenic properties, Scrib, CDC42, CTNNA1 and DLG5 were identified. Their overexpression in HCCs was associated with poor patient outcome. Notably, two of these polarity genes belong to the basolateral Scrib complex (Scrib and DLG5), indicating the importance of this complex in hepatocarcinogenesis. In addition, CTNNA1 (coding for α–catenin) also shows a close spatial proximity with the Scrib complex at the AJs [89]. A previous study demonstrated the activation of Wnt singling pathway in HCC patients with multiple intrahepatic metastasis, which was associated with β-catenin mutations in 70-100% [16]. Although little is known about α–catenin in HCC development, it has been suggested that this protein supports tumorigenesis *via* the interaction with β-catenin and the actin cytoskeleton [90]. The GTPase CDC42, which plays an important role in the dynamic reorganization of actin filament in migrating cells [39], was

overexpressed and associated with a poor HCC prognosis in our study. The oncogenic property of CDC42 identified in my study is in agreement with a previous study, which demonstrated the important role of CDC42 and other Rho GTPases in HCC invasion and migration [91].

In the subgroup of reduced polarity genes with potential tumor suppressive effects, CDH1 (coding for E-cadherin), LLGL1, TJP1, LIN7C, and MPP5 were identified. Their presence correlated with a better HCC outcome. Among these polarity genes, E-cadherin has been widely accepted as a tumor-suppressor in HCC, which is downregulated in a subgroup of HCC patients, and is associated with Wnt pathway activation in intrahepatic metastasis [16, 92]. Like E-cadherin, TJP1 is a major component of TJs. In HCC, loss of TJs and associated proteins (e.g. ZO-1 and claudin) have been connected with the tumor cell dedifferentiation and early metastasis [93]. Two other regulated factors, LIN7C and MPP5, belong to the apical Crumbs complex in association with TJs [32]. Although little is known about the role of LIN7C and MPP5 (synonyms: PALS1) in cancer development, these two polarity proteins form a complex with the apical localized membrane protein Angiomotin, which can inhibit mouse liver tumor formation *via* the Hippo/YAP signaling pathway [49, 94].

This systematic analysis of polarity genes in HCC patient material suggested the tumor-promoting role of the basolateral Scrib complex and the tumor-suppressing property of the apical Crumbs complex. In many cases, the causes for the enrichment of polarity proteins from the same complexes sharing a specific biological functionality (oncogenic or tumor-suppressive) remain unknown. One explanation could be that individual polarity complexes may preferentially modulate specific intracellular signaling pathways, which may affect different aspects of tumor cell biology [33].

6.2 The Scrib gene is frequently amplified and Scrib protein is enriched in the cytoplasm of HCC cells

Based on stringent selection criteria (significant overexpression and association with patient outcome), Scrib was further analyzed for its relevance in liver cancer. My study illustrated that Scrib overexpression in HCCs compared to normal livers was associated with poor clinical outcome. The upregulation of Scrib was also detected in other human tumor entities (e.g. breast cancer and lung adenocarcinoma), which confirmed the importance of Scrib in different cancer types [95]. Interestingly, the Scrib gene is located on chromosome 8q.24.3, which is frequently amplified in many cancer types [96, 97]. To define the cause for Scrib upregulation, Scrib expression levels in HCC samples with 8q24.3 gains were compared with samples without detectable genomic alterations. Indeed, transcriptional upregulation of Scrib was associated with chromosome amplifications at 8q24.3 (see Chapter 5.1). A meta-analysis of comparative genomic hybridization data derived from 785 HCC patients confirmed that the Scrib gene locus was amplified in more than 40% of all HCC patients [98]. Together with my study, these illustrate that the Scrib upregulation in HCC patients is probably due to the genomic amplification.

Analysis of Scrib localization in HCC tissues and healthy livers revealed the membranous loss and cytoplasmic enrichment of Scrib in the majority of HCC patients, suggesting the loss of membranous Scrib expression is one important step during liver cancer formation. Other studies have equally observed the association between cancer development and cytoplasmic Scrib localization. For example, disassembly of the Scrib complex led to ovarian tumor formation in *Drosophila melanogaster* [99], while overexpression of cytoplasmic Scrib induced hyperplastic nodules in mouse mammary glands [42]. A recent study showed Scrib was localized in the cytoplasm in all analyzed HCC tissues (n=6), whereas it was mostly membranous localized in healthy liver (3/4) [100]. These data further support that the oncogenic function of Scrib is strictly dependent on its subcellular localization.

Previous studies have identified the membranous localization of Scrib in cells depends on its LRR and PDZ domains [101], and mutations in these two domains led to cytoplasmic

mislocalization of Scrib and disturbance of epithelial polarity in *Drosophila melanogaster* embryos and breast cancer cells [42, 102]. By analyzing exome sequencing data derived from the TCGA database, two missense mutations within the LRR or PDZ domains were identified in HCC patients (n=366). These mutations represent amino acid changes (R220W and A799V), which are present in 2% of HCC patients [103]. Thus, mutations in LRR and PDZ domains can be one explanation for the cytoplasmic localization of Scrib. However, the frequency of HCC patients carrying Scrib mutations is much lower than the HCC patients with cytoplasmic-localized Scrib (2% vs. 69%), which illustrates that other mechanism may affect the subcellular Scrib localization in HCC cells.

Underlying liver diseases such as liver fibrosis and cirrhosis may represent one reason for the cytoplasmic enrichment of Scrib in hepatocytes. During this pathological process, changes in the composition of ECM due to elevated production of collagen and reorganization of cell polarity modules is detectable [19], which might affect the release of cell polarity proteins from their complexes. Another possible reason for Scrib mislocalization might be infection with is hepatitis virus. So far, only the TJ-associated protein Claudin-1 has been described to interact with HCV-derived proteins, which induces HCC invasiveness *via* ERK signaling pathway [104]. Scrib stability has been connected with human papillomavirus (HPV) infection, which induces ubiquitination and degradation of the Scrib complex [105]. However, if the infection with hepatitis viruses is a cause for the observed cytoplasmic Scrib enrichment is not clear, yet. For example, the analyzed HCC cohort consisted of HBV-positive cancer patients [65], however, only a subgroup of patients showed a clear Scrib alteration. In addition, a recent study revealed that palmitoylation of Scrib was necessary for its membranous localization [106], however, if this secondary modification is also involved in the observed mislocalization in HCC cells has not been analyzed, so far.

6.3 Cytoplasmic Scrib activates AKT signaling pathway *via* the destabilization of PHLPP1/PTEN

Because one previous study identified TAZ as the downstream effector of Scrib in breast cancer cells [50], similar effects were expected for HCC cells. However, neither was the TAZ paralogue YAP differentially phosphorylated in the $Scrib^{WT}$ and $Scrib^{P305L}$-expression cells, nor did YAP/TAZ translocate into the nucleus *via* siRNA-mediated Scrib inhibition (see Figure 15A/B), which suggested that Scrib may regulate different signaling pathways in a cell type-dependent manner. Other tumor-associated signaling pathways, including ERK1/2, JNK, AKT and p38 pathways were also not significantly affected by cytoplasmic Scrib. Instead, the AKT pathway was identified as the central downstream effector according to the used experimental setup (Figure 15C). This result is in agreement with a study in breast cancer, in which overexpression of $Scrib^{P305L}$ induced AKT-mTOR activity in cancer cells [42]. However, another breast cancer study and a recent study in HCC identified the ERK1/2 as a downstream effector of Scrib [71, 100]. In these two studies, the ERK1/2 was dephosphorylated when $Scrib^{WT}$ was overexpressed in cancer cells, although these two studies had different observations regarding the upstream activities of ERK1/2 regulators: *rapidly accelerated fibrosarcoma* (RAF) and *mitogen-activated protein kinase kinase* (MEK) [71, 100]. Taken into account a very early study in *Drosophila melanogaster*, which identified an enhanced tumor growth after *rat sarcoma* (Ras) and Scrib alterations [107], it is possible that both PI3K-AKT and Ras-ERK pathways cooperate with cytoplasmic Scrib during tumor development. Because PI3K-AKT and Ras-ERK intensively cross-talks with each other, e.g. *phosphatidyl-inositol,3,4,5-triphosphate* (PIP3) is activated by Ras [108], it is not clear if the differential activation of the two pathways is mediated through independent molecular mechanism. Because PI3K-AKT and Ras-ERK have a common downstream effector (S6 protein) [108], it is possible that similar target genes and biological processes can be induced by cytoplasmic Scrib *via* activation of AKT or ERK signaling.

The phosphatases PHLPP1 and PTEN were analyzed as potential upstream regulators of AKT because they have previously been connected with Scrib in two independent studies [109, 110]. PTEN is a negative regulator of PI3K/AKT, which dephosphorylates PIP3 and therefore blocks the recruitment and phosphorylation of AKT at cell membrane [111]. Different from PTEN, PHLPP1 directly dephosphorylates AKT (on Ser473) and protein kinase C (PKC), and both

modifications inhibit the activation of AKT and its downstream effectors [109]. In my thesis, I describe the interaction of the two important AKT phosphatases (PTEN and PHLPP1) with membranous and cytoplasmic localized Scrib. Membranous Scrib stabilized PTEN and PHLPP1 at the plasma membrane, while cytoplasmic Scrib induced the rapid proteasomal degradation of phosphatases. These results were confirmed by studies in breast cancer cells demonstrating binding capacities of Scrib with both phosphatases [42, 72]. However, my data further suggests how cytoplasmic Scrib leads to AKT activation. Here, PTEN and PHLPP1, which are tethered to cytoplasmic Scrib, are quickly degraded by ubiquitination, and thus AKT and downstream pathway are constitutively activated (Figure 17).

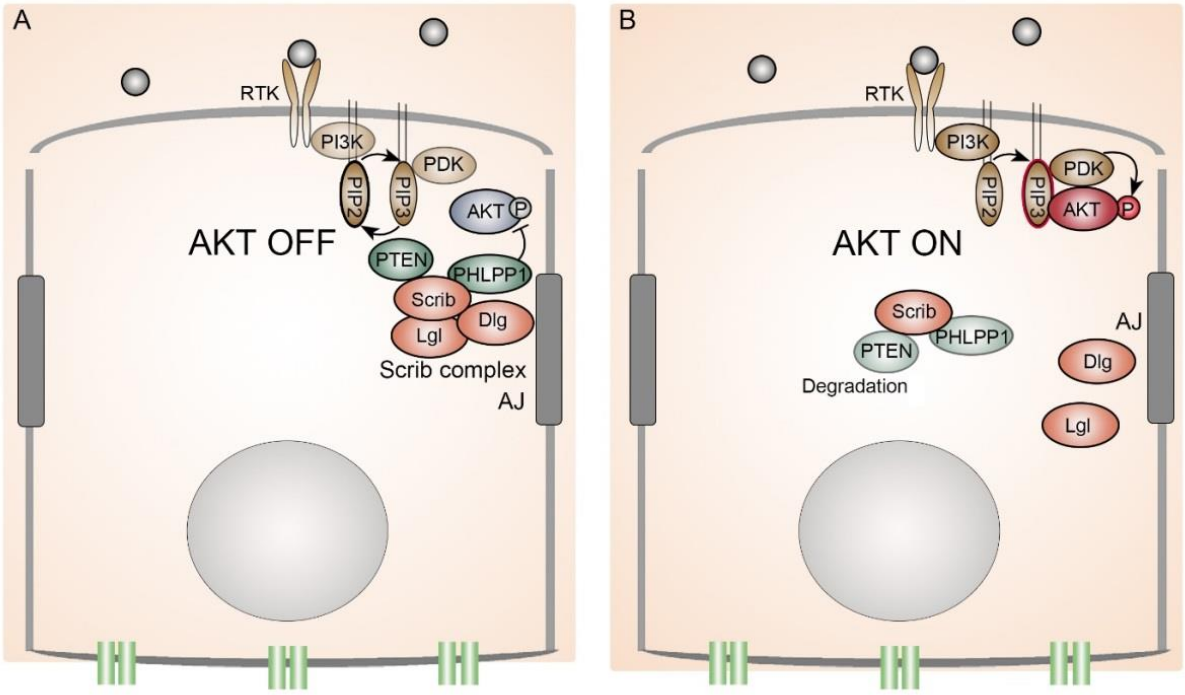

Figure 28: Cytoplasmic Scrib activates AKT signaling *via* the destabilization of PHLPP1 and PTEN. (A) Under physiological conditions, Scrib co-localizes with the AJ of the plasma membrane. It binds to the PI3K/AKT phosphatases: PHLPP1 and PTEN. PTEN dephosphorylates PIP3 to PIP2, antagonizing the effect of PI3K, while PHLPP1 directly dephosphorylates AKT [109]. AKT and the downstream pathway are negatively regulated by PHLPP1 and PTEN [109]. **(B)** In HCC cells, Scrib is enriched in the cytoplasm, which leads to a disassembly of the Scrib/PHLPP1/PTEN complex and degradation of the phosphatases. As a consequence, PI3K constantly phosphorylates PIP2 to PIP3, which allows the phosphorylation of AKT by pyruvate dehydrogenase kinase (PDK) [111]. RTK - receptor tyrosine kinases.

6.4 Cytoplasmic Scrib induces a signature associated with invasiveness in HCC

Functional analyses in the cell lines expressing $Scrib^{WT}$ and $Scrib^{P305L}$ revealed a moderate induction of proliferation and suppression of apoptosis. More strikingly, a strong induction of the cell invasive capacity was detected after cytoplasmic Scrib overexpression (Figure 14). In addition, transcriptome analysis of $Scrib^{WT}$ and $Scrib^{P305L}$ expressing cells revealed the dysregulation of invasion-associated genes in cells with cytoplasmic Scrib. These genes include cell surface adhesion molecules (N-cadherin, CEACAM1, and MCAM), an actin bundle component (Fascin1) and secreted factors (SPARC, TIMP1/2 and S100A10). Among these genes, upregulation of N-cadherin counteracts E-cadherin, which is defined as a so-called "cadherin switch" in the progression of EMT [76]. Another example for a $Scrib^{P305L}$-induced and pro-invasive gene is Fascin. This actin binding protein facilitates the dynamic reorganization of actin filament at the protruding filopodia, which is found at the leading edge of migrating cells [112]. Fascin was previously found as a target of the EMT-associated transcriptional factor *Zinc finger protein SNAI2*, which promoted tumor growth in K-Ras overexpressed mice, and was associated with early metastasis in pancreatic cancer patients [113]. Among the other identified and $Scrib^{P305L}$-induced genes with pro-invasive capacity TIMP1 and TIMP2, which can regulate the tumor microenvironment *via* the interaction with matrix metalloproteinases (MMPs), were found [114].

Previous studies discussed the tumor-supporting impact of Scrib in cancer development in the context of tumor cell proliferation, cell apoptosis as well as EMT [71, 115-117]. For example, loss of Scrib was found to induce cell proliferation via the induction of G1 to S phase cell cycle transition [116, 117]. Regarding cell invasiveness, which was the most promising aspect from my analysis; previous studies have focused on the role of membranous Scrib in inhibiting tumor cell invasion and EMT [117, 118]. Loss of Scrib induced a highly invasive tumor phenotype in *Drosophila melanogaster* in combination with Ras overexpression [115]. It has also been illustrated that this effect of membranous Scrib was dependent on its interaction with βPIX, which is a GEF protein specifically activating CDC42 and RAC1 [118, 119]. However, a different mechanism was described in breast cancer through the negative regulation on ERK pathway and *Zinc finger E-box binding homeobox* (ZEB) transcriptional factors [71]. These

studies suggest that membranous-localized Scrib may inhibit EMT/cell invasion, while my results further demonstrate that cytoplasmic-localized Scrib may promote these invasiveness *via* the activation of genes involved in EMT, actin reorganization and ECM remodeling. In addition, the secreted factors (SPARC, TIMP2 and S100A10), which were upregulated by cytoplasmic Scrib, were associated with worse clinical outcome of HCC patients (Figure 27).

6.5 SPARC in liver microenvironment induces HCC invasiveness

SPARC was identified as one of the most interesting target gene induced by cytoplasmic Scrib. Functional analysis of HCC cell lines under different culture conditions with various SPARC levels demonstrated the indispensable role of this factor in inducing HCC cell invasiveness. SPARC has important functions in the formation of collagen fibrils (I and IV) and mediating the interaction between cells and ECM [120]. Depletion of SPARC in mice caused reduced expression and stability of collagen fibers [121]. For this reason, SPARC-knockout led to embryonic lethality in *Drosophila melanogaster* due to the incomplete formation of basal lamina [122]. However, SPARC is also important in tumor development, especially in promoting migration and metastasis. Mice lacking SPARC showed increased resistant to skin papillomas under the UV exposure [123], while SPARC-knockout mice had reduced lung metastasis compared to the mice with normal SPARC expression in a breast cancer xenograft mouse model [81].

Difference studies identified multiple mechanisms explaining how SPARC can increase tumor cell invasion/metastasis and changes in ECM composition. These mechanisms include changes in the EMT process, enhanced integrin adhesion, and ECM remodeling [124-126]. SPARC was identified to activate the EMT-associated transcription factor SNAI2 in melanoma cells [124], and to decrease cell adhesion by reorganizing integrin subunits important for ovarian tumor cell invasion/metastasis [127]. Another study detected the interaction of SPARC with *vascular cell adhesion molecule 1* (VCAM) on vascular endothelial cells, which increased vascular permeability *via* activation of the p38 pathway, and promoted melanoma metastasis in a xenograft mouse model [125]. Nevertheless, there are contradicting results about the role of SPARC in tumor development. For example, SPARC inhibited tumor cell proliferation and

induced cell cycle arrest *via* the TGF-β/Smad pathway in lung epithelial cells [128], and suppressed the activation of AKT pathway in ovarian cancer cells [127]. Thus, the potential tumor-supporting role of SPARC must be evaluated for each individual tumor entity under a certain pathological process.

In case of HCC, previous findings support our results that SPARC acts as a positive regulator on liver cancer progression [129, 130]. SPARC was found to be overexpressed in poorly differentiated HCC tissues compared with non-tumor livers [130]. It was also shown that the CpG islands in the SPARC promoter were hypo-methylated in HCC primary cells, which could explain increased SPARC levels in HCC cells [129]. Interestingly, SPARC is already detectable in fibrotic livers, suggesting that early mechanisms in cancer development are responsible for its overexpression [2, 131]. Studies in fibrotic livers together with the early study in HCC described an enrichment of SPARC in liver myofibroblast, which develop from liver stellate cell under inflammatory conditions [2, 130, 131]. Based on these data, SPARC secreted by myofibroblasts may induce liver cancer progression in a paracrine manner. My data further illustrate that liver cancer cells can also produce SPARC after disturbance of cell polarity and cytoplasmic enrichment of Scrib.

6.6 Mislocalization of Scrib activates the AP1 family members ATF2 and JunB

Because cytoplasmic Scrib activated the AKT signaling pathway and cell invasion/migration-associated genes, I asked, which transcription factors were responsible for the upregulation of ttarget genes induced by AKT pathway. It is known that the cytokine and growth factor-induced AP1 protein family is sensitive to extracellular stimuli and is activated by a variety of intracellular signaling pathways such as the JNK, ERK，p38 MAPK and AKT pathways [83]. I therefore hypothesized that AP1 family members might play a key role in the regulation of $Scrib^{P305L}$-induced target genes *via* activation of AKT signaling. Indeed, my results demonstrated a higher activity of the AP1 proteins ATF2, JunB and c-Jun in $Scrib^{P305L}$ cells, indicating that AP1 family members may act as important regulators of SPARC transcription in the HCC cells.

Next, the binding capacity of the AP1 proteins ATF2 and c-Jun at the SPARC promoter was analyzed. AP1 family members belong to *leucine zipper-containing transcription factors*, which binds to DNA as homo- or heterodimers. C-Jun is regarded as a central protein of AP1 family, which can interact with both ATFs and Fos subgroup members. These subgroups recognize distinct AP1 dimer binding site. Jun/Fos dimers bind to a 7 bp DNA palindromic sequence (5'-TGAGTCA-3' or 5'-TGACTCA-3') [132], while ATF2 directly binds to a 8 bp palindrome (5'-TGACGTCA-3') [133]. Interestingly, different AP1 family members also facilitate distinct biological processes dependent on the composition of the dimer and the cell types [134, 135]. For example, c-Jun plays an important role in the regulation of cell cycle and apoptosis, which can be antagonized by JunB [134]. This suggests that the composition of AP1 dimers might affect the migratory response of HCC cells as illustrated by the different impacts of AP1 constituents on SPARC transcription.

ChIP analyses performed in my thesis showed binding of both JunB and c-Jun at the SPARC promoter/enhancer region, which contains the described 7 bp binding motif (binding site 2) in cells overexpressing $Scrib^{P305L}$. Notably, siRNA-mediated c-Jun inhibition revealed its negative regulatory impact on SPARC secretion, which illustrated that c-Jun may act as a repressor for SPARC expression. This was confirmed by a previous study showing that SPARC transcription was repressed by a viral homolog v-Jun in *Drosophila melanogaster* SL2 cells [136]. In contrast, JunB induced SPARC transcription, demonstrating that this AP-1 subunit served as a positive regulator in the used cell system. In addition to c-Jun and JunB, another AP1 protein ATF2, which showed the strongest impact on SPARC expression, bound to both potential binding sites in the SPARC promoter/enhancer. This result was in agreement with a large-scale promoter array analysis, which identified the interaction between ATF2 and SPARC promoter after cisplatin treatment [137], Notably, the second binding site was a 7-bp palindrome for Jun/Fos subgroups instead of ATF2, suggesting that the binding of ATF2 at the SPARC promoter/enhancer was probably due to other binding partners of the AP-1 dimers.

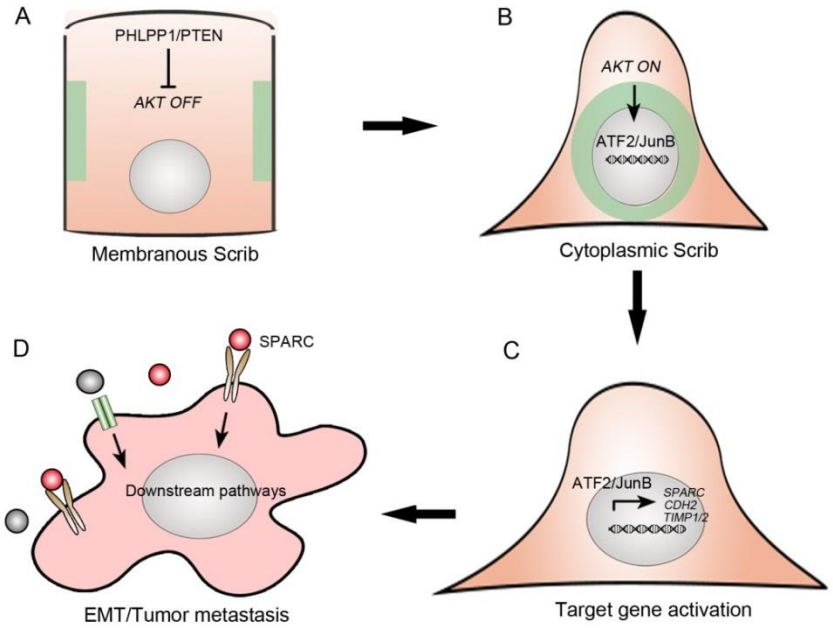

Figure 29: Summarizing scheme of how cytoplasmic Scrib induces tumor metastasis and EMT via activation of AKT pathway and AP1 transcriptional factors. (A) When Scrib locates to the plasma membrane, PHLPP1/PTEN inactivates the AKT signaling pathway in normal hepatocyte. **(B)** When Scrib locates to the cytoplasm, the AKT pathway is activated, which leads to a nuclear enrichment of AP1 transcription factors ATF2 and JunB. **(C)** ATF2 and JunB bind to respective target gene promoters, and turn on target gene expression important for EMT and cell invasiveness. **(D)** SPARC is highly expressed by cells with cytoplasmic Scrib, which binds to membranous receptors on liver cancer cells and activates downstream signaling pathways involved in EMT and metastasis [125]. In (A) and (B), green colored areas indicate different subcellular regions of Scrib. In (D), SPARC is indicated in red, while other secreted factors are presented with grey.

6.7 Cytoplasmic Scrib co-operates with c-MYC in supporting liver tumor formation in mice

In this study, I analyzed the oncogenic property of cytoplasmic Scrib in combination with the oncogene c-MYC, because c-MYC gene is located on chromosome 8q24.21 in close proximity to the Scrib gene on 8q24.3. This genomic region is known to be frequently amplified in in HCCs [86, 138]. Previous studies found that c-MYC amplification in HCC patients and induced tumor formation and progression *via* different mechanisms, including tumor cell proliferation, apoptosis and dedifferentiation [139, 140]. C-MYC promotes cell cycle progression through the activation of cell cycle proteins, e.g. cyclin D, *cyclin dependent kinase* (CDK) 4 and CDK6 [141]. In the liver, c-MYC expression synergized with AKT activation in promoting liver tumors after hydrodynamic gene delivery of both oncogenes [64]. I therefore asked if the co-delivery of c-MYC and Scrib$^{WT/P305L}$ isoforms (with Scrib^{P305L} leading to AKT activation) in mouse livers could affect c-MYC-dependent tumor formation in polarized hepatocytes.

Indeed, my data in hydrodynamic tail-vein (HDTV) mouse model demonstrated that cytoplasmic Scrib cooperates with c-MYC in hepatocarcinogenesis already in early phases of tumor development. These results are in line with a study in breast cancer, which analyzed the effect of cytoplasmic Scrib in mammary glands [42]. This study detected frequent occurrence of hyperplastic lesions and development of malignant tumors after a long-term overexpression Scrib^{P305L} for two years [42]. The results generated in my thesis, show that the co-expression of cytoplasmic Scrib and c-MYC accelerates tumor formation in hepatocytes, since first solid cancer nodules were detectable after 6-8 week. This rapid process is interesting since stable integration of the injected vectors is achieved in was about 2%-10% of all hepatocytes [64]. Importantly, HDTV-induced tumor models resemble the human situation of liver cancers, where tumor lesions are derived from single cells with several genomic alterations [64].

Most studies *in vivo* paid special attention to the activity of membranous Scrib instead of cytoplasmic Scrib in cancer development. Loss of membranous Scrib resulted in an EMT-phenotype and tumor migration in *Drosophila melanogaster* [99]. Another study showed that membranous Scrib suppressed the oncogenic property of c-MYC in mammary tumor growth in a

subcutaneous transplantation mouse model [117]. In the recent HCC study, transgenic mice with genetic Scrib deletion spontaneously developed liver tumors [100]. Together, these data all illustrate the tumor-suppressive role of membranous Scrib in different independent tumor models. However, my thesis added a new level of how cytoplasmic Scrib supports tumor development in the liver. While mice expressing $Scrib^{WT}$ and c-MYC showed few and small hepatic tumors, the $Scrib^{P305L}$/c-MYC co-expression increased the number and size of macros- and microscopically detectable tumors. These findings, together with the results from other groups, indicate that Scrib facilitates tumor-suppressor or oncogenic functions depending on its subcellular localization.

6.8 Potential application of Scrib in HCC prognosis and therapy

Current studies revealed multiple functions of how polarity proteins are involved in tumor development under pathological conditions [33]. In my study, cytoplasmic localized Scrib showed an oncogenic property in promoting liver tumor progression, while other studies in HCC and breast cancer focused on the tumor-suppressive role of Scrib [100, 117]. According to this thesis, Scrib can be used as a biomarker for the classification of highly invasive HCC; however, the localization of Scrib has to be carefully analyzed in patients. In addition, some of Scrib target genes belong to EMT markers (e.g. CDH2 and MCAM). Together with Scrib, these EMT markers may help to define the subgroup of HCC patients with higher risk of migration/metastasis.

From the therapeutic point of view, re-establishment of cell polarity with membranous Scrib localization could inhibit the progression of HCC. However, multiple factors contribute to the overexpression of Scrib (e.g. genomic alterations), while the direct molecular cause for cytoplasmic Scrib (mis-)localization is missing here. Current studies proposed an idea of re-establishing cell polarity *via* the remodeling of liver ECM, however, irreversible fibrotic collagen deposition in livers makes this approach clinically not feasible, so far [2]. Because hyperactivation of AKT pathway was connected with the overexpression of cytoplasmic Scrib in this study, this supports the idea of personalized therapeutic approach in a subgroup of patients. These patients may benefit from an AKT/mTOR pathway-directed therapy with by FDA-approved chemical compounds [142].

In this thesis, I also found that cytoplasmic Scrib induced signature gene expression (e.g., SPARC, TIMP1 and TIMP2) which was associated with remodeling of tumor microenvironment. These secreted factors are potential targets for the development of novel therapeutic approaches for the treatment of chronic liver disease and cancer [2]. Among these secreted factors, SPARC showed strongest effects on cell migration/invasion, which was confirmed by independent studies in different tumor entities [126, 127, 130]. So far, basic research for SPARC is still ongoing to define the relevant receptors and downstream signaling pathways. For example, the VCAM receptor, the *platelet-derived growth factors* (PDGF) receptor and stabilin have been identified as

potential SPARC-binding proteins. These receptors may differentially activate downstream pathways involved in, proliferation and migration of tumor cells but also vascular permeability and angiogenesis after SPARC uptake [125, 143, 144]. This thesis indicated that components targeting at SPARC or its receptors could be beneficial for a subgroup of HCC patients with early metastasis. Before this, a comprehensive understanding of the relevant SPARC receptors and their respective downstream signaling pathways is necessary.

7. REFERENCES

1. Worman, H.J., *The Liver: Biology and Pathobiology.* Gastrointest Endosc, 1995. **42**(3): p. 284.
2. Pellicoro, A., et al., *Liver fibrosis and repair: immune regulation of wound healing in a solid organ.* Nat Rev Immunol, 2014. **14**(3): p. 181-94.
3. Tsukada, N., C.A. Ackerley, and M.J. Phillips, *The structure and organization of the bile canalicular cytoskeleton with special reference to actin and actin-binding proteins.* Hepatology, 1995. **21**(4): p. 1106-13.
4. Rappaport, A.M., *Hepatic blood flow: morphologic aspects and physiologic regulation.* Int Rev Physiol, 1980. **21**: p. 1-63.
5. Bryant, D.M. and K.E. Mostov, *From cells to organs: building polarized tissue.* Nat Rev Mol Cell Biol, 2008. **9**(11): p. 887-901.
6. Treyer, A. and A. Musch, *Hepatocyte polarity.* Compr Physiol, 2013. **3**(1): p. 243-87.
7. El-Serag, H.B., *Epidemiology of viral hepatitis and hepatocellular carcinoma.* Gastroenterology, 2012. **142**(6): p. 1264-1273 e1.
8. Altekruse, S.F., K.A. McGlynn, and M.E. Reichman, *Hepatocellular carcinoma incidence, mortality, and survival trends in the United States from 1975 to 2005.* J Clin Oncol, 2009. **27**(9): p. 1485-91.
9. Balogh, J., et al., *Hepatocellular carcinoma: a review.* J Hepatocell Carcinoma, 2016. **3**: p. 41-53.
10. Asham, E.H., A. Kaseb, and R.M. Ghobrial, *Management of hepatocellular carcinoma.* Surg Clin North Am, 2013. **93**(6): p. 1423-50.
11. Mathurin, P. and R. Bataller, *Trends in the management and burden of alcoholic liver disease.* J Hepatol, 2015. **62**(1 Suppl): p. S38-46.
12. Adams, L.A., et al., *The natural history of nonalcoholic fatty liver disease: a population-based cohort study.* Gastroenterology, 2005. **129**(1): p. 113-21.
13. Oikawa, T., et al., *Multistep and multicentric development of hepatocellular carcinoma: histological analysis of 980 resected nodules.* J Hepatol, 2005. **42**(2): p. 225-9.
14. Nakano, S., et al., *Investigation of resected multinodular hepatocellular carcinoma: assessment of unicentric or multicentric genesis from histological and prognostic viewpoint.* Am J Gastroenterol, 1994. **89**(2): p. 189-93.
15. Zhu, A.X., et al., *HCC and angiogenesis: possible targets and future directions.* Nat Rev Clin Oncol, 2011. **8**(5): p. 292-301.
16. Boyault, S., et al., *Transcriptome classification of HCC is related to gene alterations and to new therapeutic targets.* Hepatology, 2007. **45**(1): p. 42-52.
17. Weiler, S.M.E., et al., *Induction of Chromosome Instability by Activation of Yes-Associated Protein and Forkhead Box M1 in Liver Cancer.* Gastroenterology, 2017. **152**(8): p. 2037-2051 e22.
18. Shen, J., et al., *Genome-wide DNA methylation profiles in hepatocellular carcinoma.* Hepatology, 2012. **55**(6): p. 1799-808.
19. Pinzani, M., *Epithelial-mesenchymal transition in chronic liver disease: fibrogenesis or escape from death?* J Hepatol, 2011. **55**(2): p. 459-65.
20. Wong, R.J., et al., *Increased long-term survival among patients with hepatocellular carcinoma after implementation of Model for End-stage Liver Disease score.* Clin Gastroenterol Hepatol, 2014. **12**(9): p. 1534-40 e1.
21. Yeo, W., et al., *A randomized phase III study of doxorubicin versus cisplatin/interferon alpha-2b/doxorubicin/fluorouracil (PIAF) combination chemotherapy for unresectable hepatocellular carcinoma.* J Natl Cancer Inst, 2005. **97**(20): p. 1532-8.

22. Lencioni, R., P. Petruzzi, and L. Crocetti, *Chemoembolization of hepatocellular carcinoma.* Semin Intervent Radiol, 2013. **30**(1): p. 3-11.
23. Llovet, J.M., et al., *Sorafenib in advanced hepatocellular carcinoma.* N Engl J Med, 2008. **359**(4): p. 378-90.
24. Bruix, J., et al., *Adjuvant sorafenib for hepatocellular carcinoma after resection or ablation (STORM): a phase 3, randomised, double-blind, placebo-controlled trial.* Lancet Oncol, 2015. **16**(13): p. 1344-54.
25. Matter, M.S., et al., *Targeting the mTOR pathway in hepatocellular carcinoma: current state and future trends.* J Hepatol, 2014. **60**(4): p. 855-65.
26. Laplante, M. and D.M. Sabatini, *mTOR signaling in growth control and disease.* Cell, 2012. **149**(2): p. 274-93.
27. Wodarz, A. and I. Nathke, *Cell polarity in development and cancer.* Nat Cell Biol, 2007. **9**(9): p. 1016-24.
28. Rodriguez-Boulan, E. and I.G. Macara, *Organization and execution of the epithelial polarity programme.* Nat Rev Mol Cell Biol, 2014. **15**(4): p. 225-42.
29. Vasioukhin, V., et al., *Directed actin polymerization is the driving force for epithelial cell-cell adhesion.* Cell, 2000. **100**(2): p. 209-19.
30. Shin, K., V.C. Fogg, and B. Margolis, *Tight junctions and cell polarity.* Annu Rev Cell Dev Biol, 2006. **22**: p. 207-35.
31. Gumbiner, B.M., *Cell adhesion: the molecular basis of tissue architecture and morphogenesis.* Cell, 1996. **84**(3): p. 345-57.
32. Bulgakova, N.A. and E. Knust, *The Crumbs complex: from epithelial-cell polarity to retinal degeneration.* J Cell Sci, 2009. **122**(Pt 15): p. 2587-96.
33. Halaoui, R. and L. McCaffrey, *Rewiring cell polarity signaling in cancer.* Oncogene, 2015. **34**(8): p. 939-50.
34. Hong, Y., et al., *Distinct roles of Bazooka and Stardust in the specification of Drosophila photoreceptor membrane architecture.* Proc Natl Acad Sci U S A, 2003. **100**(22): p. 12712-7.
35. Betschinger, J., K. Mechtler, and J.A. Knoblich, *The Par complex directs asymmetric cell division by phosphorylating the cytoskeletal protein Lgl.* Nature, 2003. **422**(6929): p. 326-30.
36. Scheffzek, K. and M.R. Ahmadian, *GTPase activating proteins: structural and functional insights 18 years after discovery.* Cell Mol Life Sci, 2005. **62**(24): p. 3014-38.
37. Michaelson, D., et al., *Differential localization of Rho GTPases in live cells: regulation by hypervariable regions and RhoGDI binding.* J Cell Biol, 2001. **152**(1): p. 111-26.
38. Maddox, A.S. and K. Oegema, *Closing the GAP: a role for a RhoA GAP in cytokinesis.* Mol Cell, 2003. **11**(4): p. 846-8.
39. Iden, S. and J.G. Collard, *Crosstalk between small GTPases and polarity proteins in cell polarization.* Nat Rev Mol Cell Biol, 2008. **9**(11): p. 846-59.
40. Atwood, S.X., et al., *Cdc42 acts downstream of Bazooka to regulate neuroblast polarity through Par-6 aPKC.* J Cell Sci, 2007. **120**(Pt 18): p. 3200-6.
41. McCaffrey, L.M., et al., *Loss of the Par3 polarity protein promotes breast tumorigenesis and metastasis.* Cancer Cell, 2012. **22**(5): p. 601-14.
42. Feigin, M.E., et al., *Mislocalization of the cell polarity protein scribble promotes mammary tumorigenesis and is associated with basal breast cancer.* Cancer Res, 2014. **74**(11): p. 3180-94.
43. Knoblich, J.A., *Asymmetric cell division: recent developments and their implications for tumour biology.* Nat Rev Mol Cell Biol, 2010. **11**(12): p. 849-60.
44. Kalluri, R. and R.A. Weinberg, *The basics of epithelial-mesenchymal transition.* J Clin Invest, 2009. **119**(6): p. 1420-8.
45. Viloria-Petit, A.M., et al., *A role for the TGFbeta-Par6 polarity pathway in breast cancer progression.* Proc Natl Acad Sci U S A, 2009. **106**(33): p. 14028-33.

46. Tschaharganeh, D.F., et al., *Yes-associated protein up-regulates Jagged-1 and activates the Notch pathway in human hepatocellular carcinoma.* Gastroenterology, 2013. **144**(7): p. 1530-1542 e12.
47. Benhamouche, S., et al., *Nf2/Merlin controls progenitor homeostasis and tumorigenesis in the liver.* Genes Dev, 2010. **24**(16): p. 1718-30.
48. Zhao, B., K. Tumaneng, and K.-L. Guan, *The Hippo pathway in organ size control, tissue regeneration and stem cell self-renewal.* Nat Cell Biol, 2011. **13**(8): p. 877-883.
49. Zhao, B., et al., *Angiomotin is a novel Hippo pathway component that inhibits YAP oncoprotein.* Genes Dev, 2011. **25**(1): p. 51-63.
50. Cordenonsi, M., et al., *The Hippo transducer TAZ confers cancer stem cell-related traits on breast cancer cells.* Cell, 2011. **147**(4): p. 759-72.
51. Zhao, B., K. Tumaneng, and K.L. Guan, *The Hippo pathway in organ size control, tissue regeneration and stem cell self-renewal.* Nat Cell Biol, 2011. **13**(8): p. 877-83.
52. Komiya, Y. and R. Habas, *Wnt signal transduction pathways.* Organogenesis, 2008. **4**(2): p. 68-75.
53. Gordon, M.D. and R. Nusse, *Wnt signaling: multiple pathways, multiple receptors, and multiple transcription factors.* J Biol Chem, 2006. **281**(32): p. 22429-33.
54. Habas, R., Y. Kato, and X. He, *Wnt/Frizzled activation of Rho regulates vertebrate gastrulation and requires a novel Formin homology protein Daam1.* Cell, 2001. **107**(7): p. 843-54.
55. Karasaki, S., *Subcellular localization of surface adenosine triphosphatase activity in preneoplastic liver parenchyma.* Cancer Res, 1972. **32**(8): p. 1703-12.
56. Kondo, Y. and T. Nakajima, *Pseudoglandular hepatocellular carcinoma. A morphogenetic study.* Cancer, 1987. **60**(5): p. 1032-7.
57. Gissen, P. and I.M. Arias, *Structural and functional hepatocyte polarity and liver disease.* J Hepatol, 2015. **63**(4): p. 1023-37.
58. Mirouse, V., et al., *LKB1 and AMPK maintain epithelial cell polarity under energetic stress.* J Cell Biol, 2007. **177**(3): p. 387-92.
59. Kim, D.H., et al., *Synthetic dsRNA Dicer substrates enhance RNAi potency and efficacy.* Nat Biotechnol, 2005. **23**(2): p. 222-6.
60. Edelheit, O., A. Hanukoglu, and I. Hanukoglu, *Simple and efficient site-directed mutagenesis using two single-primer reactions in parallel to generate mutants for protein structure-function studies.* BMC Biotechnol, 2009. **9**: p. 61.
61. Dai, M., et al., *Evolving gene/transcript definitions significantly alter the interpretation of GeneChip data.* Nucleic Acids Res, 2005. **33**(20): p. e175.
62. Artym, V.V. and K. Matsumoto, *Imaging cells in three-dimensional collagen matrix.* Curr Protoc Cell Biol, 2010. **Chapter 10**: p. Unit 10 18 1-20.
63. Kaboord, B. and M. Perr, *Isolation of proteins and protein complexes by immunoprecipitation.* Methods Mol Biol, 2008. **424**: p. 349-64.
64. Chen, X. and D.F. Calvisi, *Hydrodynamic transfection for generation of novel mouse models for liver cancer research.* Am J Pathol, 2014. **184**(4): p. 912-23.
65. Roessler, S., et al., *A unique metastasis gene signature enables prediction of tumor relapse in early-stage hepatocellular carcinoma patients.* Cancer Res, 2010. **70**(24): p. 10202-12.
66. Roessler, S., et al., *Integrative genomic identification of genes on 8p associated with hepatocellular carcinoma progression and patient survival.* Gastroenterology, 2012. **142**(4): p. 957-966 e12.
67. Budczies, J., et al., *Cutoff Finder: a comprehensive and straightforward Web application enabling rapid biomarker cutoff optimization.* PLoS One, 2012. **7**(12): p. e51862.
68. Sandelin, A., et al., *JASPAR: an open-access database for eukaryotic transcription factor binding profiles.* Nucleic Acids Res, 2004. **32**(Database issue): p. D91-4.
69. Navarro, C., et al., *Junctional recruitment of mammalian Scribble relies on E-cadherin engagement.* Oncogene, 2005. **24**(27): p. 4330-9.

70. Le Clainche, C. and M.F. Carlier, *Regulation of actin assembly associated with protrusion and adhesion in cell migration.* Physiol Rev, 2008. **88**(2): p. 489-513.
71. Elsum, I.A., C. Martin, and P.O. Humbert, *Scribble regulates an EMT polarity pathway through modulation of MAPK-ERK signaling to mediate junction formation.* J Cell Sci, 2013. **126**(Pt 17): p. 3990-9.
72. Li, X., et al., *Scribble-mediated membrane targeting of PHLPP1 is required for its negative regulation of Akt.* EMBO Rep, 2011. **12**(8): p. 818-24.
73. Vazquez, F., et al., *Phosphorylation of the PTEN tail regulates protein stability and function.* Mol Cell Biol, 2000. **20**(14): p. 5010-8.
74. Kanehisa, M. and S. Goto, *KEGG: kyoto encyclopedia of genes and genomes.* Nucleic Acids Res, 2000. **28**(1): p. 27-30.
75. Belinky, F., et al., *PathCards: multi-source consolidation of human biological pathways.* Database (Oxford), 2015. **2015**.
76. Lamouille, S., J. Xu, and R. Derynck, *Molecular mechanisms of epithelial-mesenchymal transition.* Nat Rev Mol Cell Biol, 2014. **15**(3): p. 178-96.
77. Ebrahimnejad, A., et al., *CEACAM1 enhances invasion and migration of melanocytic and melanoma cells.* Am J Pathol, 2004. **165**(5): p. 1781-7.
78. Jansen, S., et al., *Mechanism of actin filament bundling by fascin.* J Biol Chem, 2011. **286**(34): p. 30087-96.
79. Wu, Z.S., et al., *Prognostic significance of MMP-9 and TIMP-1 serum and tissue expression in breast cancer.* Int J Cancer, 2008. **122**(9): p. 2050-6.
80. Ito, Y., et al., *S100A10 expression in thyroid neoplasms originating from the follicular epithelium: contribution to the aggressive characteristic of anaplastic carcinoma.* Anticancer Res, 2007. **27**(4C): p. 2679-83.
81. Sangaletti, S., et al., *Macrophage-derived SPARC bridges tumor cell-extracellular matrix interactions toward metastasis.* Cancer Res, 2008. **68**(21): p. 9050-9.
82. Nagaraju, G.P., et al., *Molecular mechanisms underlying the divergent roles of SPARC in human carcinogenesis.* Carcinogenesis, 2014. **35**(5): p. 967-73.
83. Shaulian, E. and M. Karin, *AP-1 as a regulator of cell life and death.* Nat Cell Biol, 2002. **4**(5): p. E131-6.
84. Mathelier, A., et al., *JASPAR 2014: an extensively expanded and updated open-access database of transcription factor binding profiles.* Nucleic Acids Res, 2014. **42**(Database issue): p. D142-7.
85. Ho, C., et al., *AKT (v-akt murine thymoma viral oncogene homolog 1) and N-Ras (neuroblastoma ras viral oncogene homolog) coactivation in the mouse liver promotes rapid carcinogenesis by way of mTOR (mammalian target of rapamycin complex 1), FOXM1 (forkhead box M1)/SKP2, and c-Myc pathways.* Hepatology, 2012. **55**(3): p. 833-45.
86. Okamoto, H., et al., *PTK2 and EIF3S3 genes may be amplification targets at 8q23-q24 and are associated with large hepatocellular carcinomas.* Hepatology, 2003. **38**(5): p. 1242-9.
87. Lee, J.S., et al., *Classification and prediction of survival in hepatocellular carcinoma by gene expression profiling.* Hepatology, 2004. **40**(3): p. 667-76.
88. Subramanian, A., et al., *Gene set enrichment analysis: a knowledge-based approach for interpreting genome-wide expression profiles.* Proc Natl Acad Sci U S A, 2005. **102**(43): p. 15545-50.
89. Kobielak, A. and E. Fuchs, *Alpha-catenin: at the junction of intercellular adhesion and actin dynamics.* Nat Rev Mol Cell Biol, 2004. **5**(8): p. 614-25.
90. Drees, F., et al., *Alpha-catenin is a molecular switch that binds E-cadherin-beta-catenin and regulates actin-filament assembly.* Cell, 2005. **123**(5): p. 903-15.
91. Grise, F., A. Bidaud, and V. Moreau, *Rho GTPases in hepatocellular carcinoma.* Biochim Biophys Acta, 2009. **1795**(2): p. 137-51.

92. Osada, T., et al., *E-cadherin is involved in the intrahepatic metastasis of hepatocellular carcinoma.* Hepatology, 1996. **24**(6): p. 1460-7.
93. Lee, N.P. and J.M. Luk, *Hepatic tight junctions: from viral entry to cancer metastasis.* World J Gastroenterol, 2010. **16**(3): p. 289-95.
94. Yi, C., et al., *The p130 isoform of angiomotin is required for Yap-mediated hepatic epithelial cell proliferation and tumorigenesis.* Sci Signal, 2013. **6**(291): p. ra77.
95. Lin, W.H., Y.W. Asmann, and P.Z. Anastasiadis, *Expression of polarity genes in human cancer.* Cancer Inform, 2015. **14**(Suppl 3): p. 15-28.
96. Sato, K., et al., *Clinical significance of alterations of chromosome 8 in high-grade, advanced, nonmetastatic prostate carcinoma.* J Natl Cancer Inst, 1999. **91**(18): p. 1574-80.
97. Rummukainen, J., et al., *Aberrations of chromosome 8 in 16 breast cancer cell lines by comparative genomic hybridization, fluorescence in situ hybridization, and spectral karyotyping.* Cancer Genet Cytogenet, 2001. **126**(1): p. 1-7.
98. Moinzadeh, P., et al., *Chromosome alterations in human hepatocellular carcinomas correlate with aetiology and histological grade--results of an explorative CGH meta-analysis.* Br J Cancer, 2005. **92**(5): p. 935-41.
99. Zhao, M., et al., *Basolateral junctions utilize warts signaling to control epithelial-mesenchymal transition and proliferation crucial for migration and invasion of Drosophila ovarian epithelial cells.* Genetics, 2008. **178**(4): p. 1947-71.
100. Kapil, S., et al., *The cell polarity protein Scrib functions as a tumor suppressor in liver cancer.* Oncotarget, 2017. **8**(16): p. 26515-26531.
101. Albertson, R., et al., *Scribble protein domain mapping reveals a multistep localization mechanism and domains necessary for establishing cortical polarity.* J Cell Sci, 2004. **117**(Pt 25): p. 6061-70.
102. Bilder, D. and N. Perrimon, *Localization of apical epithelial determinants by the basolateral PDZ protein Scribble.* Nature, 2000. **403**(6770): p. 676-80.
103. Gao, J., et al., *Integrative analysis of complex cancer genomics and clinical profiles using the cBioPortal.* Sci Signal, 2013. **6**(269): p. pl1.
104. Stebbing, J., A. Filipovic, and G. Giamas, *Claudin-1 as a promoter of EMT in hepatocellular carcinoma.* Oncogene, 2013. **32**(41): p. 4871-2.
105. Nakagawa, S. and J.M. Huibregtse, *Human scribble (Vartul) is targeted for ubiquitin-mediated degradation by the high-risk papillomavirus E6 proteins and the E6AP ubiquitin-protein ligase.* Mol Cell Biol, 2000. **20**(21): p. 8244-53.
106. Chen, B., et al., *ZDHHC7-mediated S-palmitoylation of Scribble regulates cell polarity.* Nat Chem Biol, 2016. **12**(9): p. 686-93.
107. Wu, M., J.C. Pastor-Pareja, and T. Xu, *Interaction between Ras(V12) and scribbled clones induces tumour growth and invasion.* Nature, 2010. **463**(7280): p. 545-8.
108. Mendoza, M.C., E.E. Er, and J. Blenis, *The Ras-ERK and PI3K-mTOR pathways: cross-talk and compensation.* Trends Biochem Sci, 2011. **36**(6): p. 320-8.
109. Gao, T., F. Furnari, and A.C. Newton, *PHLPP: a phosphatase that directly dephosphorylates Akt, promotes apoptosis, and suppresses tumor growth.* Mol Cell, 2005. **18**(1): p. 13-24.
110. Brognard, J. and A.C. Newton, *PHLiPPing the switch on Akt and protein kinase C signaling.* Trends Endocrinol Metab, 2008. **19**(6): p. 223-30.
111. Carnero, A., et al., *The PTEN/PI3K/AKT signalling pathway in cancer, therapeutic implications.* Curr Cancer Drug Targets, 2008. **8**(3): p. 187-98.
112. Mattila, P.K. and P. Lappalainen, *Filopodia: molecular architecture and cellular functions.* Nat Rev Mol Cell Biol, 2008. **9**(6): p. 446-54.
113. Li, A., et al., *Fascin is regulated by slug, promotes progression of pancreatic cancer in mice, and is associated with patient outcomes.* Gastroenterology, 2014. **146**(5): p. 1386-96 e1-17.

114. Kessenbrock, K., V. Plaks, and Z. Werb, *Matrix metalloproteinases: regulators of the tumor microenvironment.* Cell, 2010. **141**(1): p. 52-67.
115. Pagliarini, R.A. and T. Xu, *A genetic screen in Drosophila for metastatic behavior.* Science, 2003. **302**(5648): p. 1227-31.
116. Nagasaka, K., et al., *Human homolog of Drosophila tumor suppressor Scribble negatively regulates cell-cycle progression from G1 to S phase by localizing at the basolateral membrane in epithelial cells.* Cancer Sci, 2006. **97**(11): p. 1217-25.
117. Zhan, L., et al., *Deregulation of scribble promotes mammary tumorigenesis and reveals a role for cell polarity in carcinoma.* Cell, 2008. **135**(5): p. 865-78.
118. Audebert, S., et al., *Mammalian Scribble forms a tight complex with the betaPIX exchange factor.* Curr Biol, 2004. **14**(11): p. 987-95.
119. Osmani, N., et al., *Scrib controls Cdc42 localization and activity to promote cell polarization during astrocyte migration.* Curr Biol, 2006. **16**(24): p. 2395-405.
120. Bradshaw, A.D., *The role of SPARC in extracellular matrix assembly.* J Cell Commun Signal, 2009. **3**(3-4): p. 239-46.
121. Rentz, T.J., et al., *SPARC regulates processing of procollagen I and collagen fibrillogenesis in dermal fibroblasts.* J Biol Chem, 2007. **282**(30): p. 22062-71.
122. Martinek, N., et al., *Haemocyte-derived SPARC is required for collagen-IV-dependent stability of basal laminae in Drosophila embryos.* J Cell Sci, 2008. **121**(Pt 10): p. 1671-80.
123. Aycock, R.L., et al., *Development of UV-induced squamous cell carcinomas is suppressed in the absence of SPARC.* J Invest Dermatol, 2004. **123**(3): p. 592-9.
124. Fenouille, N., et al., *The epithelial-mesenchymal transition (EMT) regulatory factor SLUG (SNAI2) is a downstream target of SPARC and AKT in promoting melanoma cell invasion.* PLoS One, 2012. **7**(7): p. e40378.
125. Tichet, M., et al., *Tumour-derived SPARC drives vascular permeability and extravasation through endothelial VCAM1 signalling to promote metastasis.* Nat Commun, 2015. **6**: p. 6993.
126. Arnold, S.A. and R.A. Brekken, *SPARC: a matricellular regulator of tumorigenesis.* J Cell Commun Signal, 2009. **3**(3-4): p. 255-73.
127. Said, N., I. Najwer, and K. Motamed, *Secreted protein acidic and rich in cysteine (SPARC) inhibits integrin-mediated adhesion and growth factor-dependent survival signaling in ovarian cancer.* Am J Pathol, 2007. **170**(3): p. 1054-63.
128. Schiemann, B.J., J.R. Neil, and W.P. Schiemann, *SPARC inhibits epithelial cell proliferation in part through stimulation of the transforming growth factor-beta-signaling system.* Mol Biol Cell, 2003. **14**(10): p. 3977-88.
129. van Zijl, F., et al., *A human model of epithelial to mesenchymal transition to monitor drug efficacy in hepatocellular carcinoma progression.* Mol Cancer Ther, 2011. **10**(5): p. 850-60.
130. Le Bail, B., et al., *Osteonectin/SPARC is overexpressed in human hepatocellular carcinoma.* J Pathol, 1999. **189**(1): p. 46-52.
131. Blazejewski, S., et al., *Osteonectin (SPARC) expression in human liver and in cultured human liver myofibroblasts.* Am J Pathol, 1997. **151**(3): p. 651-7.
132. Angel, P. and M. Karin, *The role of Jun, Fos and the AP-1 complex in cell-proliferation and transformation.* Biochim Biophys Acta, 1991. **1072**(2-3): p. 129-57.
133. Hai, T.W., et al., *Transcription factor ATF cDNA clones: an extensive family of leucine zipper proteins able to selectively form DNA-binding heterodimers.* Genes Dev, 1989. **3**(12B): p. 2083-90.
134. Reddy, S.P. and B.T. Mossman, *Role and regulation of activator protein-1 in toxicant-induced responses of the lung.* Am J Physiol Lung Cell Mol Physiol, 2002. **283**(6): p. L1161-78.
135. Hess, J., P. Angel, and M. Schorpp-Kistner, *AP-1 subunits: quarrel and harmony among siblings.* J Cell Sci, 2004. **117**(Pt 25): p. 5965-73.

136. Chamboredon, S., et al., *v-Jun downregulates the SPARC target gene by binding to the proximal promoter indirectly through Sp1/3.* Oncogene, 2003. **22**(26): p. 4047-61.
137. Hayakawa, J., et al., *Identification of promoters bound by c-Jun/ATF2 during rapid large-scale gene activation following genotoxic stress.* Mol Cell, 2004. **16**(4): p. 521-35.
138. Schlaeger, C., et al., *Etiology-dependent molecular mechanisms in human hepatocarcinogenesis.* Hepatology, 2008. **47**(2): p. 511-20.
139. Kawate, S., et al., *Amplification of c-myc in hepatocellular carcinoma: correlation with clinicopathologic features, proliferative activity and p53 overexpression.* Oncology, 1999. **57**(2): p. 157-63.
140. Lin, C.P., et al., *Targeting c-Myc as a novel approach for hepatocellular carcinoma.* World J Hepatol, 2010. **2**(1): p. 16-20.
141. Marian, C., et al., *Search for germline alterations in CDKN2A/ARF and CDK4 of 42 Jewish melanoma families with or without neural system tumours.* Br J Cancer, 2005. **92**(12): p. 2278-85.
142. Sharlow, E.R., et al., *A Small Molecule Screen Exposes mTOR Signaling Pathway Involvement in Radiation-Induced Apoptosis.* ACS Chem Biol, 2016. **11**(5): p. 1428-37.
143. Hirose, Y., et al., *Inhibition of Stabilin-2 elevates circulating hyaluronic acid levels and prevents tumor metastasis.* Proc Natl Acad Sci U S A, 2012. **109**(11): p. 4263-8.
144. Brekken, R.A. and E.H. Sage, *SPARC, a matricellular protein: at the crossroads of cell-matrix.* Matrix Biol, 2000. **19**(7): p. 569-80.

8. ACKNOWLEDGEMENTS

I would like to give my sincere acknowledgements to the people who have helped me to the successful completion of my PhD thesis.

First of all, I would thank my supervisor Dr. Kai Breuhahn, who always gives valuable support and guidance for my thesis. I learned from him how to carry out scientific research, how to solve problems in the study of liver cancer. He also gives me great opportunities to collect ideas from scientific conferences and meetings. With his help, I have improved my knowledge of tumor biology, and the skills for scientific research, which is important for my further professional career.

I would like to thank Prof. Dr. Peter Angel for the guidance of my PhD thesis. He and Dr. Marina Schorpp-Kistner provided me the knowledge and valuable support for the study of AP1 transcriptional factors in liver cancer.

I would like to give my thanks to Dr. Federico Pinna. He gave me great guidance during the first two years of my PhD study. I learned from him different laboratory skills, and he provided me valuable ideas for the study of cell polarity proteins.

I would like to thank Prof. Peter Schirmacher, for giving me the opportunity to study and carry out research in the group of AG Breuhahn of Pathology Institute.

I would like to thank my colleague Sofia Maria Elisabeth Weiler, who is always ready to help and give me suggestions during my PhD thesis. She is always willing to share her knowledge and experiences in the experimental work.

I would like to thank my colleague Anne-Sophie Meyer for the collection of HCC patient tissues, and the analysis of Scrib localizations.

I would like to thank the members of AG Breuhahn, Jennifer Schmitt and Michaela Bissinger for the valuable technical support. They are always ready to help when I have problems in my

experiments.

I would like to thank Dr. Stephanie Roessler who provided the HCC patient data and shared the knowledge of hydrodynamic tail-vein injection.

I would like to thank Prof. Dr. Jens Marquardt from University Hospital of Mainz, for providing the valuable patient materials and giving suggestions for my thesis.

I would like to thank Dr. Carsten Sticht and Prof. Dr. Norbert Gretz from Medical Faculty Mannheim. They helped me with the trancriptome analysis, which was important for the identification of Scrib-target genes.

I would like to thank Dr. Darjus Felix Tschaharganeh for providing the plasmids for hydrodynamic tail-vein injection. He also gave me suggestions for the scientific research.

I would like to thank Heike Conrad, who did the immunohistochemistry stains of HCC patient tissues and mouse tissues.

I also would like to give my thanks to the people in the department of Molecular Hepatology, Eva Eiteneuer, Marcell Toth, Dr. Carolin Plöger, Dr. Stefan Thomann and Dr. Margarita González-Vallinas Garrachón who helped me during the laboratory work. I enjoyed the cooperation with these people during my PhD study.

Last but not the least; here I would like to express my gratitude and love to my husband and my beloved parents for their support, encouragement and help to my life.

ERKLÄRUNG GEMÄß § 8 (3B, C) DER PROMOTIONSORDNUNG

Hiermit erkläre ich, dass die vorgelegte Dissertation mit dem Titel „Impact of the cell polarity protein Scribble on liver cancer formation and progression“ selbst verfasst und mich dabei keiner anderen als der von mir ausdrücklich bezeichneten Quellen und Hilfen bedient habe. Des Weiteren bestätige ich, dass ich an keiner anderen Stelle ein Prüfungsverfahren beantragt bzw. die Dissertation in dieser oder anderer Form bereits anderweitig als Prüfungsarbeit verwendet oder einer anderen Fakultät als Dissertation vorgelegt habe.

11/07/2017, Heidelberg

Shan Wan